NAVAL POSTGRADUATE SCHOOL
Monterey, California

THESIS

A DEMONSTRATION OF THE USE OF WALSH FUNCTIONS FOR MULTIPLEXED IMAGING

by

Robert Hugh McKenzie III
DECEMBER 1990

Thesis Advisor: David S. Davis

Approved for public release: Distribution is unlimited

NCLASSIFIED

CURITY CLASSIFICATION OF THIS PAGE

REPORT DOCUMENTATION PAGE

Form Approved
OMB No 0704-0188

a REPORT SECURITY CLASSIFICATION: Unclassified	1b RESTRICTIVE MARKINGS
a SECURITY CLASSIFICATION AUTHORITY	3 DISTRIBUTION / AVAILABILITY OF REPORT: Approved for public release: Distribution is unlimited
b DECLASSIFICATION / DOWNGRADING SCHEDULE	
PERFORMING ORGANIZATION REPORT NUMBER(S)	5 MONITORING ORGANIZATION REPORT NUMBER(S)
a NAME OF PERFORMING ORGANIZATION: Naval Postgraduate School; 6b OFFICE SYMBOL (If applicable): 61Dv	7a NAME OF MONITORING ORGANIZATION: Naval Postgraduate School
c ADDRESS (City, State, and ZIP Code): Monterey, CA 93943-5000	7b ADDRESS (City, State, and ZIP Code): Monterey, CA 93943-5000
a NAME OF FUNDING / SPONSORING ORGANIZATION; 8b OFFICE SYMBOL (If applicable)	9 PROCUREMENT INSTRUMENT IDENTIFICATION NUMBER
c ADDRESS (City, State, and ZIP Code)	10 SOURCE OF FUNDING NUMBERS: PROGRAM ELEMENT NO; PROJECT NO; TASK NO; WORK UNIT ACCESSION NO

11 TITLE (Include Security Classification)
A DEMONSTRATION OF THE USE OF WALSH FUNCTIONS FOR MULTIPLEXED IMAGING

12 PERSONAL AUTHOR(S)
ROBERT HUGH McKENZIE III

13a TYPE OF REPORT	13b TIME COVERED	14 DATE OF REPORT (Year, Month, Day)	15 PAGE COUNT
Master's Thesis	FROM _____ TO _____	DECEMBER 1990	131

16 SUPPLEMENTARY NOTATION
The views expressed in this thesis are those of the author and do not reflect the official policy or position of the Department of Defense or the U.S. Government

17 COSATI CODES			18 SUBJECT TERMS (Continue on reverse if necessary and identify by block number)
FIELD	GROUP	SUB-GROUP	Spectroscopy; Walsh Functions; Sequency Theory; infrared imaging

19 ABSTRACT (Continue on reverse if necessary and identify by block number)

A proof-of-concept experimental validation of a proposed idea for encoding spatial images using masks with patterns based on a set of ortnogonal Walsh functions was conducted. Simple images were encoded via a multiplexing technique, and computer algorithms were developed to decode and to display the results. Photographs of the re-constructed images offer incontestable proof of the validity of this hypothesis for multiplexed imaging. Further research of this technology is expected to lead to full development of an extremely efficient infrared imaging system, with additional applications to passive surveillance, target signature identification, and airborne infrared astrophysics.

20 DISTRIBUTION / AVAILABILITY OF ABSTRACT: ☒ UNCLASSIFIED/UNLIMITED ☐ SAME AS RPT ☐ DTIC USERS	21 ABSTRACT SECURITY CLASSIFICATION: unclassified
22a NAME OF RESPONSIBLE INDIVIDUAL: David S. Davis	22b TELEPHONE (Include Area Code): (408) 646-2116; 22c OFFICE SYMBOL: 61Dv

DD Form 1473, JUN 86 *Previous editions are obsolete* SECURITY CLASSIFICATION OF THIS PAGE

S/N 0102-LF-014-6603 UNCLASSIFIED

Approved for public release: Distribution is unlimited

A Demonstration of the
Use of Walsh Functions
for Multiplexed Imaging

by

Robert Hugh McKenzie III
Captain, United States Marine Corps
B.S., United States Naval Academy, 1982

Submitted in partial fulfillment of the
requirements for the degree of

MASTER OF SCIENCE
IN ENGINEERING SCIENCE

from the

NAVAL POSTGRADUATE SCHOOL
DECEMBER 1990

Author: Robert Hugh McKenzie III
Robert Hugh McKenzie III

Approved by: David Scott Davis
David S. Davis, Thesis Advisor

Donald L. Walters
D.L. Walters, Second Reader

K.E. Woehler, Chairman
Department of Physics

ABSTRACT

A proof-of-concept experimental validation of a proposed idea for encoding spatial images using masks with patterns based on a set of orthogonal Walsh functions was conducted. Simple images were encoded via a multiplexing technique, and computer algorithms were developed to decode and to display the results. Photographs of the re-constructed images offer incontestable proof of the validity of this hypothesis for multiplexed imaging. Further research of this technology is expected to lead to full development of an extremely efficient infrared imaging system, with additional applications to passive surveillance, target signature identification, and airborne infrared astrophysics.

TABLE OF CONTENTS

LIST OF FIGURES

I. INTRODUCTION

A. MOTIVATION

Since the time of the discovery of the characteristics of thermal (blackbody) radiation almost a century ago, it has been known that most commonplace objects on the earth emit most of their thermal radiation at infrared wavelengths. This is because most objects are in approximate thermal equilibrium with the ambient terrestrial environment, whose absolute temperatures lie in the range of 250-300 Kelvin. Hence, it follows that the infrared (IR) wavelengths constitute an important channel for the conveyance of information about objects in the terrestrial environment.

However, environmental remote sensing by means of infrared thermal measurements is not the only reason for pursuing infrared methods. The IR portion of the spectrum carries a vast amount of useful information. In particular, most molecules are capable of emitting and/or absorbing infrared radiation with ease. This makes IR observations, particularly IR spectroscopy, an important agent for the remote sensing of fundamental physical properties, such as chemical composition, temperature, and chemical abundances, It is evident, therefore, that detailed measurements of the spatial and

spectral characteristics of the radiation distribution emitted from an object can be of significant value.

Our primary regime of interest, then, is the remote sensing of the spatial and spectral properties of IR radiation. This area of technology is called infrared imaging spectroscopy, or, alternatively, spectroscopic imaging. It is a comparatively new field of study. Diverse types of instrumentation exist for either IR imaging or spectroscopy, but efficient and sensitive devices that are capable of both functions at once are rare. The development of such technology should be of great utility to many areas of remote sensing, particularly in surveillance/target signature identification and in more "pure" scientific disciplines, like infrared astrophysics.

This thesis has its origins in the infrared astrophysical instrumentation background of the author's thesis advisor, D.S. Davis. He has been the developer of state-of-the-art IR spectroscopic instrumentation for an extended period, particularly devices that are deployed aboard NASA's Kuiper Airborne Observatory. This thesis project marks the extension of his interests into the realm of imaging spectroscopy.

The Kuiper Airborne Observatory (KAO), operated by the Medium Altitude Missions Branch at NASA's Ames Research Center in California since 1975, has exploited the superior transmission of the atmosphere at altitudes above 40,000 feet and produced a wealth of significant astronomical information.

An airborne platform is required for much IR astronomical work, in order to get above terrestrial water vapor, an IR absorber. Researchers aboard the KAO are credited with such discoveries as the unique ring system around Uranus in 1977, a ring of dust emission about the galactic center, an understanding of the composition of Halley's Comet, and precision measurements of the chemical constituents of planetary atmospheres.

Recently, NASA has proposed a successor to the KAO to be called SOFIA -- Stratospheric Observatory For Infrared Astronomy. SOFIA will be a modified Boeing 747 jet aircraft carrying a Nasmyth three meter open-port telescope supplied by the Federal Republic of Germany. Designed to "address fundamental questions in galactic and extragalactic astronomy and in the origin and evolution of the Solar System" [Ref. 1], Sofia will extend airborne observation capabilities well beyond those of the KAO. With an evolving complement of focal plane instrumentation, SOFIA should have 10 times the point source sensitivity and three times the angular resolution of its predecessor. With these vast improvements, scientists believe SOFIA will provide the capability to study the entire cycle of the birth and death of stars and planets by examining infrared emissions of different phases of the interstellar medium.

Davis' principal contribution to KAO research has been in the development and use of a cryogenically-cooled infrared

multiplexing Fourier Transform Spectrometer. The spectrometers that are to fly aboard SOFIA will need to take advantage of its augmented sensitivity to increase their spectral resolving powers where needed. The proposed availability of SOFIA has sparked recent developments in spectrometer design, including an innovative optical multiplexing technique for infrared imaging being pursued by Davis [Ref. 2]. This technique is based on the use of orthogonal functions to encode entire images at once, rather than on traditional scanning methods. Davis proposes a unique state-of-the-art imaging/spectroscopic system that will operate over a wide range of infrared wavelengths and resolving powers. For the first time such a system will achieve in both the spatial and spectral domains, all of the advantages now enjoyed by Fourier spectroscopic methods alone. Davis believes such a system would provide extreme sensitivity and versatility on a platform such as SOFIA, and have major effects on such areas of infrared remote sensing as passive surveillance and target signature identification. [Ref. 2]

B. THESIS GOAL

The goal of this thesis is to investigate the idea of encoding electromagnetic energy using masks encoded with patterns based on the products of Walsh functions, as proposed by Davis. This is a proof-of-concept project; it has not attempted to achieve the goals of high sensitivity and

versatility of which the technique is hypothetically capable. We have set out to encode simple images via a multiplexing technique, to develop the necessary computer algorithms to decode and to display results, and to demonstrate that the method is conceptually sound. Successful achievement of these goals will prove the validity of Davis' hypothesis. This will lay the groundwork for future experimentation leading to the development of infrared spectroscopic imaging instruments using this technique to its fullest potential.

II. A NEW TECHNIQUE IN INFRARED IMAGING SPECTROSCOPY

A. GOAL AND METHODOLOGY OF IMAGING SPECTROSCOPY

The basic goal of imaging spectroscopy is to measure simultaneously the spatial and spectral characteristics of an observed electromagnetic radiation field. The desired measurements are functions of three independent variables, typically the X and Y coordinates of each image pixel, along with a spectral variable, such as wavelength or wave number. Theoretically, the direct determination of the intensity of such a radiation field would require the use of some sort of complex three-dimensional (3-D) detector whose geometric structure could be mapped into the 3-D spatial and spectral parameter space required by the application. Such detectors, and instruments to use them, do not exist. Therefore, some sort of opto-mechanical scanning in the spectral and/or spatial domain is usually employed. Such sequential scanning does not produce a simultaneous measurement of the entire pattern of radiation. Yet, if the field under observation is temporally stable during the scanning period, satisfactory results may be obtained for comparatively bright sources.

The development of a new generation of imaging spectrometers is by no means an idle academic exercise. This is particularly true in the realm of IR technology.

Currently, various types of IR imaging devices exist that use opto-mechanical scanners, vidicons, and array detectors. Such devices yield only limited information about the radiation field under study. They are IR relatives of black-and-white television, revealing the intensities of a target field's spatial components without measuring anything about that field's spectral characteristics. By the same token, IR spectrometers abound. These devices disclose an abundance of data about a target's temperature, chemical composition, and range. They do so, however, at the expense of spatial information, by averaging their spectroscopic capabilities over an entire field of view. Details about which spectral composition is produced by which portion of the target are thereby lost in the process.

An efficient IR imaging spectrometer can, at least hypothetically, overcome both of these limitations by providing simultaneous, detailed spectral and spatial information about the radiation field being emitted from a target. Citing again the analogy with television, the goal of such an imaging spectrometer is to measure IR spatial and spectra signatures by means of high definition color television. It is actually better than that, for the resulting "colors" are actually detailed spectra, characterizing the target's composition, temperature, and other signature components.

For example, suppose that we are interested in characterizing the exhaust of a jet engine. Conventional IR imaging methods, such as Forward-looking infrared, record the spatial distribution of the exhaust's emitted IR flux, but nothing abouts its spectrum. A conventional spectrometer can measure the spectrum of the exhaust plume, but spatial information is lost. If we want to know what molecular species are present and where in the plume they occur, we need imaging spectroscopy for the task.

B. SCANNING VERSUS MULTIPLEXING

It has been demonstrated repeatedly that, for optical measurements which must employ some type of scanning to achieve their purpose, significant improvement in the quality of experimental results may be realized by using multiplexing methods in lieu of traditional scanning methods. [Ref. 3] Traditional scanning approaches usually involve a sequential set of observations made while one of the independent optical variables, for example, wavelength or pointing angle, varies in a systematic manner. This is the technique used in raster scanning of an image or in the recording of a spectrum with a conventional monochromator.

There is a fundamental inefficiency associated with this approach, however. By recording only one sample at a time, the instrument is ignoring the rest of the radiation field during that time. If the measurement is to be of an

inherently weak source, then this waste of incoming photons at other wavelengths of interest, or from other parts of the source, results in a gross inefficiency in the entire measurement process. Multiplexing avoids this waste by recording all of the information of interest all of the time. The experimental apparatus encodes the radiation field in such a way that the optical detector sees not a time sequence of isolated samples of the field, but rather a time sequence of linear combinations of all samples from the entire field. The information is encoded so that these linear combinations may be unscrambled later by a digital computer. By employing such a procedure, the experimenter gains enormous optical efficiency with his device. The cost in doing so is an increase in instrumental complexity; nevertheless, the effort can be more than amply rewarded.

C. FOURIER TRANSFORM SPECTROSCOPY

1. Methodology

The most widely exploited multiplexing technique is Fourier Transform Spectroscopy (FTS) [Ref. 3]. In FTS, each spectral element's intensity appears as the coefficient of a simple sinusoidal function; the spectrometer produces a sequence of measurements of linear sums of such terms. A Fourier transform of the sequence of measurements recovers the spectral intensity distribution.

2. Advantages

Fourier transform spectrometers have virtually revolutionized IR spectroscopy. There are now many commercial instruments in widespread use. Several physical reasons exist for the remarkable successes of IR multiplexing, but five prominent factors stand out. They are listed herein and described briefly below:

the Fellgett multiplexing advantage [Ref. 3]

the Jacquinot throughput advantage [Ref. 3]

the excellent thermal background signal cancellation of properly designed multiplexing systems [Refs. 2,4]

the immense versatility of the technique [Ref. 2]

the simple internal metrological consistency of the resulting measurements. [Ref. 4]

a. The Felgett Advantage

When multiplexed instruments are operated in noise regimes where the dominant noise source is not correlated with detected signal levels, those instruments possess a significant signal-to-noise advantage over traditional scanning devices. This is because the noise fluctuations in signal level are distributed uniformly over all measurement channels, while all channels are being recorded simultaneously. When the measurements are later demultiplexed in the computer, this uniform noise distribution is divided

equally among the various channels, so that each channel receives only a fraction of the total noise distribution.

b. The Jacquinot Advantage

This consideration is of particular relevance to Fourier transform spectrometers and related instruments. Since such devices do not employ slits or similar one-dimensional field stops, they collect much more light than that collected by a conventional dispersive spectrometer of comparable resolving power. Comparing a multiplexed instrument and a dispersive instrument for observations of the same spatially extended field, the multiplexed one will typically record many orders of magnitude more photons in a given time, yielding an attendant enhancement in signal-to-noise ratio (SNR).

c. Thermal Background Reduction

The form of optical multiplexing inherent in Fourier spectrometers makes these instruments excellent for measurements of comparatively weak signals embedded within strong thermal background emissions from the environment and/or from the instruments themselves. The cancellation of this background interference is accomplished by purely passive means. Two input beams are employed: one looks at the field of interest, while the other looks at a neighboring blank field. Both fields are then combined out of phase at the spectrometer's beamsplitter, so that, ideally, the common

background component does not produce a measured modulated signal.

d. The Versatility Advantage

In order to make major changes in experimental parameters, such as resolving power, with traditional instruments, it is usually necessary to make a complete interchange of key optical components. For example, the experimenter may be required to switch diffraction gratings in order to obtain the best blaze angle and spectral resolution for a particular application. Optical changes of this kind are a complicated exercise and are not conducive to the rapid adaptation of the apparatus to diverse experimental objectives under real-time operating constraints.

Multiplexed instruments, however, need no such major overhaul for their conversion to different objectives. For example, the airborne Fourier transform spectrometer used by Davis aboard the KAO can be converted, in flight, from low (100) to ultra-high (1,000,000) resolving power in about 10 seconds. Similar reconfiguration times are involved in its conversion to different wavelength bands and different sensitivities. Therefore, multiplexed approaches have a distinct edge in applications such as airborne spectrometry and "in-the-field" remote sensing, which require that a single instrument be readily adjustable to a wide variety of experimental objectives.

e. Metrological Consistency

The simultaneous acquisition of all measurements via a single detection channel automatically cancels any channel-to-channel discrepancies and systematic calibration errors. All observations have the same experimental frame of reference, yielding remarkable internal consistency and ease of calibration. The experimenter generally does not have to resort to laborious secondary calibration procedures.

3. Limitations

As of this time, FTS represents the most successful refinement of optical multiplexing methods as applied to spectroscopic measurement. Spectroscopist A.H. Gebbie stated [Ref. 5] in 1970 that he believes "it has been perfected during the recent revival in two beam interferometric spectroscopy due to the advent of very fast and cheap digital computation, which allows the time variable to be inverted to the required frequency variable." Computers are much faster and cheaper now than they were 20 years ago. Efficient digital processing techniques, such as the fast Fourier transform and its cousins, make it feasible to consider the use of other orthogonal function families for optical multiplexing.

4. Hadamard Spectroscospy

a. Methodology

The use of binary orthogonal functions in multiplex spectrometry was pursued by Gebbie and others a number of years ago. The most familiar example of this approach is probably the so-called Hadamard transform spectrometer of Harwit and Decker. [Refs. 6,7] Despite its name, it does not actually use Hadamard matrices in its operation; it encodes the elements of a spectrum as coefficients of orthogonal cyclic-redundancy functions by modulating the instrumental field of view with optical masks that are alternately transparent or opaque at each image pixel. In the cyclic-redundancy form of the Hadamard tactic, 2^n-1 separate two-dimensional encoding masks are required to multiplex n image pixels.

b. Limitations

There are some obvious limitations with this approach. First, it is difficult to register so many two-dimensional masks precisely and reproducibly within the field of view. Second, the optical efficiency of the Hadamard system is at best 50%, owing to the opacity of the "off" pixels for any given mask. Third, there is no way to invoke the equivalent two-beam background compensation scheme that is an key contributor to the success of IR FTS systems. Fourth, the method lacks versatility; different spatial resolving

powers require a set of different masks. The new image multiplexing scheme proposed by Davis will overcome each of these deficiencies while preserving the other advantages of multiplexing at the same time.

D. DAVIS' PROPOSED TECHNIQUE

Davis' proposed new technique is based upon the tenets of sequency theory as detailed by Harmuth [Ref. 8]. Instead of using opaque and transparent masks as in the Hadamard approach this technique uses reflecting and transmitting encoding masks formed from photo-etched metal films on transparent substrates. These masks will consist of patterns of two-dimensional sequency-ordered Walsh functions as shown in Figure II-1. This technique achieves passive background compensation exactly analogous to the FTS's technique by using two input beams to illuminate opposite sides of such a mask encoder. Furthermore, with proper material selection, few photons will be absorbed by the encoder and optical efficiencies can, at least theoretically, approach 100%.

There is one overriding advantage to be gained by using Walsh functions instead of the cyclic-redundancy functions associated with the Hadamard technique. As will be shown in the next chapter, Walsh functions form an orthogonal basis set which can be synthesized by means of Kronecker products of other Walsh bases of lower order. This will permit the generation of 2^n encoding masks in the two-dimensional (2-D)

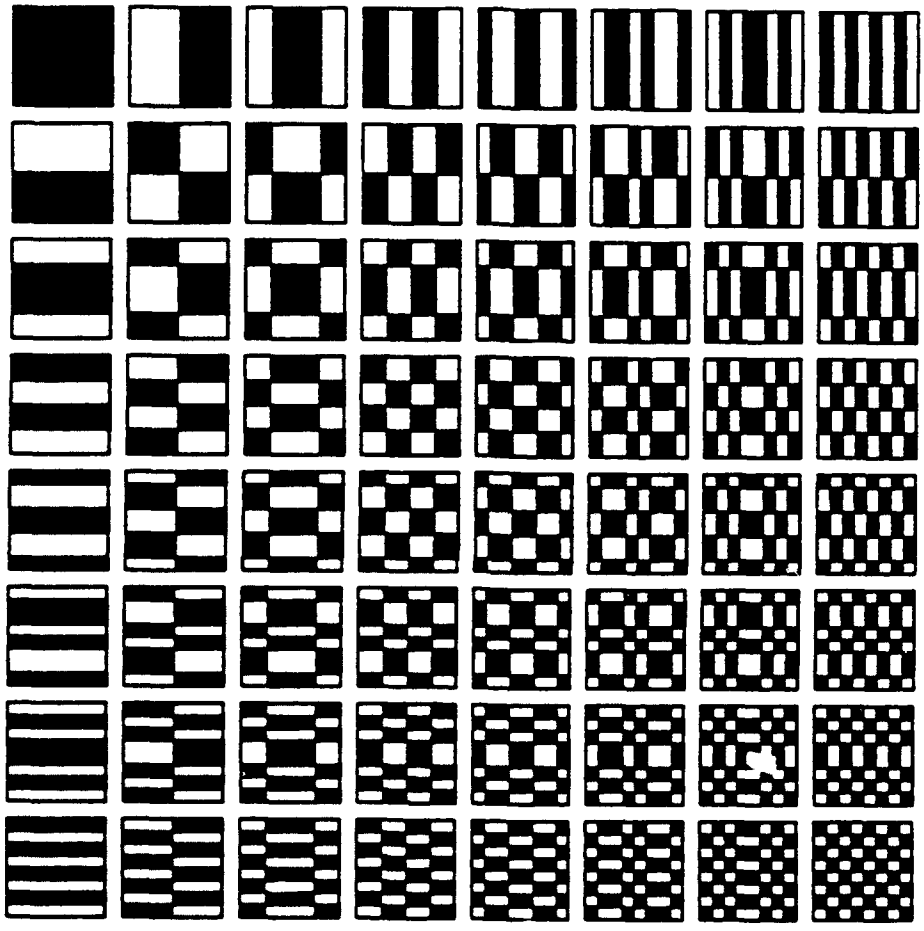

Figure II-1. Two-Dimensional Sequency-Ordered Walsh Functions.

image plane by employing two one-dimensional (1-D) masks of order 2^j and 2^k, where j+k=n. There are tremendous potential gains to be derived by exploiting this fact. To encode, for instance, a 32 x 32 pixel image, the Hadamard approach would require the precise manipulation of 2,047 2-D masks. The Walsh method will require that only two 1-D masks be used, each with only 32 patterns! The opto-mechanical servo system for 1-D control will be much simpler than a 2-D system. Also, proper sequency ordering of the basis masks will permit the complete decoupling of the measured spatial frequencies of the image, so that wide versatility of spatial resolving power with respect to two independent spatial coordinates may be realized.

The patterns shown in Figure II-1 are actually entries in a multiplication table of Walsh functions; only those encoding patterns displayed along the top and left margins of each array are required to synthesize the remainder of the patterns and thus the entire encoding basis. In addition, the technique is not confined to simple cartesian arrays, as shown by the patterns in Figures II-2 and II-3.

Figure II-2 shows a multiplication table for projected spherical coordinates, such as might be employed for global surveillance; Figure II-3 displays an equivalent table mapped into modified polar coordinates. Any arbitrary distribution of pixel sizes and shapes, even non-contiguous configurations, is possible. The only restriction is that the number of

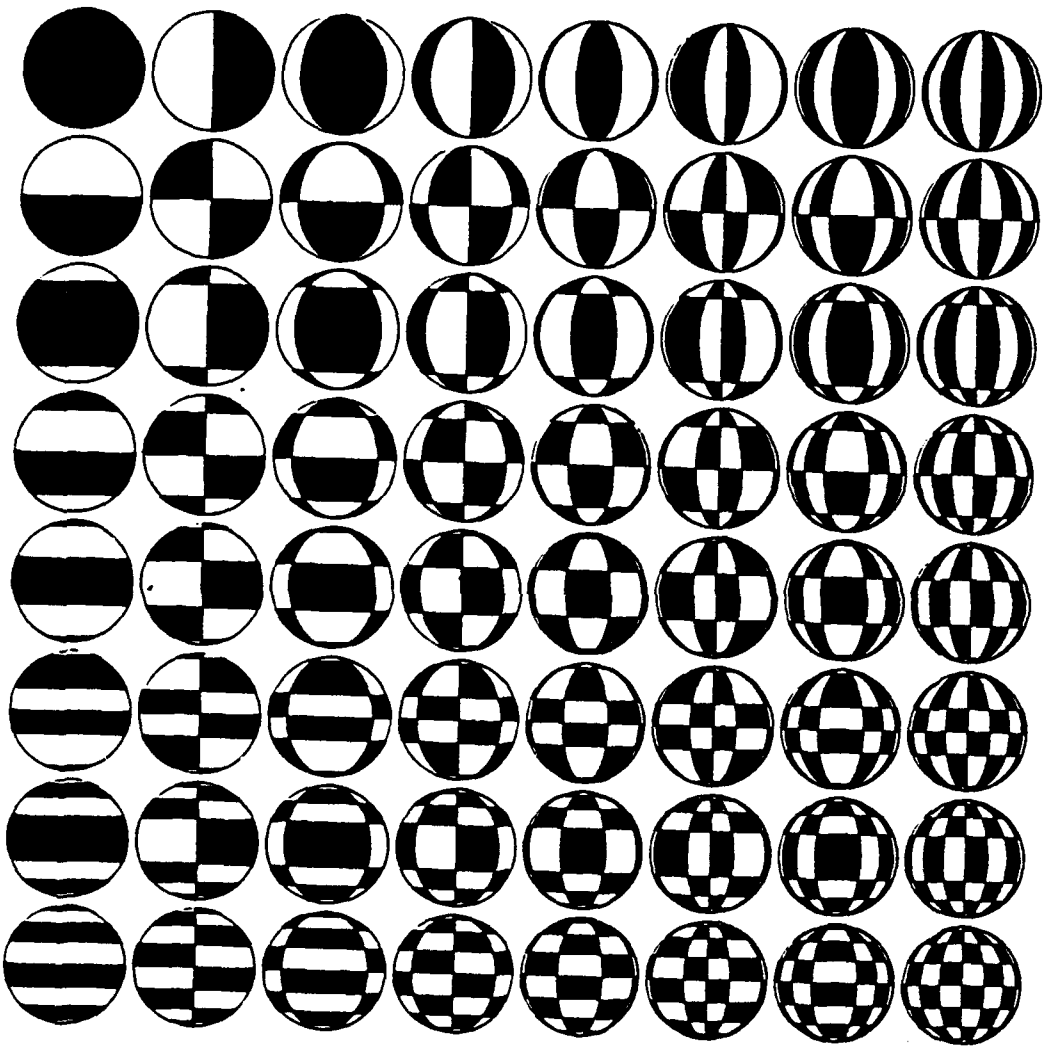

Figure II-2. Walsh Functions in Projected Spherical Coordinates.

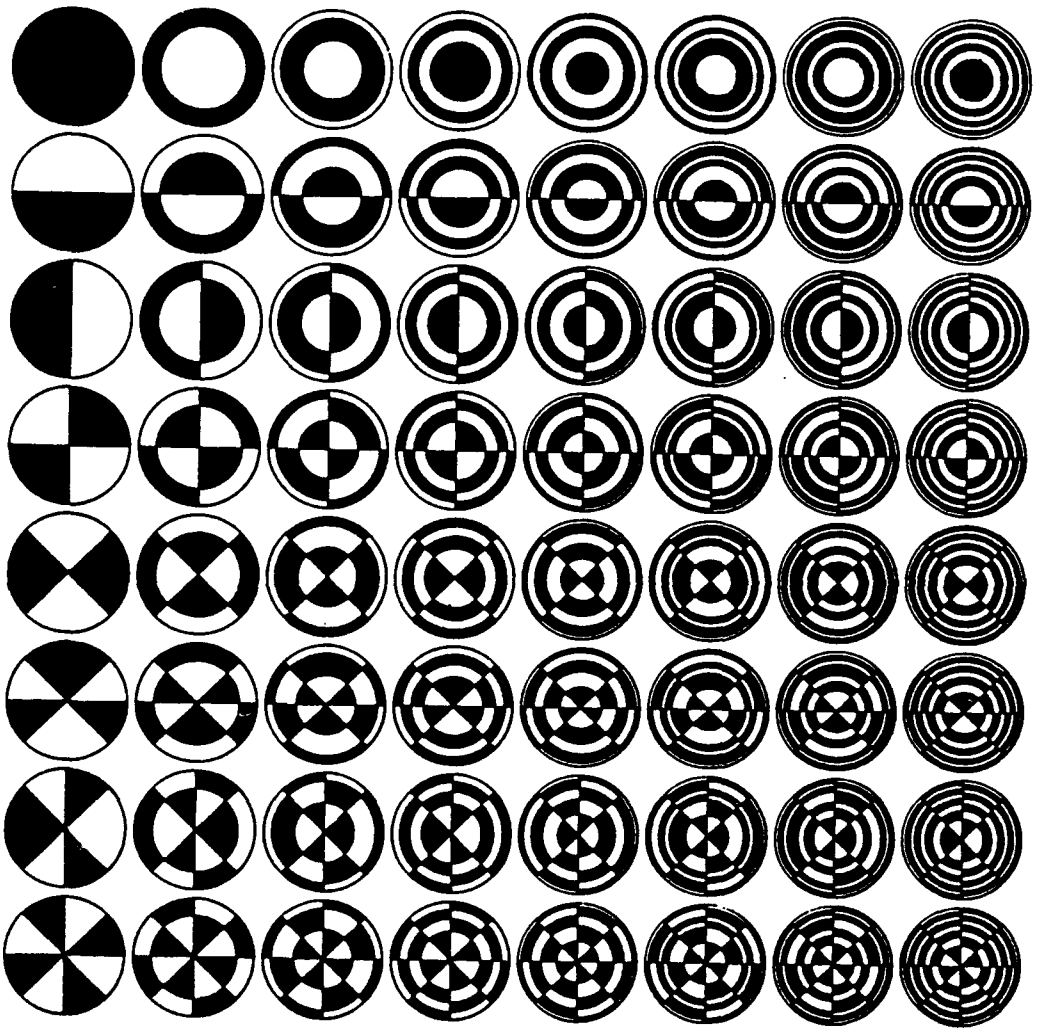

Figure II-3. Walsh Functions in Modified Polar Coordinates.

samples to be encoded must be 2^n, where n is an integer. If an instrument is pre-configured with a sufficiently large pair of masks, any complete sub-basis of spatial frequencies, in 1 or 2 dimensions, may be scanned independently.

Once this new approach to imaging is realized in a practical IR instrument, it can be coupled to either a conventional dispersive array detector system to record spatially multiplexed and spectroscopically dispersed spectral images. Or, in wavelength regions where efficient array detectors are not available, it could be combined with a two-input Fourier transform spectrometer to produce completely multiplexed spectral images. Figure II-4 illustrates Davis' concept for a possible hybrid multiplexed imaging-FTS system. It contains the two orthogonal Walsh encoders, a stigmatic optical train to perform the optical analog of the Kronecker product, and an output FTS of the proven KAO type.[Ref. 2]

As stated in the introduction, the goal of this thesis project has been to demonstrate that the Walsh multiplexing scheme for image encoding/decoding will work. The ultimate goal of producing an efficient imaging spectrometer is left for the future.

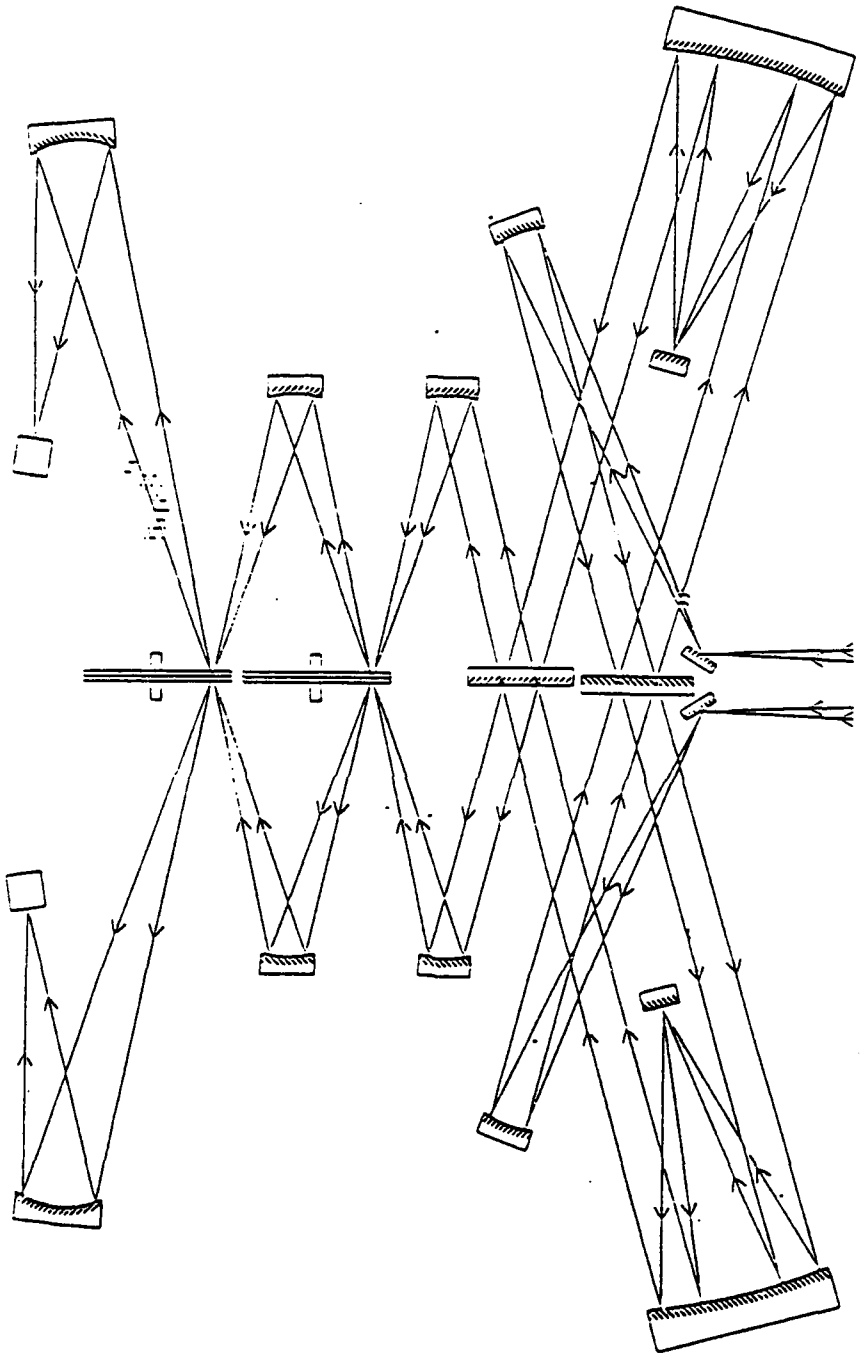

Figure II-4. Davis' Proposed Hybrid Multiplexed Imaging-FTS System.

III. WALSH FUNCTIONS

A. DESCRIPTION

Walsh functions are a closed set of orthogonal functions first developed by J.L. Walsh in 1923 [Ref. 9]. They form an ordered set of rectangular waveforms, taking on amplitude values of ±1 only. They are defined over a limited argument range, such as some domain of length, T. For the multiplexing applications described in this thesis, T is actually a spatial, rather than a temporal argument. Two parameters are required for a complete description of a Walsh function, just as with the familiar sine and cosine trigonometric functions, $\sin(\omega t)$ and $\cos(\omega t)$. For Walsh functions, the necessary parameters are an argument t (often normalized to the domain width T as $\theta = t/T$), and an ordering number, n, which is analogous to the frequency parameter of the trigonometric functions. An arbitrary Walsh function may be written as:

$$\mathrm{Wal}(n,t) \quad \text{for } n = 0,1,2,\ldots,N-1$$

$$\text{where } N=2^m, \ m \text{ integer} \geq 1.$$

The ordering parameter is usually referred to as the sequency of the Walsh function. Sequency is a term originally coined by Harmuth [Ref. 8] to describe a waveform-independent repetition rate. It is similar to the frequency concept associated with sinusoidal functions. Frequency may be

thought of as a specification of ½ the number of a sinusoid's zero crossings in a given interval. Similarly, sequency is the number of zero crossings that a Walsh, or related functions, exhibit in a given interval, although the zero crossings do not have to be uniformly spaced. For our purpose and many other applications, the set of Walsh functions is ordered in ascending sequency. The first eight sequency-ordered Walsh functions are shown Figure III-1.

In addition to sequency order, other conventions in common use include dyadic order (Paley order), natural order (Hadamard order), and Gray code order. These orderings, their origins, and their uses are fully described by Harmuth [Ref. 8] and Beauchamp [Ref. 10].

B. ORTHOGONALITY

1. Definition

Two functions $\phi_i(x)$ and $\phi_j(x)$ in the set $\{\phi_n(x)\}$ are said to be orthogonal with respect to each other over the interval $a < x < b$ if they satisfy the conditions

$$\int_a^b \phi_i(x)\,\phi_j^*(x)\,dx = K_i\delta_{ij}$$

where

$$\delta_{ij} \triangleq \begin{cases} 1, & i=j \\ 0, & i=j \end{cases}$$

and $K_i \neq 0$.

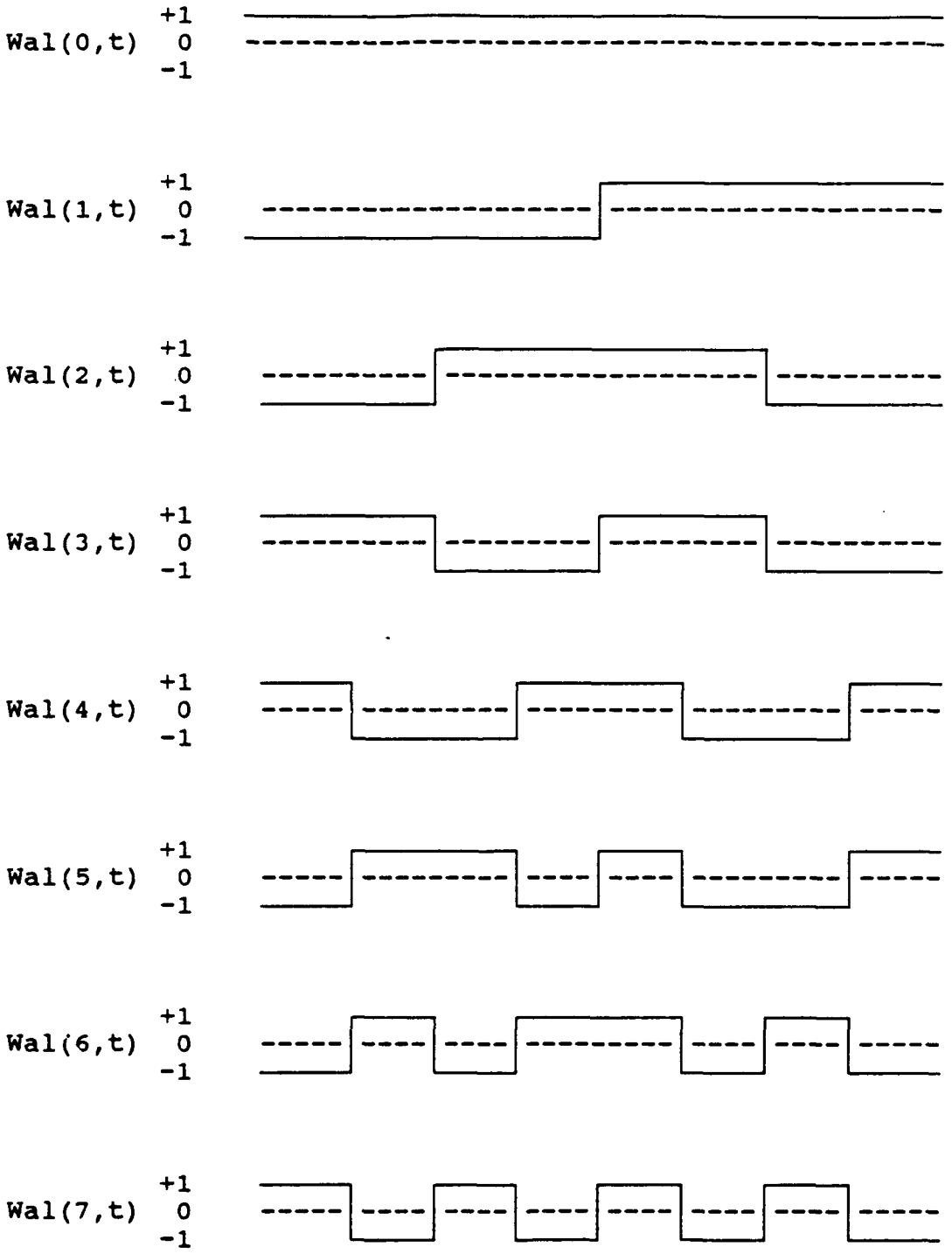

Figure III-1. The First Eight Sequency-ordered Walsh Functions.

δ is called the Kronecker delta. If the constants K_i are all equal to 1, the ϕ_i (x) are said to be orthonormal functions. The term "orthogonal" is borrowed from vector algebra in analogy to perpendicular vectors, because the above integral resembles the dot product operation for ordinary vectors.

2. Demonstration

The orthogonality of the discrete Walsh function set is proven by Walsh [Ref. 9], Harmuth [Ref. 8], and Beauchamp [Ref. 10]. The result is

$$\int_{t=0}^{t=1} WAL(m,t)\,WAL(n,t)\,dt = \delta_{mn}.$$

The reader can demonstrate this characteristic easily and convincingly using the Walsh functions shown in Figure III-1. Arbitrarily choose any two of these functions. Working from left to right over the entire interval, multiply the amplitudes of the two functions together for each sub-interval (a sub-interval is the domain over which there are no zero crossings). Next, add up the values for all sub-intervals. The sum will be zero in all cases in which the two functions are not identical, and will be exactly one when the two functions are the same.

For example, choose WAL(3,t) and WAL(7,t). Note that WAL(7,t) has seven zero crossings, or discontinuities, resulting in eight sub-intervals where the sign changes,

whereas WAL(3,t) has only four sub-intervals (which are twice the length of those for Wal(7,t)) over the same interval of time. Working from left to right over the entire interval, take the product of these two functions over eight sub-intervals. Next, total the values for all sub-intervals and note that the sum is indeed zero. Results are listed below in Table III-1.

TABLE III-1
SUMMARY OF ORTHOGONALITY DEMONSTRATION

SUB-INTERVAL	WAL(3,t)	WAL(7,t)	WAL(3,t)*WAL(7,t)
1	+1	+1	+1
2	+1	-1	-1
3	-1	+1	-1
4	-1	-1	+1
5	+1	+1	+1
6	+1	-1	-1
7	-1	+1	-1
8	-1	-1	+1
		SUM TOTAL	0

Now repeat the same procedure multiplying one function by itself and adding up the amplitude values. In all cases, wherever the function equals -1, then the function multiplied by itself gives (-1 x -1) = +1; wherever the function is +1, then (+1 x +1) = +1. Therefore, the function multiplied by itself (or squared) is +1 everywhere and the integral over the entire unit interval will always be 1!

After trying these exercises with several different combinations, the reader will be convinced of the orthogonality of Walsh functions, an important characteristic which we will later exploit.

C. ADDITIONAL PROPERTIES

There are two additional properties of Walsh functions which should be noted. The first is the limitation on the number of individual functions in an orthogonal basis set and the second is the concept of phasing.

1. Limitation on the Number of Individual Functions

Unlike the orthogonal trigonometric functions which form the basis set for conventional Fourier analysis, the Walsh functions have a restriction on the number of component functions that constitute a complete orthogonal basis set. That number must be an integer power of two; that is, the complete basis set must contain N distinct members, where $N = 2^m$ and m is a positive integer. The sequency of the individual member functions will range from 0 to N-1, as Figure III-1 shows for the case of N = 8.

2. Phasing Concept

The phasing concept for Walsh functions is actually simpler than that for the trigonometric functions. Since the functions take on only the values ±1, the only possible alteration or ambiguity in their specification is that they can be multiplied by -1, if desired, either individually or as an entire basis set. It is easy to show that such a sign inversion does not affect the orthogonality or normalization properties of the Walsh functions. Harmuth phasing and positive phasing are two sign conventions in common use [Ref.

10]. For Harmuth phasing, the function is required to have a positive algebraic sign for argument values that lie just above the midpoint of the argument's domain, as shown in Figure III-1. Alternatively, positive phasing demands that the initial portion of the function, for the smallest values of its argument, have a value of +1.

D. APPLICATIONS

Walsh functions have proven to be useful in many engineering applications, especially electronics and communication signal processing. Beauchamp [Ref. 10] presents a survey which includes such diverse applications as speech processing, seismology, electrocardiograms, digital filtering techniques, and pattern recognition. Annual "Proceedings of the Symposium on the Applications of Walsh Functions" were published in the early 1970's [Refs. 11,12], and are now published as regular IEEE proceedings. They contain abtracts from international contributors on a variety of projects where Walsh function are especially practical and/or useful.

E. WALSH FUNCTIONS WITH SEVERAL VARIABLES

Many signals in communications are functions of several variables. For example, television signals have two spatial variables and one time variable. The Walsh functions are readily extended to several variables by means of a remarkably simple characteristic of this class of functions: the product

of two or more Walsh functions is itself another Walsh function. More properly stated, the Kronecker product of the Walsh functions is another Walsh function [Ref. 8]. This theme is crucial to the image encoding masks employed in this research and will be explained in more detail in later chapters.

By way of example, consider the graphical representation of Wal(k,x) x Wal(m,y) as shown in Figure III-2. The functions shown in the top row are Wal(k,x) for k = {0,1,2,...,7} and the functions in the left column are Wal(m,y) for m = {0,1,2,...,7}. Black areas represent the value +1 and white areas represent the value -1. All of the other patterns are entries in a multiplication table: the pattern formed by the product Wal(k,x) x Wal(m,y) is located at the intersection of the column denoted Wal(k,x) and the row denoted Wal(m,y). The product function, Wal(0,x) x Wal(0,y), located in the top left corner, is +1 everywhere and its areal integral equals +1. Notice that all other functions Wal(k,x) and Wal(m,y) for k,m ≠ 0 are +1 (black) as often as -1 (white), and their areal integrals equal zero. Also notice that all the products of these two Walsh functions are themselves Walsh functions whose areal integrals also equal zero.

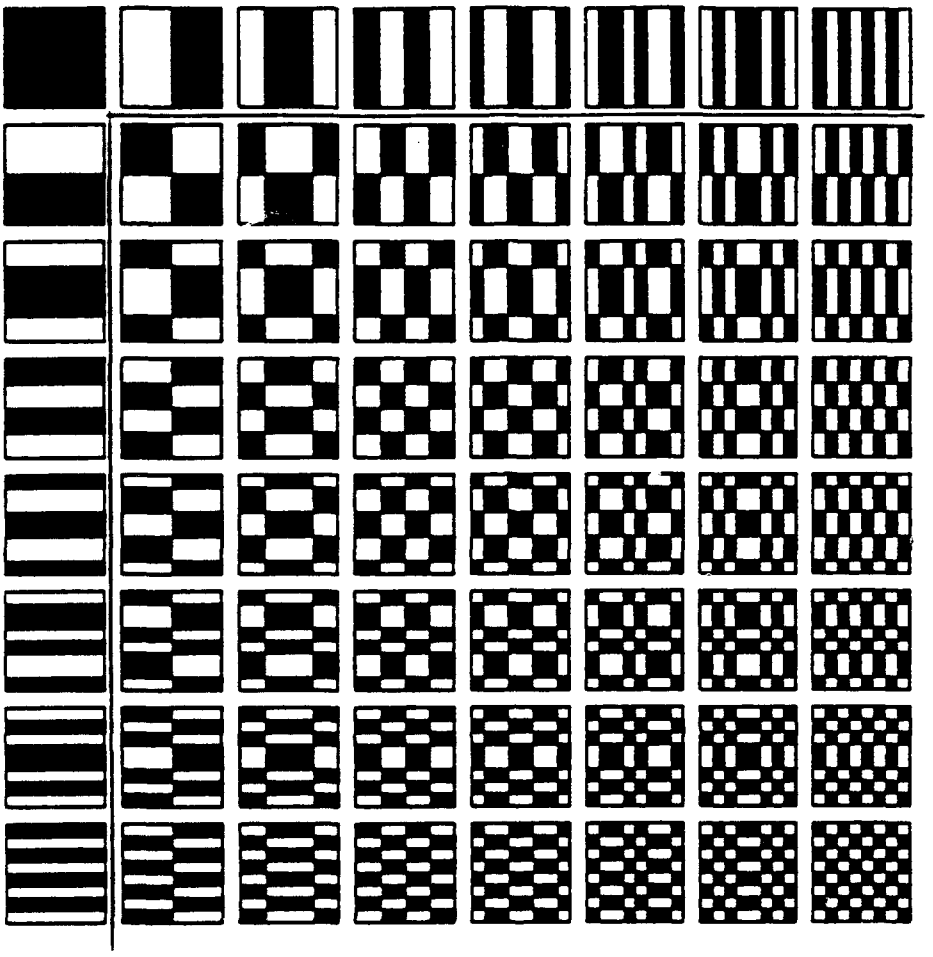

Figure III-2. Walsh Functions Wal(k,x) and Wal(m,y) and Their Products Wal(k,x) x Wal(m,y) for k,m = (0,...,7). Black Areas Represent +1; White Areas Represent -1.

These are the patterns which were computer-generated and used to make encoding masks for this thesis. The many intrinsic symmetries of the family of Walsh functions make this encoding approach a particularly interesting one.

IV. MULTIPLEXED IMAGING WITH WALSH FUNCTIONS

A. OVERVIEW

The reader should recall that the primary objective of this thesis project has been to demonstrate that the proposed technique of optical multiplexing by means of Walsh functions is a viable one. The ultimate goal of the entire project, of which this thesis effort is but a part, is to develop a very sensitive and efficient means of measuring spectroscopic images. The novel aspect of our approach entails the encoding of image, as opposed to spectral, information by multiplexed means. Therefore, the thrust of this project so far has been concerned with imaging methods, rather than with spectroscopic techniques. Incorporation of spectroscopic capability into a final instrumental configuration has been left for future work.

In this chapter the basic formalism behind the multiplexed imaging approach will be outlined. In order to understand this approach, the reader will need to become acquainted with the logical steps that were followed in the development of crucial ideas, beginning with the familiar concepts of radiometry, scanning and multiplexing in the spectral domain. These ideas are then extended to incorporate the Walsh function multiplexing of images.

B. RADIOMETRY

It is well-known that electromagnetic radiation consists of discrete quanta, or photons, of energy that correspond to oscillations of the electromagnetic field. For our purposes, we are not concerned with this quantum aspect of the radiation process, nor are we interested in the vector or polarization characteristics of the field. Imaging spectroscopy deals with only a subset of the complete properties of the electromagnetic field: how much energy a target is radiating at different wavelengths and from what region of the target that radiation originates. Our interests are the spectral and angular energy (or power) distributions of the radiation field.

The simplest radiometric situation is shown in Figure IV-1. Similar illustrations may be found in many texts on radiative transfer [Refs. 13, 14].

The source consists of some very small radiating area, A_s, and the receiver of a small collecting area, A_R, separated by a linear distance, r. A_s and A_R are oriented so that their normal vectors make angles of Θ_s and Θ_R with respect to r. The flow of radiative energy from A_s to A_R is governed by two classes of parameters: geometric and electromagnetic. The geometric parameters are just A_s, Θ_s, A_R, Θ_R, and r. The relevant electromagnetic quantity is the specific intensity, or simply intensity, I, of the radiation field. I defines the amount of radiative energy passing through some small area dA

Figure IV-1. A Simple Radiometric Situation.

per unit solid angle dω per wavelength interval dλ per unit time dt. As Figure IV-2 illustrates, the small solid angle dω intersects the normal to dA at some angle Θ.

The parcel of energy that crosses dA is then used to define I as

$$dE = I(\vec{r}, w, \lambda)\cos\theta\, dA\, d\omega\, d\lambda\, dt\,. \qquad (1)$$

The ultimate purpose of imaging spectroscopy is to measure the spatial $(\vec{r})$ and spectral (λ) dependencies of a target's $I(\vec{r}, \omega, \lambda)$, thereby enabling the observer to infer the physical characteristics of that target, as discussed in Chapter II.

We are interested in remote sensing applications of imaging spectroscopy, which allows us to simplify the radiometric config-uration above. For remote sensing, we may safely assume that the line-of-sight separation between the

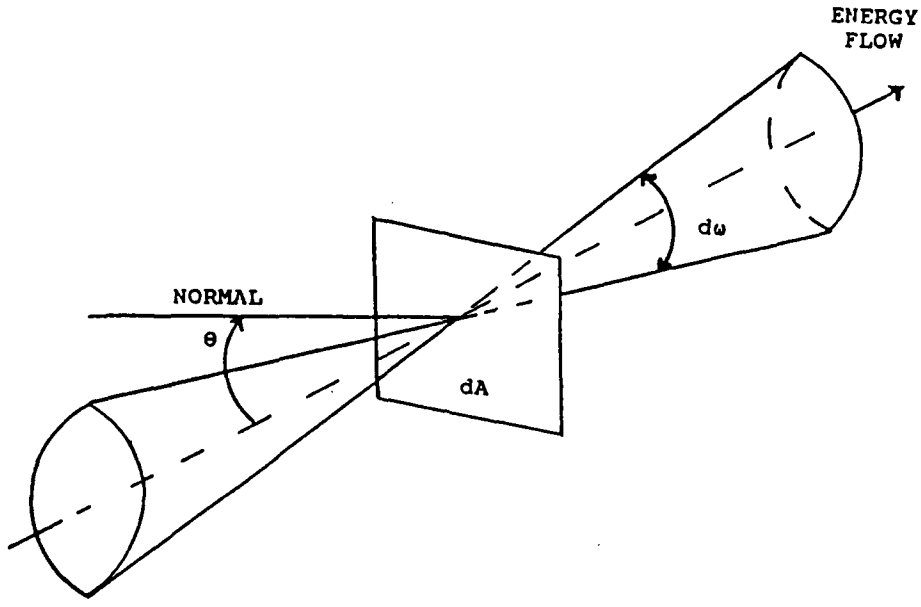

Figure IV-2. Radiative Energy Passing Through a Small Area.

source and the receiver, r, is much larger than the characteristic linear dimensions of either the source or the receiver. In fact, we must typically use some sort of antenna or telescope to collect radiation from a distant target, as shown schematically in Figure IV-3.

Such a telescope will be used in the paraxial limit [Ref. 15], so its Θ_R, as shown in Figure IV-1, will be ≈ 0. Since r » source dimensions, each radiating point on the source will see the telescope's entrance aperture subtending the same solid angle Ω. If that entrance aperture is a conventional

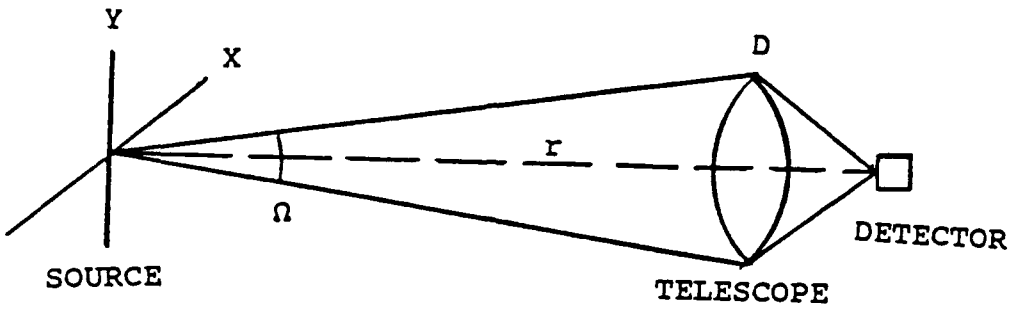

Figure IV-3. Collection of Radiation from a Distinct Target.

round antenna or optical objective of diameter D, then

$$\Omega \approx \frac{\pi D^2}{4r^2} . \qquad (2)$$

When a target is to be observed by remote, telescopic means, there is seldom an opportunity to control the spatial orientation of the target. We have to observe whatever face the source presents to us, and there is no way to judge the surface aspect angle Θ_s or the actual surface area of the target. This restricts us to measuring the projected <u>perspective</u> properties of the target. In effect, we are forced to treat the source as a two-dimensional object whose plane is oriented perpendicular to the line-of-sight. The angle Θ in Figure IV-2 and equation (1) is effectively zero as a result of this projection.

Combining these ideas, we see that a small, planar target source, like that shown in Figure IV-3, will illuminate the

telescope during a time interval dt, with an amount of energy given by

$$dE = I(x, y, \lambda)\left(\frac{\pi D^2}{4r^2}\right) dx\,dy\,d\lambda\,dt, \qquad (3)$$

where x and y are the two spatial coordinates specifying a location on the target. Most electro-optic detectors used in infrared observations respond to incident power rather than the accumulated deposition of radiant energy. Therefore, a more useful form of equation (3) would be

$$dP = I(x, y, \lambda)\left(\frac{\pi D^2}{4r^2}\right) dx\,dy\,d\lambda, \qquad (4)$$

in which dP is the radiant power entering the telescope. The total power received is obtained by integrating equation (4) over the target's spatial area A_s and the effective wavelengths over which the detector operates, giving

$$P = \frac{\pi D^2}{4r^2} \int_{\lambda}^{\lambda^2} \int\int_{A_s} I(x, y, \lambda)\, dx\,dy\,d\lambda \qquad (5)$$

The imaging spectroscopy problem is then stated succinctly: from remotely-sensed power measurements P, we wish to determine the functional form of $I(x,y,\lambda)$.

C. MULTIPLEXING VERSUS CONVENTIONAL SCANNING

In Chapter II the need for some sort of scanning approach in imaging spectroscopy was discussed. In summary, it was

argued that, since I is a function of three independent parameters and since 3-D detector systems do not exist, at least one of the three functional dependencies must be deduced by means of a scanning procedure. In that procedure, a sequence of detector signals, P, is recorded as one of the arguments of I is varied in successive steps.

For example, consider a conventional scanning grating monochromator spectrometer, which are common in many physics laboratories. A simple form of a monochromator might consist of an entrance slit, two lenses, a plane grating, and a detector, as shown in Figure IV-4.

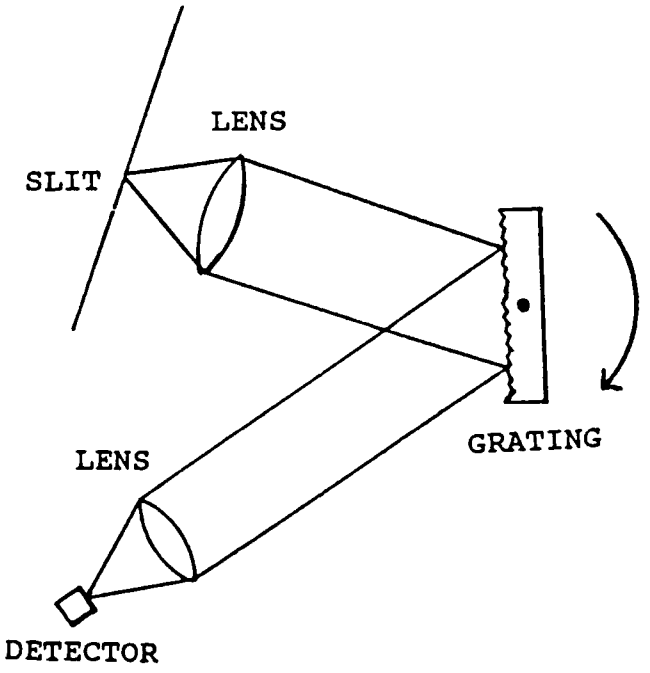

Figure IV-4. A Simple Form of a Monochromator.

The grating pivots about an axis that is parallel to the rulings. Each angular position of the grating sends a different narrow band of wavelengths toward the detector.

Therefore, the detected power might be represented as the sequence of values

$$P_i = \frac{\pi D^2}{4r^2} \int_{\lambda_j}^{\lambda_{j+1}} \int\int_A I(x, y, \lambda)\, dx dy d\lambda \qquad (6)$$

for {i = 0,1,2,...,n}. In this way, we can measure the wavelength dependence of I, but we lose spatial information because the monochromator averages the power flux over its entire entrance aperture.

By the same token, a conventional image scanner records a two-dimensional set of samples,

$$P_{ij} = \frac{\pi D^2}{4r^2} \int_{\lambda_i}^{\lambda_2} \int_{y_j}^{y_{j+1}} \int_{x_i}^{x_{i+1}} I(x, y, \lambda)\, dx dy d\lambda \qquad (7)$$

for {i = 0,1,2, ..., n}.

Typically, a scanner sequences through its scan parameters x and y in a raster pattern, much like a television camera. Of course, an imaging spectrometer system could be constructed by scanning in all three parameters: x, y, and λ. However, it was argued in Chapter II that such a straightforward sequential scanning approach is inherently wasteful of information. Power from only one narrow volume, dxdydλ, of the experimental parameter space falls on the detector at any one time.

Multiplexing is an efficient and elegant solution to this problem. For instance, in a Fourier transform spectrometer, the desired spectral information is not recorded directly.

A two-beam interferometer is used to encode the data as an interferogram [Refs. 16, 17, 18]. Equation (6) would be replaced by

$$P_i = \frac{\pi D^2}{4r^2} \int_{\lambda_1}^{\lambda_2} \iint_A I(x, y, \lambda) \cos(2\pi k_i \lambda)\, dx dy d\lambda . \qquad (8)$$

(Equation (8) is not strictly accurate, since an FTS actually encodes I as a function of reciprocal wavelength, or wavenumber. It is meant to express only the spirit of the Fourier technique in compact notation.)

Recovery of the desired I involves performing an inverse Fourier cosine transform on the P_i. What has been accomplished by this added complexity? Notice that the limits of integration of the wavelength interval, λ, span the entire spectrum at once. So, incident power is not wasted by looking at only one narrow range of wavelengths at a time.

D. IMAGE ENCODING AND DECODING WITH WALSH FUNCTIONS

For the remainder of this discussion, it will be convenient to have an abbreviation for a recurring quantity which we will use repeatedly. We shall define a spatial intensity distribution function I'(x,y), such that

$$I'(x, y) = \frac{\pi D^2}{4r^2} \int_{\lambda_1}^{\lambda_2} I(x, y, \lambda)\, d\lambda . \qquad (9)$$

In other words, I'(x,y) embodies those properties of the radiation field which characterize the spatial dependence of

the target's luminosity over the wavelength range $\lambda_1 \leq \lambda \leq \lambda_2$. Therefore, the detected power is simply expressed in analogy with equation (5) as:

$$P = \int\int_A I'(x, y)\, dxdy . \qquad (10)$$

An optical configuration that is capable of multiplexing the spatial intensity distribution is constructed quite simply. If one takes the stylized remote sensing apparatus of Figure IV-3 and extends it by adding a field aperture mask as shown below in Figure IV-5, that mask can provide the desired multiplexing.

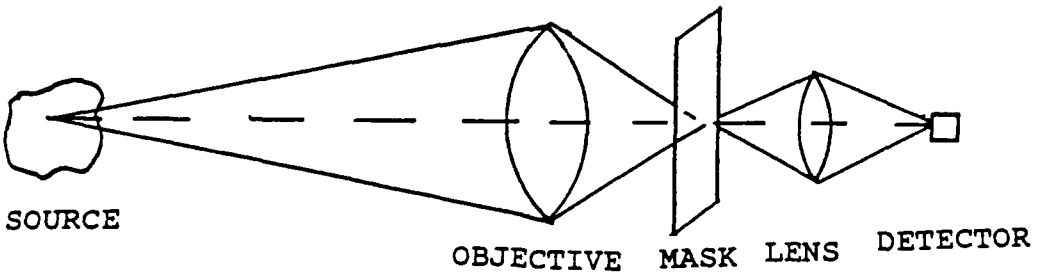

Figure IV-5. A Simple Multiplexing Configuration.

For example, suppose that the source target area A consists of a square region. The objective portion of the optical system will produce a scaled square image on the mask

plane. Decompose the image region into small, discrete image pixels in such a way that, if the pixel pattern could be imaged back upon the source itself, the re-imaged pattern would completely cover area A. Then equation (10) could be expressed as :

$$P = \int\int_{a_0} I'(x, y)\, dxdy + \int\int_{a_1} I'(x, y)\, dxdy + \ldots, + \int\int_{a_{n-1}} I'(x, y)\, dxdy \quad \textbf{(11)}$$

where a_0, a_1, ..., a_{n-1} represent the areas of the n individual pixels at the source.

Now, suppose that the mask is somehow capable of passing the power fluxes from some pixels with a plus sign and others with a minus sign. (How this is achieved will be discussed below.) Then we could design a mask such that each pixel corresponds to one of the sub-intervals of a Walsh function, as outlined in Chapter III. Of course, the number of pixels would be constrained to be $n=2^m$. This would require that n masks be used to encode n pixels. By sequencing through these masks, we could measure n multiplexed incident radiative power values P_j, which, according to equation (10), could be expressed as

$$P_j = \sum_{i=0}^{n-1} Wal(j, i) \int\int_{a_i} I'(x, y)\, dxdy . \quad \textbf{(12)}$$

Remember that we are trying to measure the integrals within equation (12). If we define $I'_i = \int\int_{a_i} I'(x, y)\, dxdy$, then clearly equation (12) becomes

$$P_j = \sum_{i=0}^{n-1} Wal(j,i) \times I_i . \qquad (13)$$

The P_j are fully multiplexed linear combinations of the I_i'. The form of equation (13) is that of a simple n-dimensional matrix equation. The matrix coefficients Wal(j,i) are either ± 1. Since the Walsh functions are orthogonal, the matrix Wal(j,i), a Walsh matrix, is also orthogonal. In fact, the matrix inverse of a Walsh matrix is simply 1/n times the transpose of the original Walsh matrix [Ref. 8]. The inversion of equation (13) to produce the pixel intensities I_i' is accomplished by multiplying the vector of P measurements by the inverse of the Walsh matrix.

How is the sequence of Walsh encoding masks actually constructed? In the instrumental configuration proposed by Davis, optical transmission and reflection will correspond to the two algebraic values that Walsh functions may assume. In this thesis project, proof-of-concept is emphasized, not optical efficiency. Therefore, we have used simple, photographically-produced opaque and transmitting masks. Encoding via this technique requires that each Walsh mask be accompanied by its complement, where the complement of +1 (opaque) is -1 (transmitting), and vice versa.

This is demonstrated as follows: Suppose that we have four pixels that we wish to encode, according to the matrix equation

$$\begin{pmatrix} P_0 \\ P_1 \\ P_2 \\ P_3 \end{pmatrix} = \begin{pmatrix} +1 & +1 & +1 & +1 \\ -1 & -1 & +1 & +1 \\ -1 & +1 & +1 & -1 \\ +1 & -1 & +1 & -1 \end{pmatrix} \begin{pmatrix} I_0 \\ I_1 \\ I_2 \\ I_3 \end{pmatrix}. \qquad (14)$$

If we use an opaque-transmitting mask instead, we measure

$$\begin{pmatrix} Q_0 \\ Q_1 \\ Q_2 \\ Q_3 \end{pmatrix} = \begin{pmatrix} +1 & +1 & +1 & +1 \\ 0 & 0 & +1 & +1 \\ 0 & +1 & +1 & 0 \\ +1 & 0 & +1 & 0 \end{pmatrix} \begin{pmatrix} I_0 \\ I_1 \\ I_2 \\ I_3 \end{pmatrix}. \qquad (15)$$

With the complementary mask, we measure

$$\begin{pmatrix} R_0 \\ R_1 \\ R_2 \\ R_3 \end{pmatrix} = \begin{pmatrix} 0 & 0 & 0 & 0 \\ +1 & +1 & 0 & 0 \\ +1 & 0 & 0 & +1 \\ 0 & +1 & 0 & +1 \end{pmatrix} \begin{pmatrix} I_0 \\ I_1 \\ I_2 \\ I_3 \end{pmatrix}. \qquad (16)$$

Now, if we combine the Q and R vectors by subtraction,

$$\begin{pmatrix} Q_0 \\ Q_1 \\ Q_2 \\ Q_3 \end{pmatrix} - \begin{pmatrix} R_0 \\ R_1 \\ R_2 \\ R_3 \end{pmatrix} = \begin{pmatrix} +1 & +1 & +1 & +1 \\ 0 & 0 & +1 & +1 \\ 0 & +1 & +1 & 0 \\ +1 & 0 & +1 & 0 \end{pmatrix} \begin{pmatrix} I_0 \\ I_1 \\ I_2 \\ I_3 \end{pmatrix} - \begin{pmatrix} 0 & 0 & 0 & 0 \\ +1 & +1 & 0 & 0 \\ +1 & 0 & 0 & +1 \\ 0 & +1 & 0 & +1 \end{pmatrix} \begin{pmatrix} I_0 \\ I_1 \\ I_2 \\ I_3 \end{pmatrix}$$

$$\begin{pmatrix} Q_0-R_0 \\ Q_1-R_1 \\ Q_2-R_2 \\ Q_3-R_3 \end{pmatrix} = \begin{pmatrix} +1 & +1 & +1 & +1 \\ -1 & -1 & +1 & +1 \\ -1 & +1 & +1 & -1 \\ +1 & -1 & +1 & -1 \end{pmatrix} \begin{pmatrix} I_0 \\ I_1 \\ I_2 \\ I_3 \end{pmatrix}. \qquad (17)$$

This approach is identical in its consequences to the "ideal" multiplexed apparatus described by Equation (14). There is a price to pay, however. To encode n pixels, 2n measurements (nQ's and nR's) must be made. Nevertheless, the simplicity of

this approach has made it the technique of choice for this thesis project.

V. EXPERIMENTAL PROCEDURE

A. GENERAL APPROACH

1. Outline

The goal of this thesis has been to demonstrate that the proposed methods for encoding and decoding images are conceptually sound. To do this, masks were created from the patterns shown in Figure III-2. They were used to encode a variety of targets. The corresponding Walsh functions were used to decode the data and to recreate a reasonable facsimile of the image on a computer CRT. An outline of the major steps taken to achieve this thesis goal are listed here and described in this chapter.

COMPUTER GENERATION OF WALSH-CODED MASK PATTERNS

PHOTOGRAPHIC TECHNIQUES USED TO CREATE THE MASKS

OPTICAL ENCODING PROCEDURES

DECODING

IMAGE RECONSTRUCTION AND DISPLAY

SIMULATION

2. Computer configuration

a. Hardware

An IBM Personal System/2 Model 70 386 personal computer was used for all programs. The prototype encoding

masks were drawn on a Hewlett-Packard model 7550A pen plotter connected to the IBM computer via a conventional 9600 baud RS-232 interface. The decoded images were plotted on an IBM model 8513 VGA color monitor.

b. Software

The Pascal programming language was selected for most of the project's program development tasks, based on the author's familiarity with that language. An additional contributing factor in that choice of language was the ready availability of the IBM personal computer version of Turbo Pascal 4.0 software (Borland International), and its compatibility with the plotter. Microsoft C 5.1 was used to develop the image display program because that language is equipped with an efficient library of routines to control the VGA monitor. All programs are explained herein and included in the appendices.

B. COMPUTER GENERATION OF WALSH-CODED MASK PATTERNS

1. Kronecker Product Method

For an initial attempt, this project used the 8 x 8 mask pattern shown in Figure III-2. A 2 x 2 pattern and a 4 x 4 pattern would provide insufficient image resolution; a 16 x 16 mask would be too cumbersome to work with at this stage. However, the mask generation software was written to accommodate mask geometries of other resolutions, for flexibility of future use. As a first step, a computer

program was written to generate the first eight sequency-ordered Walsh functions, Wal(0,t) - Wal(7,t) as shown in Figure III-1. The function values were streamlined from ±1 to simply +/- signs. This program utilized a recursive Kronecker product method to compute these functions, beginning with the simplest basis set of two Walsh functions: Wal(0,t) and Wal(1,t). These functions, in simplified sign form for each of their sub-intervals are:

$$\text{Wal}(0,t) = \quad + \; +$$

$$\text{Wal}(1,t) = \quad - \; +.$$

Alternatively, we can express the same concept in 2 x 2 Walsh matrix as:

$$\begin{bmatrix} + & + \\ - & + \end{bmatrix}.$$

Using the Kronecker method, each element of this array is used to multiply each element in the same array in the following manner to produce a 4 x 4 array of signs:

$$\begin{bmatrix} - \times \begin{bmatrix} + & + \\ - & + \end{bmatrix} & + \times \begin{bmatrix} + & + \\ - & + \end{bmatrix} \\ - \times \begin{bmatrix} + & + \\ - & + \end{bmatrix} & + \times \begin{bmatrix} + & + \\ - & + \end{bmatrix} \end{bmatrix} = \begin{bmatrix} + & + & + & + \\ - & + & - & + \\ - & - & + & + \\ + & - & - & + \end{bmatrix}.$$

The multiplication rules used are : "+" x "+" = "+"

"+" x "-" = "-"

"-" x "-" = "+"

To get the first eight Walsh functions, this procedure is repeated using the first 2 x 2 matrix to multiply each element in the 4 x 4 matrix to produce an 8 x 8 matrix of signs:

$$\begin{bmatrix} + \times \begin{bmatrix} + & + & + & + \\ - & + & - & + \\ - & - & + & + \\ + & - & - & + \end{bmatrix} & + \times \begin{bmatrix} + & + & + & + \\ - & + & - & + \\ - & - & + & + \\ + & - & - & + \end{bmatrix} \\ - \times \begin{bmatrix} + & + & + & + \\ - & + & - & + \\ - & - & + & + \\ + & - & - & + \end{bmatrix} & + \times \begin{bmatrix} + & + & + & + \\ - & + & - & + \\ - & - & + & + \\ + & - & - & + \end{bmatrix} \end{bmatrix} = \begin{bmatrix} + & + & + & + & + & + & + & + \\ - & + & - & + & - & + & - & + \\ - & - & + & + & - & - & + & + \\ + & - & - & + & + & - & - & + \\ - & - & - & - & + & + & + & + \\ + & - & + & - & - & + & - & + \\ + & + & - & - & - & - & + & + \\ - & + & + & - & + & - & - & + \end{bmatrix}.$$

This 8 x 8 array represents the first eight Walsh functions, but they are not in sequency order nor are they of the same (Harmuth) phase as the 2 x 2 basis with which we started. So, the computer program sorts the functions into sequency order and then changes the phase of some of the functions, as necessary. Harmuth phasing was used in Figure III-1, wherein the value of the function just to the right of the mid-point of the interval is always positive. Below, the functions are arranged in increasing sequency order, as can be verified by counting the number of times the sign changes along each row:

```
+ + + + + + + +
- - - - + + + +
- - + + + + - -
- - + + - - + +
+ - - + + - - +
- + + - + - - +
+ - + - - + - +
- + - + - + - +   .
```

Since the first sign to the right of the mid-point (the fifth sign from the left) in some of these functions is not a "+" sign, those functions are multiplied by a "-" sign to correct the phase. The result is that the program generates the first eight sequency-ordered Walsh functions with the desired Harmuth phase. Compare Figure III-1 with the functions labeled below:

```
WAL(0,t)    + + + + + + + +
WAL(1,t)    - - - - + + + +
WAL(2,t)    - - + + + + - -
WAL(3,t)    + + - - + + - -
WAL(4,t)    + - - + + - - +
WAL(5,t)    - + + - + - - +
WAL(6,t)    - + - + + - + -
WAL(7,t)    + - + - + - + -    .
```

2. Product Functions

These Walsh function sign patterns were then written into two identical disk data files: "HDATA.TXT" and "VDATA.TXT", which correspond to the eight one-dimensional Walsh functions shown along the horizontal axis and also along the vertical axis in Figure III-2. The two-dimensional Walsh encoding masks that we wished to generate were simply algebraic products of the one-dimensional vertical and horizontal functions. In other words, a given mask is, in effect, a multiplication table of horizontal and vertical Walsh functions. Therefore, another computer program was written to calculate the products. It multiplied the 64 signs in the first data file by the same 64 signs in the second file to produce a 64 x 64 array of values. These values were written into a separate data file called "PDATA.TXT". They are shown in Figure V-1. These two programs were later combined to form the single program called "WALSHPRODUCTS" listed in Appendix A.

3. Plotting

a. General Description

The values stored in the file "PDATA.TXT" were then read into another program, called "PRODUCTPLOTS", which performed the actual mask plotting. Appendix B lists this plotting routine. This program uses standard commands from the Hewlett-Packard Graphics Language (HP-GL) [Ref. 15]. The

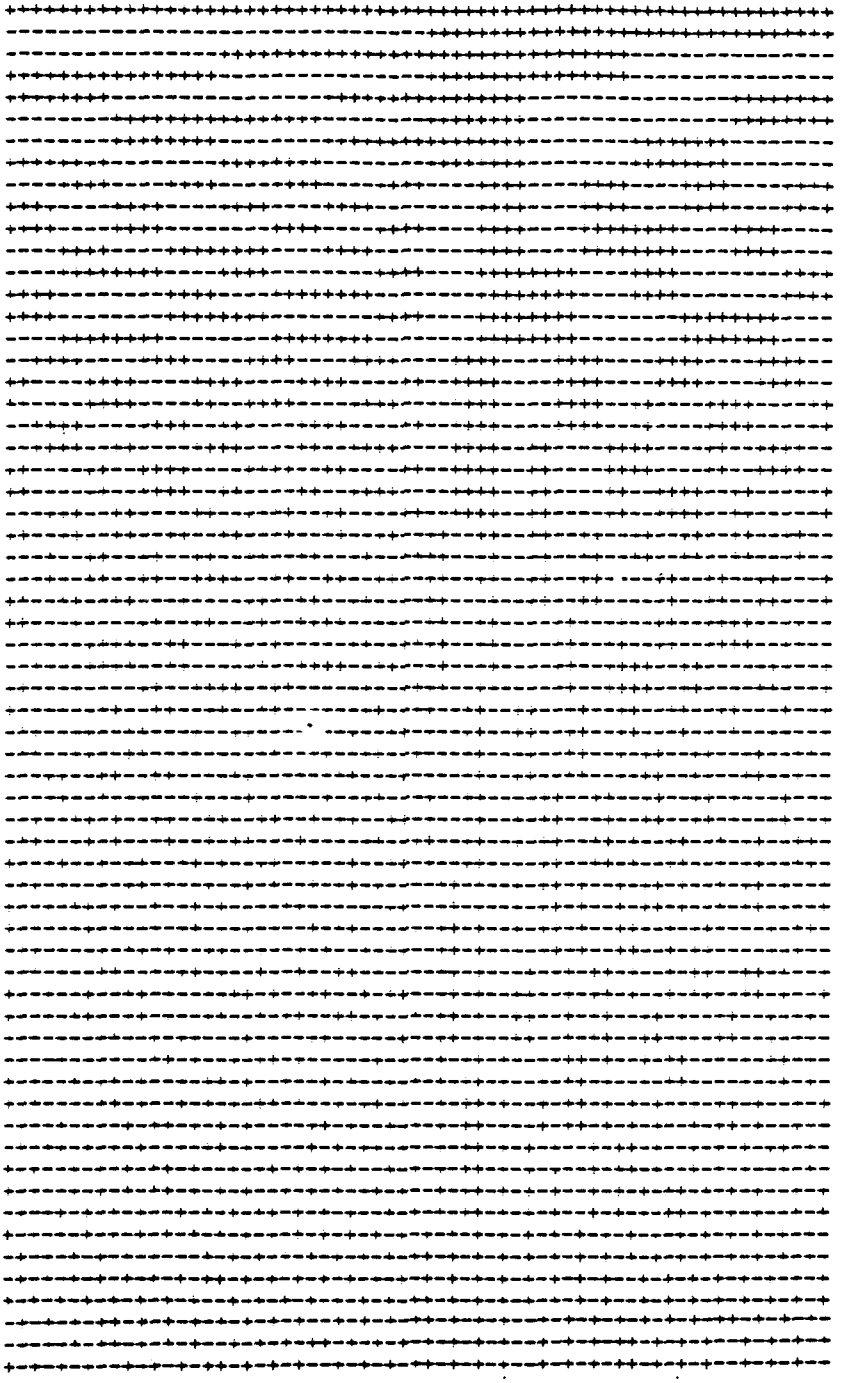

Figure V-1. Contents of File "PDATA.TXT": a 64 x 64 Array of +/- Signs Created by the Program "WALSHPRODUCTS".

plots were generated using the Hewlett-Packard 7550A Graphics Plotter interfaced with the computer.

b. HP-GL Instructions

HP-GL Instructions are codes that access the plotter's graphics functions and consist of a two-letter mnemonic followed by numerical parameters. To program the plotter, HP-GL instructions can be included in appropriate output statements from any programming language that outputs literal strings. Turbo Pascal was chosen for uniformity with the other programs. Programming the plotter was accomplished by creating a separate file called "Plotfile" and using Pascal "write" and "writeln" commands to load HP-GL instructions into this file.

The HP-GL instructions allow both absolute and relative coordinate addressing to be used. The absolute system and its associated mnemonic instructions were used for positioning the pen at the desired starting position on the paper. The relative system proved useful for offsetting coordinates in a nested loop structure to plot the patterns. Parameters which follow the HP-GL instructions are given as integer values, and usually consist of the X and Y coordinates of either the fixed or the relative system, in plotter units.

c. Plotting Procedure

The plotting procedure "PRODUCTPLOTS" consists of nested loops of instructions to plot a mask of 64 separate

"windows", each consisting of 64 filled or unfilled "blocks", or pixels. If the value read from the file "PDATA.TXT" is a "+" sign, the corresponding block of that mask is filled; otherwise it is left blank. The blocks and windows are filled in a manner that reproduces the pattern shown in Figure III-2. The contrast-complement ("negative") of this mask was easily created by instructing the plotter to fill a block if the value read from the data file was a "-" sign, vice a " +" sign. The plots are shown in Figures V-2 and V- 3. These figures have been photo-copied and reduced to fit in this document. Their dimensions are not those of the originals, as stated below.

d. Dimensions

Each square pixel block measures approximately 100 plotter units (2.5 mm) per side and, when filled, is done so using Fill-Type 1, a solid bi-directional filling pattern. Each 8 x 8-block window measures 800 plotter units (20 mm or 2 cm) per side; window spacing is 150 plotter units (3.75 mm).

e. Additional Parameters

In addition to the parameters used to program the plotter, two plotter front panel settings used for best results were found to be: (1) Pen Speed = 10 (Slowest) and (2) Pen Force = 8 (Heaviest).

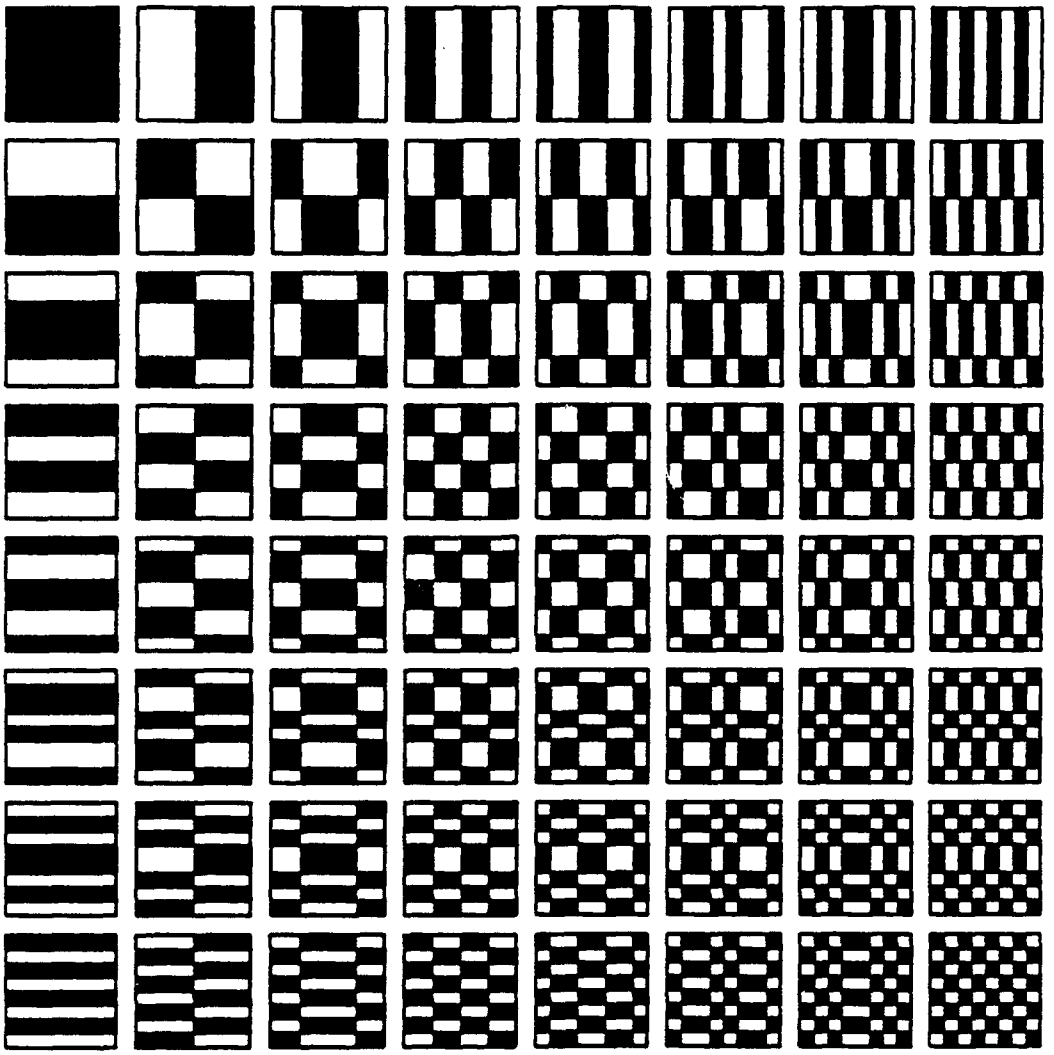

Figure V-2. Plot of Walsh Function Products Produced by the Program "PLOTPRODUCTS".

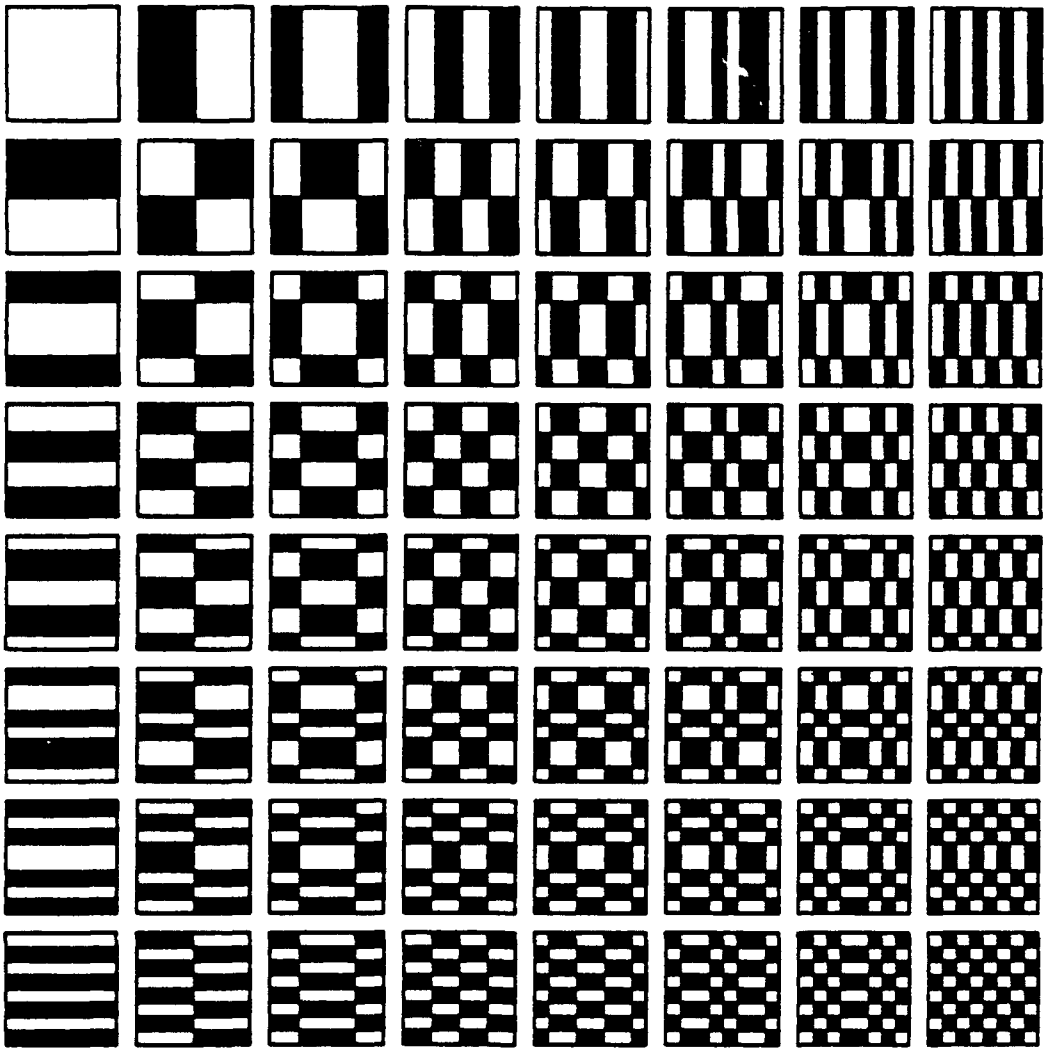

Figure V-3. Plot of the Contrast-Complement of the Walsh Function Products Shown in Figure V-2.

Also, Hewlett-Packard brand A-size (8 ½" x 11") non-glossy plotter paper and a black fiber-tip paper plotter pen with narrow line width (0.3 mm) were used in accordance with the manufacturer's recommendations.

f. Plotting Problems

Many attempts were made to create precision patterns with the proper size and spacing between windows to fit on a sheet of plotting paper. The most difficult problem encountered was trying to compensate for the finite pen thickness. This caused an undesired distortion in the size of blocks as ink from a filled block spread over into adjacent unfilled blocks. Different pen speed and pen force values caused the amount of spreading to change. To minimize distortion, the plotter was instructed to fill an area somewhat smaller than the final desired area (98 vice 100 plotter units per side). As the ink spread, the entire area was filled.

Another distortion caused by the pen thickness was the ink bleeding over into unfilled areas along the border, or frame, of each mask window. This adverse effect was abated by instructing the plotter to move five plotter units beyond the edge of the finished window.

C. PHOTOGRAPHIC TECHNIQUES USED TO CREATE THE MASKS

1. Photographing the plots

a. Camera

To create masks on transparent/opaque material in the desired patterns, photographs of each of the two original plots, depicted in Figures V-2 and V-3, were taken. The desired masks were then simply the resulting negatives. A Graflex Speed Graphic camera, shown in Figure V-4, was available from the NPS Optics Laboratory and mounted on a stable copy table. To keep the camera as still as possible, a remote shutter release cable was used. This camera had an OPTAR brand copy lens, adjustable from f/4.5 - f/32.

b. Film

A local camera shop supplied Kodalith Ortho film 2556 type 3, manufactured by Kodak. This black and white film is rated as extremely high-contrast and is recommended for making line and half-tone negatives and positives. The film was used in 4" x 5" sheet form. The camera's film holder could accommodate two sheets at a time.

c. Illumination

The paper plots shown in Figures V-2 and V-3 were individually placed on the copy stand 35 cm below the outer casing of the camera lens. Uniform illumination was provided by two Sylvania 150-Watt flood lamps mounted on arms, as shown in Figure V-4.

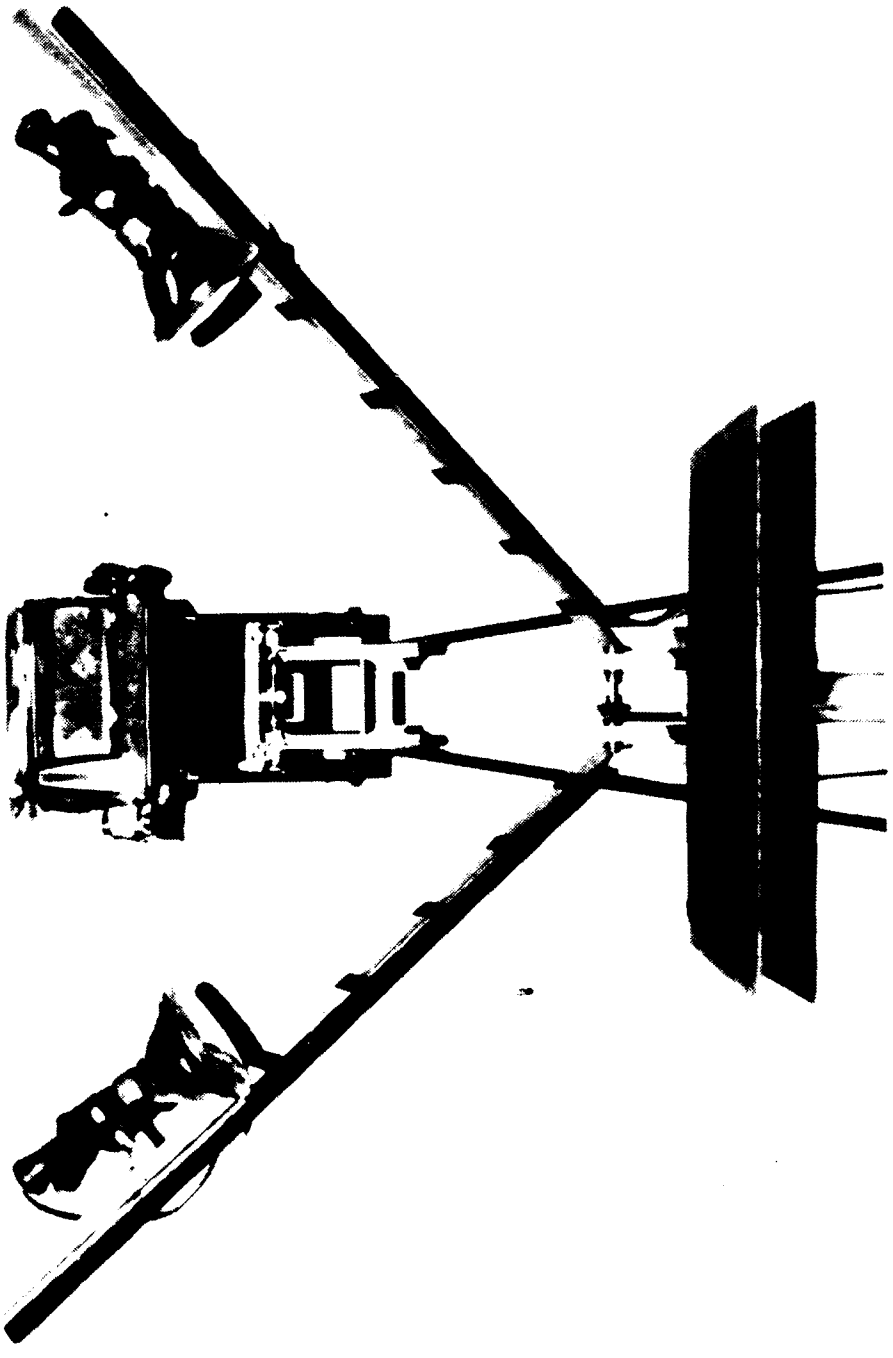

Figure V-4. Photograph of Camera Mount.

d. Camera Settings

Determining the proper camera settings took several trial exposures. The plots were focused by adjusting the lens- film spacing. An f-number of f/22 was set and the film was exposed for various lengths of time, ranging from 0.1 to 20 seconds. An optimum exposure time was found to be 2.0 seconds. Since the camera's timed shutter release could only go as slow as 1.0 second, it was necessary to time the exposure with a stopwatch.

2. Developing the Negatives

a. Darkroom Procedures

Once the photographs were taken, the film was developed in a darkroom. After removal from the film holder, the film was placed in a bath of Kodak D-19 developer for five minutes. It was then transferred to a stop bath solution of Kodak Indicator in water (1:128) for about 30 seconds, followed by immersion in Kodak Kodafix and water (1:3) for about 30 seconds. All three immersion steps were performed at room temperatures of about 20 degrees Celsius. After these standard chemical treatments, the film was rinsed in cold tap water for 30 minutes, then hung to dry. These times were derived after several trial-and-error experiments. The primary criterion in evaluating these trials was image contrast. The resulting negatives became the actual masks and are shown together in Figure V-5.

b. Masks

The patterns on the mask were photo-reduced in size from the plots to fit within the 4" x 5" area of the film. Each mask window is approximately 9 mm per side. It should be noted that the photographic negative of each mask was the contrast-complement of the plot that was photographed. These masks were labeled Mask #1, with the transparent window located in the upper left hand corner, and Mask #2, with the opaque window in the same position. Notice that the frame around each window, which was a black border on the plot, has become a transparent border on the mask; a significant area where stray, unencoded light could pass through.

D. OPTICAL ENCODING

1. General Description

Once the set of two masks was finished, the next step was to encode an image as described in Chapter IV. An illuminated pattern was projected through a rectangular aperture and an optical chopper onto one window of a mask and then onto the face of a photodetector. Figure V-6 shows the initial physical arrangement of components mounted on an optical bench. In order to avoid interference from stray light sources, all measurements were performed in a darkened room. Several early attempts at encoding proved to be unsuccessful due to problems with mechanical stability, detector non-linearities, and sensitivity to electrical noise. The

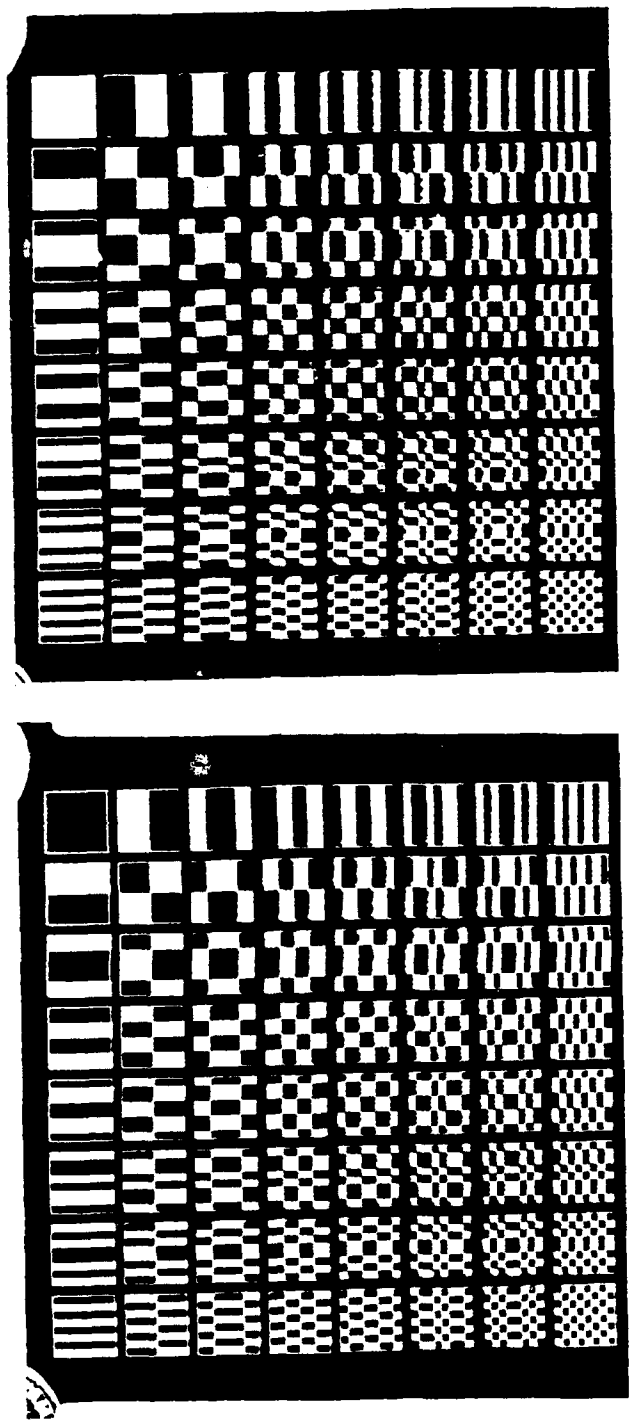

Figure V-5. The Two Walsh Function Encoding Masks on Photographic Film. Top: Mask #1. Bottom: Mask #2.

procedures outlined below were found to be adequate to yield a recognizable decoded image.

2. **Components**

a. Object Pattern Selection

As a first attempt at imaging, a black pattern on a white background was selected as the object. An eye chart with various letters of the alphabet was a convenient source of patterns. A photocopy of a section of an eye chart was made, then mounted on white paper and hung from a ring stand.

b. Illumination

The letter was uniformly illuminated by a laboratory lamp aimed at the letter from the front. This lamp was a General Electric brand 18 amp/6 volt Microscope Illuminator bulb mounted in a collimator, powered by 110 volt line source through a AC-to-DC transformer. This light was then projected through a 1½" diameter thin, positive lens with a focal length of 15 cm onto the transparent window of an aperture. Here, the image was reduced in size and inverted.

c. Aperture

A square aperture of the same dimensions as the square windows on the masks was created by plotting and photographing a third mask with only a single window. This was accomplished by altering the plotting program "PRODUCTPLOT" to read only the first row of "PDATA.TXT" and then plot just the first window of Mask #2, which is

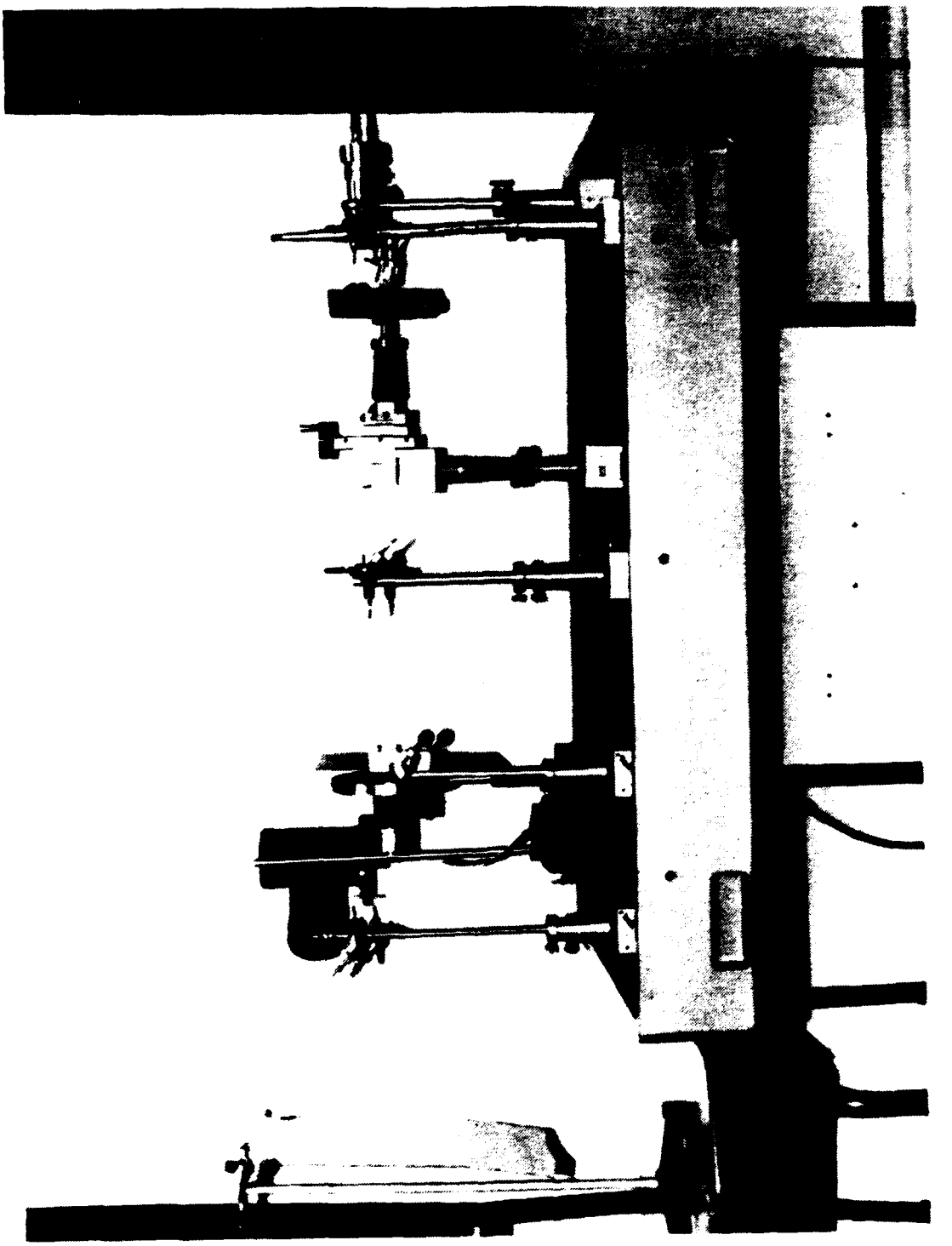

Figure V-6. Inital Physical Arrangement of Encoding components.

completely opaque. When this mask was later photographed and developed, the negative resulted in a fully transparent window surrounded by opaque film material.

d. Mask Positioning

The light emanating from the aperture was focused through another 1½" diameter thin, positive lens, this one with a focal length of 10 cm, onto the face of the mask. The mask as mounted in another film holder for our Graflex camera, with a 4" x 5" glass plate behind it to hold it in place. Masks were moved transversely and vertically in the vertical plane, at a fixed horizontal distance between the object and the detector, until an entire window was fully illuminated. Crude, manually-operated X and Y positioners with screw drives were adapted to translate the masks.

e. Detector

The light which passed through each mask window was optically encoded by the two-dimensional Walsh function pattern. It then passed through a third 1½" diameter thin, positive lens with a focal length of 5 cm and focused onto a photodiode detector, model UDT-PIN 10DP 145-3, manufactured by United Detector Technology. This photovoltaic zero-bias photodiode is designed with an active area of 1.0 cm^2 and is optimized for a spectral range of 350 to 1100 nm, as shown in Figure V-7. The detector converted the incident light intensity into an electric current.

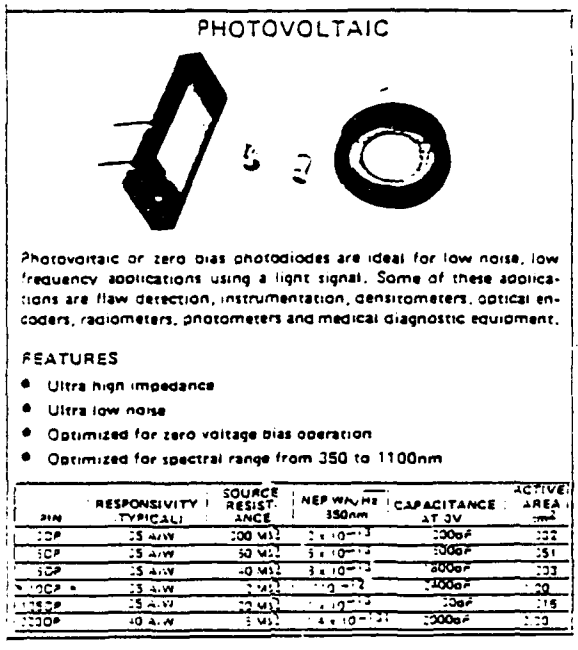

PHOTOVOLTAIC

Photovoltaic or zero bias photodiodes are ideal for low noise, low frequency applications using a light signal. Some of these applications are flaw detection, instrumentation, densitometers, optical encoders, radiometers, photometers and medical diagnostic equipment.

FEATURES

- Ultra high impedance
- Ultra low noise
- Optimized for zero voltage bias operation
- Optimized for spectral range from 350 to 1100nm

PIN	RESPONSIVITY TYPICAL	SOURCE RESISTANCE	NEP W/√Hz 350nm	CAPACITANCE AT 3V	ACTIVE AREA
[illegible]DP	.25 A/W	100 MΩ	[illegible]	250pF	[illegible]
[illegible]DP	.25 A/W	50 MΩ	[illegible]	500pF	[illegible]
[illegible]DP	.25 A/W	40 MΩ	[illegible]	600pF	[illegible]
[illegible]DP	.25 A/W	[illegible]	[illegible]	2400pF	[illegible]
[illegible]DP	.25 A/W	[illegible]	[illegible]	[illegible]pF	[illegible]
[illegible]DP	.40 A/W	[illegible]	[illegible]	[illegible]pF	[illegible]

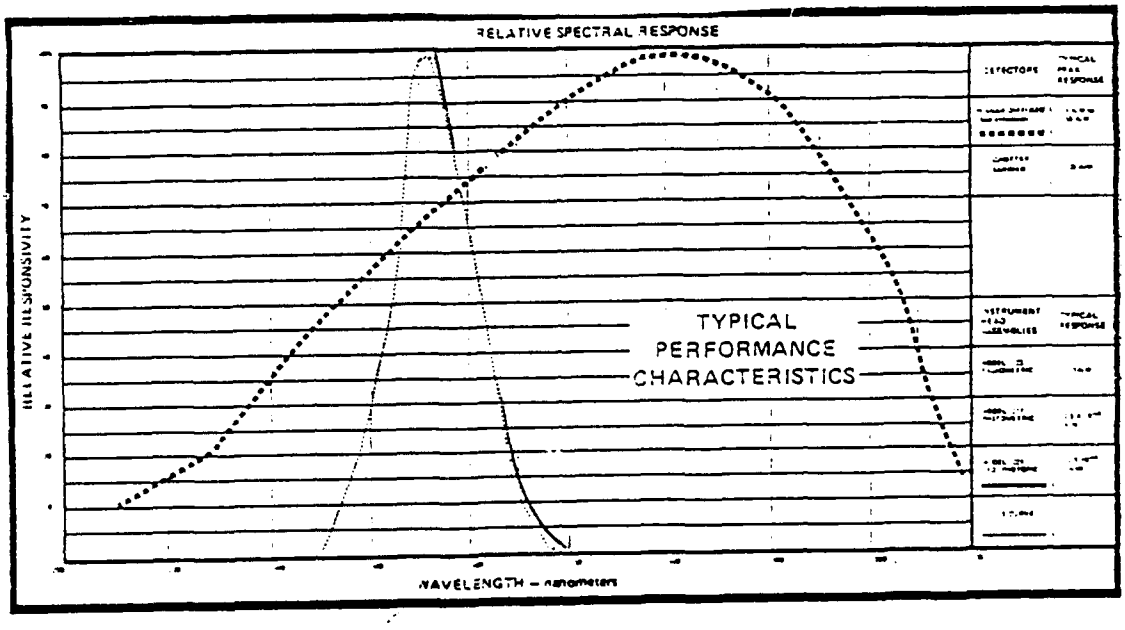

Figure V-7. Photodetector and its Spectral Range.

f. Background Light (Noi[illegible] Suppression

A variable speed optical chopper, model CTX-534 manufactured by Laser Precision Corporation, modulated the light at a frequency of 100 Hertz. The reference signal from the chopper controller and the chopped, encoded light signal were fed into a model 121 Lock-In Amplifier manufactured by Princeton Applied Research. The lock-in acted essentially as a filter with an extremely narrow bandwidth tuned to the frequency of the chopper. It rejected all signals which were not of the same frequency or of the same phase as the modulated signal, thereby suppressing all unwanted noise. Figure V-6 show[illegible]e location of the optical chopper.

g. Digital Multimeter

The lock-in amplifier was equipped with an analog voltmeter to monitor its output, however an illuminated digital multimeter was much easier to read in the darkened laboratory. A model 177 Microvolt Digital Multimeter (DMM) manufactured by Keithley Corporation was connected to the output of the lock-in amplifier to display the relative light intensity.

h. Oscilloscope

A dual channel oscilloscope, model 2336 YA manufactured by Tektronix Corporation was used to display the chopper reference signal and the modulated optical signal and to verify the chopper frequency.

3. Initial Optical Alignment Procedure

The optical encoding components were mounted on an optical bench for ease of alignment. After the bench components were in line, the next step was to illuminate a blank sheet of paper and move the second lens and aperture so that the square beam of light out of the aperture exactly filled the transparent window of Mask #1. Next, it was necessary to position the detector for a maximum value readout on the DMM. Once this optimization was completed, the target object had to be positioned so that it was within the aperture and it was focused on the mask window. This procedure was best accomplished by two people, with one person adjusting optical components and the other always doing the visual alignment verification so that the same standards were maintained every time a different object was used.

Because of the finite plotter pen thickness on the original plots, which resulted in transparent borders around each mask window, it was necessary to check the alignment of each aperture so that windows did not have light projecting through these borders. (The distinct border is not evident on the fully transparent window of Mask #1, so other windows were positioned for this check.) These borders could have been eliminated by not framing each window when plotting. However, these borders proved to be useful as a guide when aligning the windows during each measurement. Once the initial alignment of the aperture was verified, the mask was translated until no

light was visible around the border of a window. This was an effective method of visually ensuring conformity in each measurement procedure, despite the unrefined nature of the apparatus.

4. Recording the Data

a. Relative Values

After each mask window was properly positioned, the Light Intensity Measurement Data (LIMDATA), in mV DC, was recorded by hand on a pre-printed form. Generally, these values ranged between zero and minus ten mV DC and were read to the nearest 1/100 th of a mV. The sign and the absolute voltage values were not of concern, but rather the relative values resulting from the different windows. Any amplification performed by the lock-in was not important as long as each recorded value was equally treated. Recorded values, therefore, ignore the algebraic sign of the signal.

b. Duration

With a little practice, it took an average of about 45 seconds to move each succeeding window into position, another 15 seconds for the lock-in amplifier to provide a stable output to the DMM, and about five seconds to write the data in the proper box. This worked out to over an hour per mask, or more than two hours for a complete set of data for each object.

There were several problems associated with these long sessions, leading to probable, but unquantifiable inconsistencies in the numerical data. One was that the electrical power source for the target illumination was not stable so fluctuations in light intensity of a few hundredths of a millivolt were common. Another problem was reduced precision in mask window alignment. This was caused by moderate eye fatigue. Although the alignment procedures described above were repeated for each measurement, the experimenter had to look at the mask window from various angles from behind the detector instead of directly at it because the detector blocked direct line-of-sight observation. Continuous demand for the eye to adjust to dark and light conditions while scanning the pattern from different perspectives undoubtedly reduced the alignment accuracy during the course of data collection.

E. COMPUTER DECODING

1. Difference values

Using the recorded data, the values from each window on Mask #2 were manually subtracted from the values from the corresponding positions on Mask #1 in accordance with the approach discussed in Chapter IV. These "Difference" values were recorded on a separate table and then typed into the Turbo Pascal file "LIMDATA.TXT" as a column of 64 values.

2. Mathematical transformation

a. Filling arrays

The program "IMAGE.PAS" listed in Appendix C was used to decode these Difference values. These values were read from the file "LIMDATA.TXT" and written into an array. The 64 x 64 array of +/- signs used to make the mask patterns and encode the light were read from the file "PDATA.TXT", converted into values of +1/-1, and stored in another array.

b. Matrix Multiplication

The first array of measured difference values, a 1 x 64 matrix, was then multiplied by the transpose of the encoding array, a 64 x 64 matrix. The resulting 1 x 64 matrix of decoded values was then written to the file "IMAGDATA.TXT", to be used by another program that displayed the reconstructed image on the computer CRT screen.

F. IMAGE RECONSTRUCTION AND CRT DISPLAY

The data in "IMAGDATA.TXT" were then used to reconstruct the image on the computer CRT monitor. A user-defined gray scale could not be implemented with Turbo Pascal 4.0. A separate program written by Davis, using Microsoft C 5.1, was used. This program, called "WALSQR", is listed in Appendix D. This program offers the user a choice of gray scales composed of 2,4,8, or 16 levels. It instructs the monitor to divide up the display screen into 64 equal-sized squares, or pixels. It then reads all the values from "IMAGDATA.TXT" and divides

this range by the number of levels selected. For each value read from "IMAGDATA.TXT", the program computes its appropriate level of gray, from white to black, and paints the corresponding pixel on the screen. The resulting image should be a reasonable facsimile of the originally encoded object if the entire encoding/decoding technique works as conceived.

G. SIMULATION

In order to test the decoding and image display programs, simulation of an object's image was performed using artificially encoded, idealized data. These simulations provided an indication of what, theoretically, should result from actual experiments under ideal conditions.

For the strictly black and white objects this simulation was very simple to do. A facsimile of each object was drawn on graph paper in an 8 x 8 window of blocks; a filled block was given the value of +1 while an unfilled block was given a value of zero. These 64 values were read from top to bottom, left to right, then typed into the "IMAGDATA.TXT" file, just as if they were the decoded values from the program "IMAGE.PAS". The "WALSQR" program was then run using any gray scale level since the values were all known to be either +1 or 0. The images were all sharp black and white reproductions and provided a baseline for comparing the experimental results, as detailed in the next chapter.

VI. RESULTS

A. INITIAL RESULTS

1. First Attempt

The first object that we attempted to image was the letter "P" copied from a conventional eye chart. The decoded image did not resemble the original object at all. We noticed that the raw encoded data did not show pronounced variations, or modulation efficiency, from one encoding mask to another. It was thought that a significant amount of near-infrared radiation was leaking through the ostensibly opaque mask regions, thereby saturating the detector. (As Figure V-7 shows, the PIN detector is sensitive to near-IR radiation.) However, inserting an IR blocking filter did not improve the modulation efficiency, so the IR leakage idea was rejected.

Another possible reason for the disappointing results was that the letter "P" was not a good choice due to its shape. With only an 8 x 8 pixel image area, it would be inherently difficult to encode efficiently an object with highly curved contours, such as those on the letter "P". Therefore, we decided to try an object with more rectilinear features.

2. Second Attempt

The letter "Z", also copied from the eye chart, was substituted for the letter "P" and the experiment was run again. As before, the decoded image did not resemble the original object. However, an important discovery was made when examining the raw data. Because the letter "Z" is symmetric about one of its diagonals, the value for the fully transparent window in Mask #1 (see Figure V-5) was expected to be twice the value for the first window to the right and the first window below, since these windows should have admitted exactly half of the object's flux to the detector. This was not the case. When a blank, uniformly illuminated sheet of white paper was substituted for the object, the observed signal levels were not at all compatible with a linear response from the optical detector. This non-linear response was traced to the high output impedance of the detector, which was measured to be 1.2 Meg-ohm, far to high to drive the lock-in amplifier without distortion.

As an additional source of potential problems, it was also noticed that the second lens was not large enough for the image to pass through without some vignetting. In addition, we observed that the lock-in amplifier was erratic. Although conventional wisdom would dictate that elimination of one problem source at a time as sound scientific procedure, a major revision of our approach, correcting all these perceived deficiencies at once, was deemed necessary. A trans-impedance

amplifier circuit [Ref. 20] was designed and built to correct the problem of detector non-linearity. A new arrangement of components, including object backlighting, a larger lens, a more stable optical bench, and a different lock-in amplifier, was substituted to correct the other problems.

3. Modifications

a. Trans-impedance Amplifier Circuit

The trans-impedance amplifier circuit, shown in Figure VI-1, was inserted between the output of the detector and the input to the lock-in amplifier. The circuit was designed around a low-power enhanced junction field effect transistor operational amplifier (JFET OP AMP) type TL031CP, manufactured by Texas Instruments. This op amp was packaged as a single device on a standard eight-pin integrated circuit. Data and a pin-out diagram for this device were reproduced from the manufacturer's data book [Ref. 21], and can be found in Figure VI-2.

A feedback resistor, a voltage divider, and power supply filter capacitors were connected with the chip on an Analog/Digital Proto-Board brand breadboard, model PB-503, manufactured by Global Specialties. The breadboard with the electronic components installed is shown in Figure VI-3. BNC-type connectors on the breadboard facilitated the input and output connections of this circuit to the other components of the system.

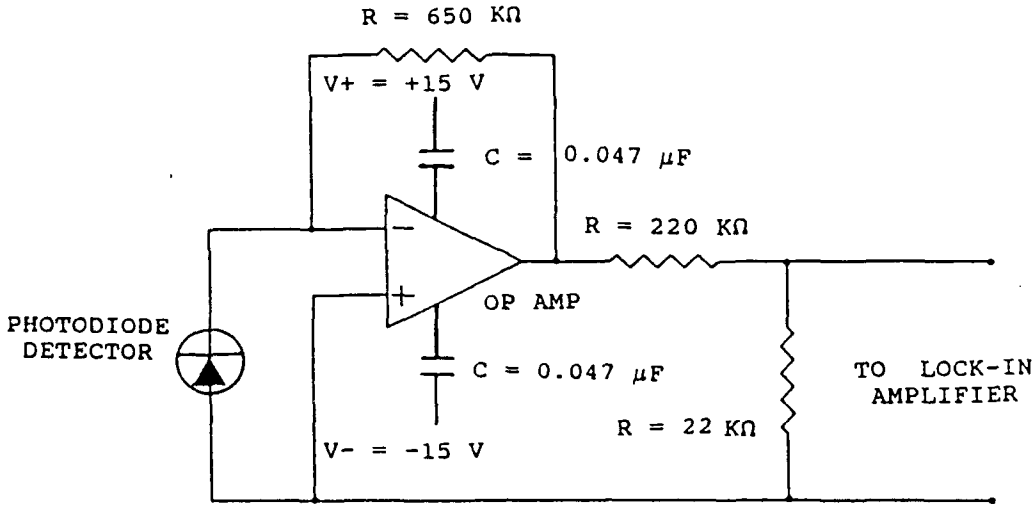

Figure VI-1. Trans-impedance Amplifier Circuit.

b. Backlighting

The light was moved to shine directly at the rear of the object pattern. This meant that the patterns had to be opaque and transparent instead of black and white. So, the patterns were copied onto transparency film and were then framed with black construction paper. The patterns were sized

TL031, TL031A
ENHANCED JFET LOW-POWER LOW-OFFSET OPERATIONAL AMPLIFIERS

D3151, JULY 1988 – REVISED JANUARY 1989

- Maximum Offset Voltage ... 800 µV
- High Slew Rate ... 2.9 V/µs Typ
- Low Input Bias Current ... 2 pA Typ
- Very Low Power Consumption ... 6.5 mW Typ
- Output Short-Circuit Protection

D, JG, or P PACKAGE
(TOP VIEW)

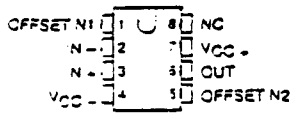

FK PACKAGE
(TOP VIEW)

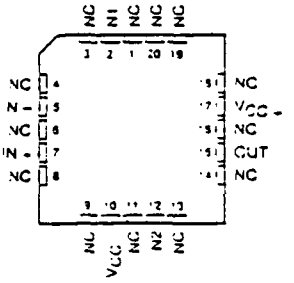

L PACKAGE
(TOP VIEW)

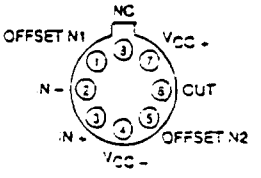

Pin 4 (L Package) is in electrical contact with the case

NC – No internal connection

description

The TL031 and TL031A operational amplifiers incorporate well-matched, high-voltage JFET and bipolar transistors in a monolithic integrated circuit. These devices offer the significant advantages of Texas Instruments new enhanced JFET process. This process affords not only low initial offset voltage due to the on-chip zener trim capability but also stable offset voltage over time and temperature. In comparison, traditional JFET processes are plagued by significant offset voltage drift.

This new enhanced process still maintains the traditional JFET advantages of fast slew rates and low input bias and offset currents. These advantages, coupled with low power consumption, make the TL031 well-suited for new state-of-the-art designs as well as existing design upgrades. The TL031 has been designed to be functionally compatible and pin compatible with the TL061.

AVAILABLE OPTIONS

T_A	V_{IO} max AT 25°C	PACKAGE				
		SMALL-OUTLINE (D)	CHIP CARRIER (FK)	CERAMIC DIP (JG)	METAL CAN (L)	PLASTIC DIP (P)
0°C to 70°C	3 mV	TL031ACD	—	TL031ACJG	TL031ACL	TL031ACP
	5 mV	TL031CD	—	TL031CJG	TL031CL	TL031CP
−40°C to 85°C	3 mV	TL031AID	—	TL031AIJG	TL031AIL	TL031AIP
	5 mV	TL031ID	—	TL031IJG	TL031IL	TL031IP
−55°C to 125°C	3 mV	TL031AMD	TL031AMFK	TL031AMJG	TL031AML	TL031AMP
	5 mV	TL031MD	TL031MFK	TL031MJG	TL031ML	TL031MP

D packages are available taped-and-reeled. Add "R" suffix to device type (e.g., TL031CDR).

DISTRIBUTION OF TL031A
INPUT OFFSET VOLTAGE

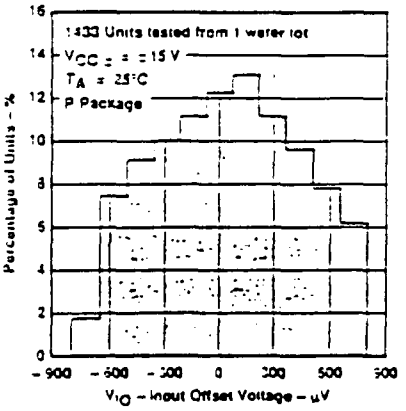

Figure VI-2. Operational Amplifier Data Sheet.

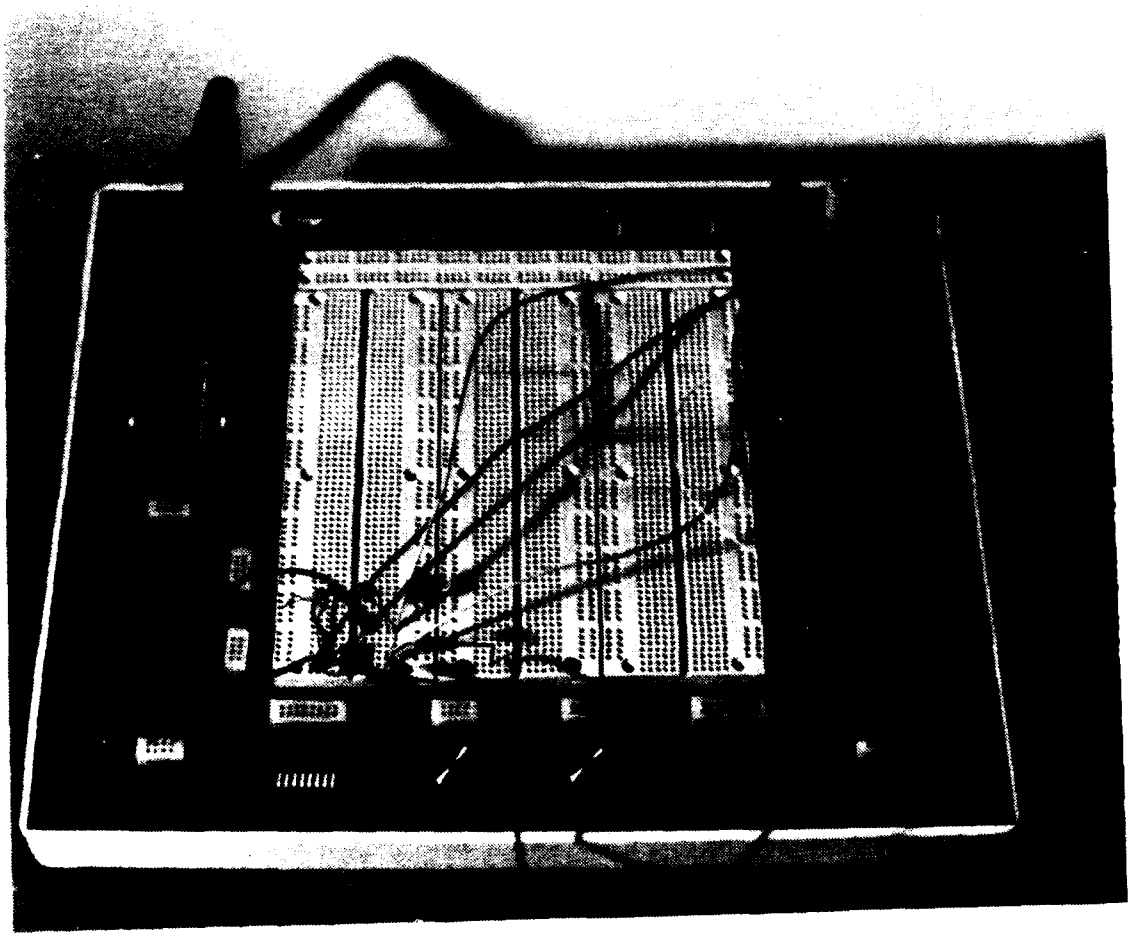

Figure VI-3. Bread Board with Amplifier Circuit.

to fit into a square area whose dimensions were identical to those of the mask windows, so that, with proper longitudinal positioning of the compound lens on the optical bench, the geometry of the object was projected without magnification onto the encoding masks.

c. Replacement Lens

An adjustable, compound, 1¾" diameter camera lens was used to replace the first two smaller 1½" diameter positive lenses in the optical train. This was an Apochromat Artar 19" focal length lens, model # 776116 manufactured by the C. P. Goerz American Optical Company. Close observation indicated that this lens was far superior to its predecessors in its image-forming characteristics.

d. Optical Bench

Two linear rail-type optical benches were used to replace the original table-type bench due to the longer focal length of the replacement lens. The revised system of components is shown in Figure VI-4.

e. Replacement Lock-In Amplifier

A model SR530 Lock-In amplifier manufactured by Stanford Research Systems was found to be a suitable replacement for the erratic amplifier initially used. Careful monitoring of its output under quiescent optical conditions indicated that it was far more stable than the earlier model.

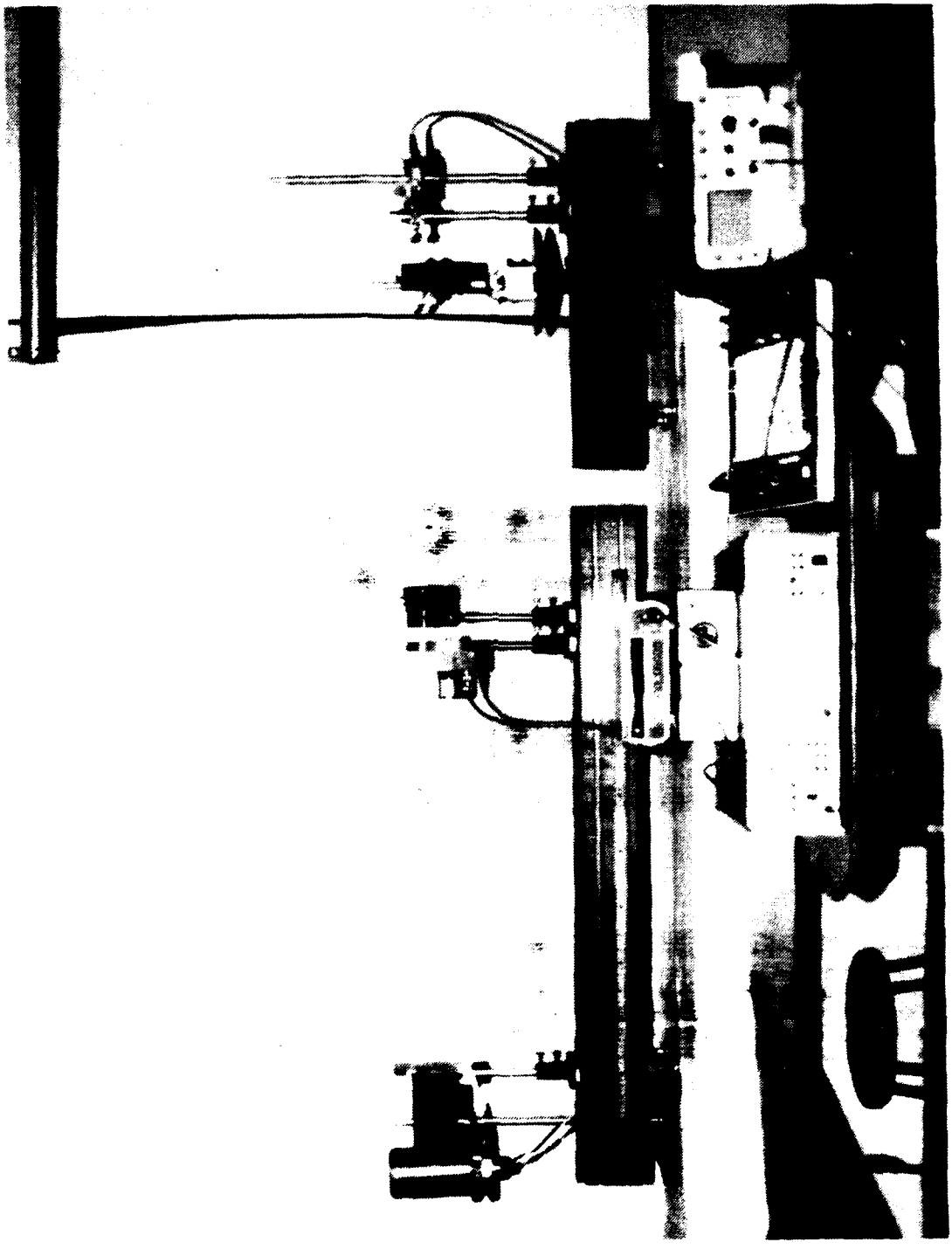

Figure VI-4. Photograph of Revised Optical Arrangement.

4. Third Attempt

a. System Linearity Check.

After aligning the new optical system and connecting the new electronics, the first order of business was evaluation of the detector linearity. With a blank, uniformly illuminated sheet of paper as the target object, the detector out-put decreased from 9.51 mV through the fully-transparent window to 4.77 mV, almost half, as half of the incident light was blocked by another window with 50% opacity. We therefore concluded that the detector linearity difficulties had been remedied.

b. A Different Object.

With a linear response from the detector and the new lock-in behaving in a stable manner, another attempt was made, this time with a different object. The letter "Z" previously used has a dominant diagonal component. With only an 8 x 8 square encoding scheme, faithful reproduction of such a diagonal is not really possible. To avoid this problem, a new object pattern, consisting of four black stripes separated by equal thickness white gaps was chosen from an Air Force resolution chart. The original chart pattern was photo-copied and reduced onto transparency film at a scale that caused the object's spatial structures to coincide closely with those of the Walsh encoding masks' pixel widths and spacings. In fact, this object, shown in Figure VI-5, was identical to the

pattern shown in the window on the bottom row of the first column of Mask #1; see Figure V-5 for comparison. It was expected that this correspondence of sizes would enhance the modulation efficiency and maximize the output for this particular window.

c. Success

At last we were successful at encoding and decoding an image. The decoded pattern was recognizable on the computer CRT screen. Appendix E lists the measured data. Figure VI-6 (a)-(d) show the simulated and actual images reproduced on the screen. These results were very encouraging. They assured us that the radical changes that were made to the encoding system were not in vain.

The lack of distinct contrast in the decoded image was attributed to the difficu' y in aligning many of the encoding masks. It was hard to distinguish between the edges of many of the mask windows and the edges of the projected image. Recall that such alignment was performed manually, in a darkened room. The previous, unsuccessful encoding sessions were tedious; this successful one was even more so. Recording data with both masks took almost twice as long as the previous sessions. We concluded that the primary source of experimental uncertainty at this juncture was simple, random mask alignment error, due to operator fatigue and the

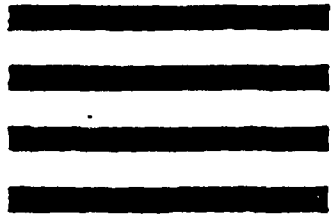

Figure VI-5. Four-stripe Object Pattern.

relatively crude mechanical means by which masks were positioned.

5. A Fourth Attempt

a. Another New Pattern

To overcome the perceived positioning problem, another target object was selected which would be easier to center on the individual mask windows. This pattern consisted of a black square in the middle of a white background. The black square had an area equal to four times that of the individual mask pixel blocks. It was drawn with a black marking pen then photo-copied and reduced onto transparency film. Figure VI-7 shows this object pattern.

b. Another Success

The image of this pattern, when decoded and displayed on the CRT was again recognizable. Appendix E lists the measured data. Figures VI-8 (a)-(d) show the simulated and actual images reproduced on the screen. Recording data for this run took just under two hours due to the improved ease of centering the masks.

6. A Final Convincing Demonstration

a. Yet Another Pattern

To demonstrate that our procedure was indeed valid, another attempt was performed, this time with an object shaped like the letter "T". This letter had a top bar that was two mask pixel blocks high and eight blocks wide and a center

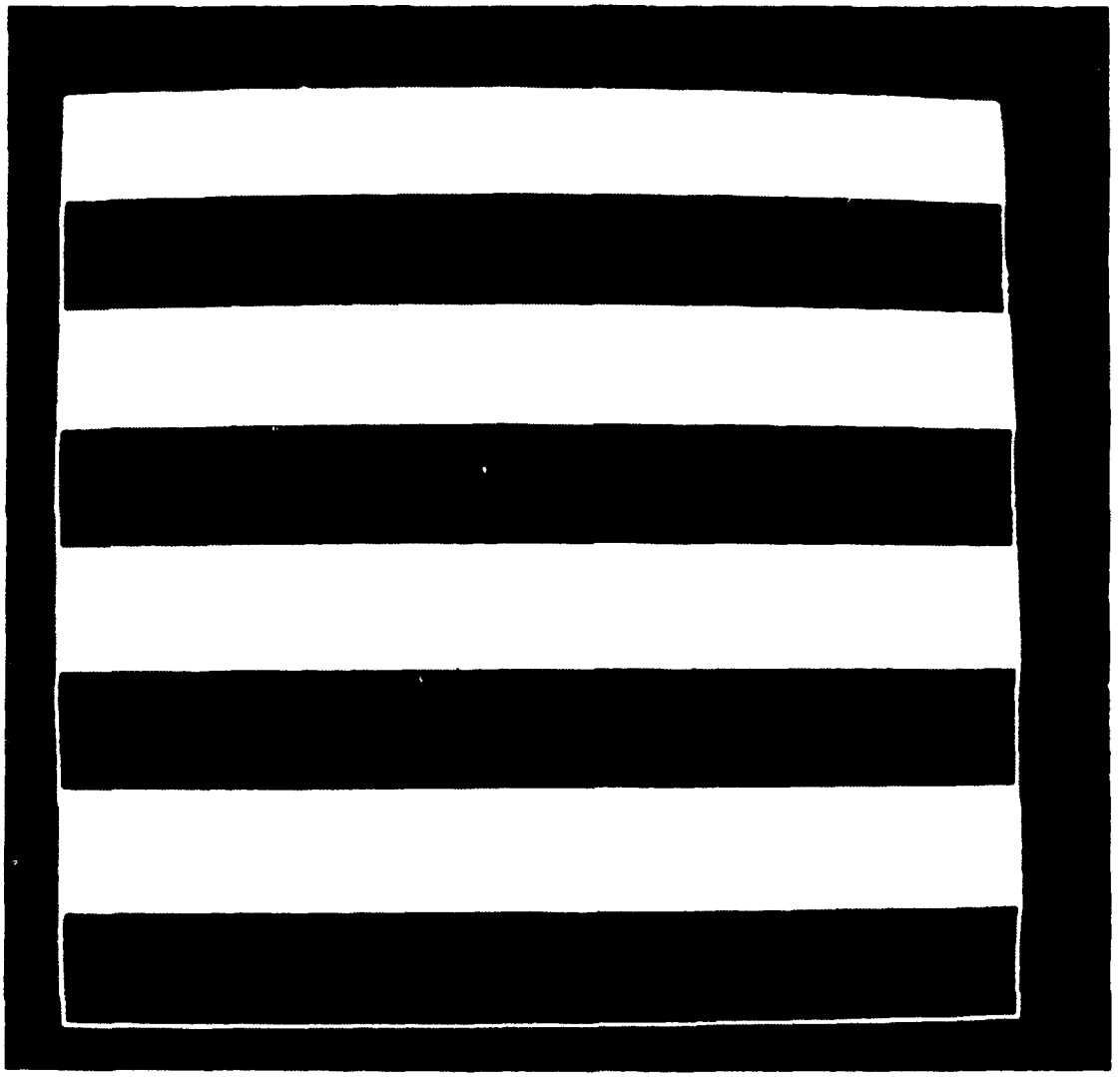

Figure VI-6 (a). Simulated Image of Four-stripe Object Pattern.

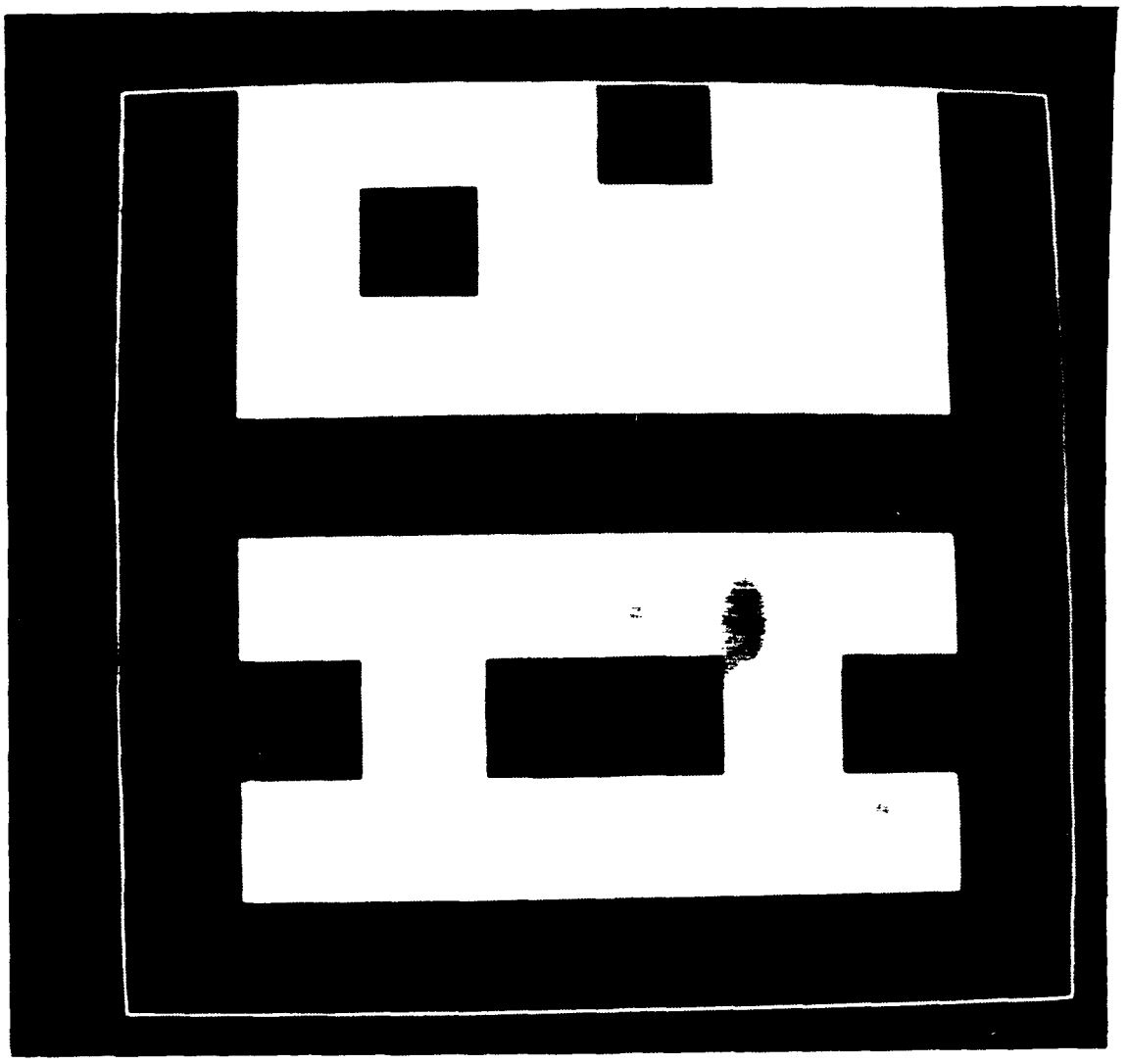

Figure VI-6 (b). Reproduced Image of Four-stripe Object Pattern Using Two-level Gray Scale.

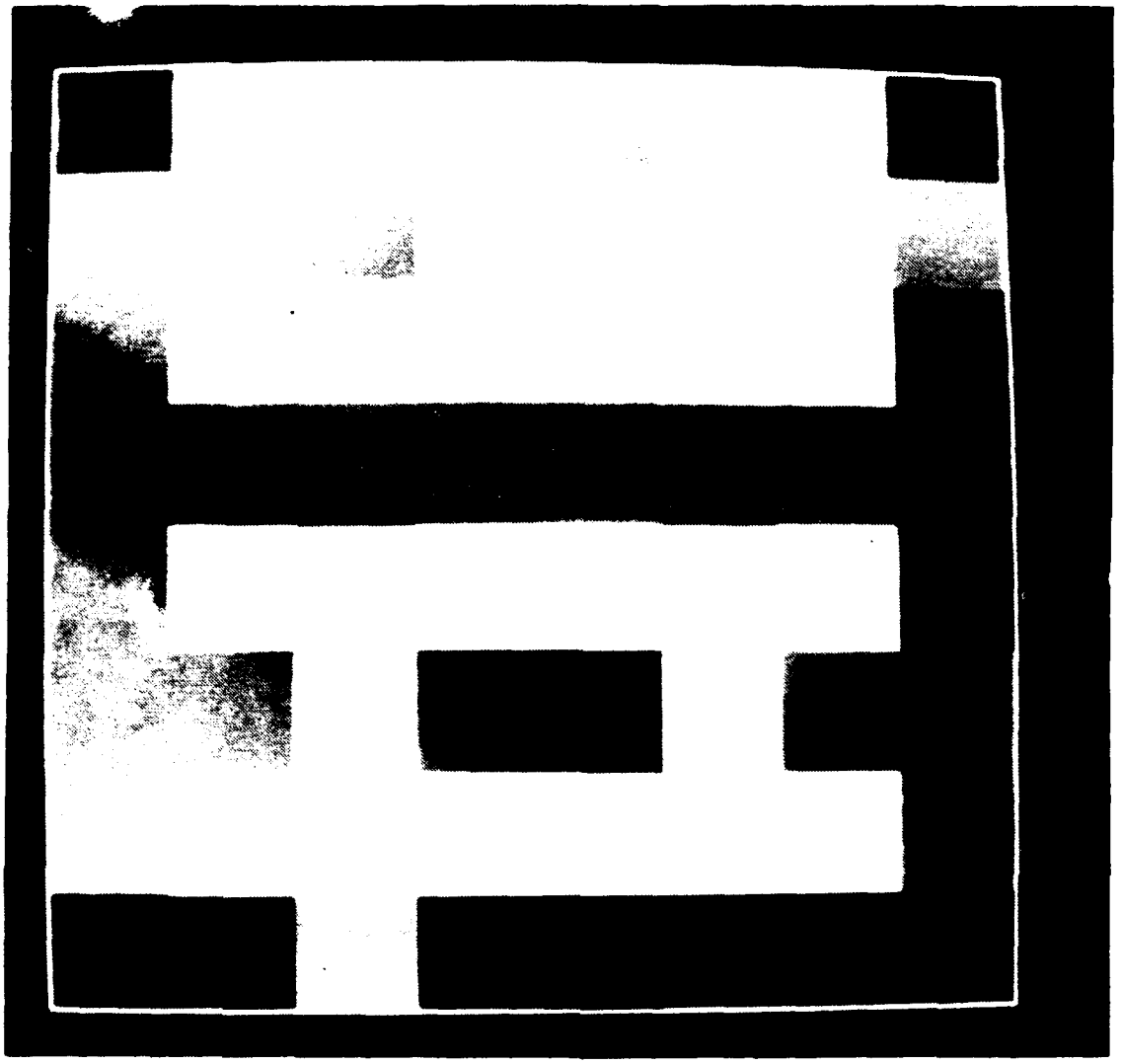

Figure VI-6 (c). Reproduced Image of Four-stripe Object *Pattern Using Four-level Gray Scale.*

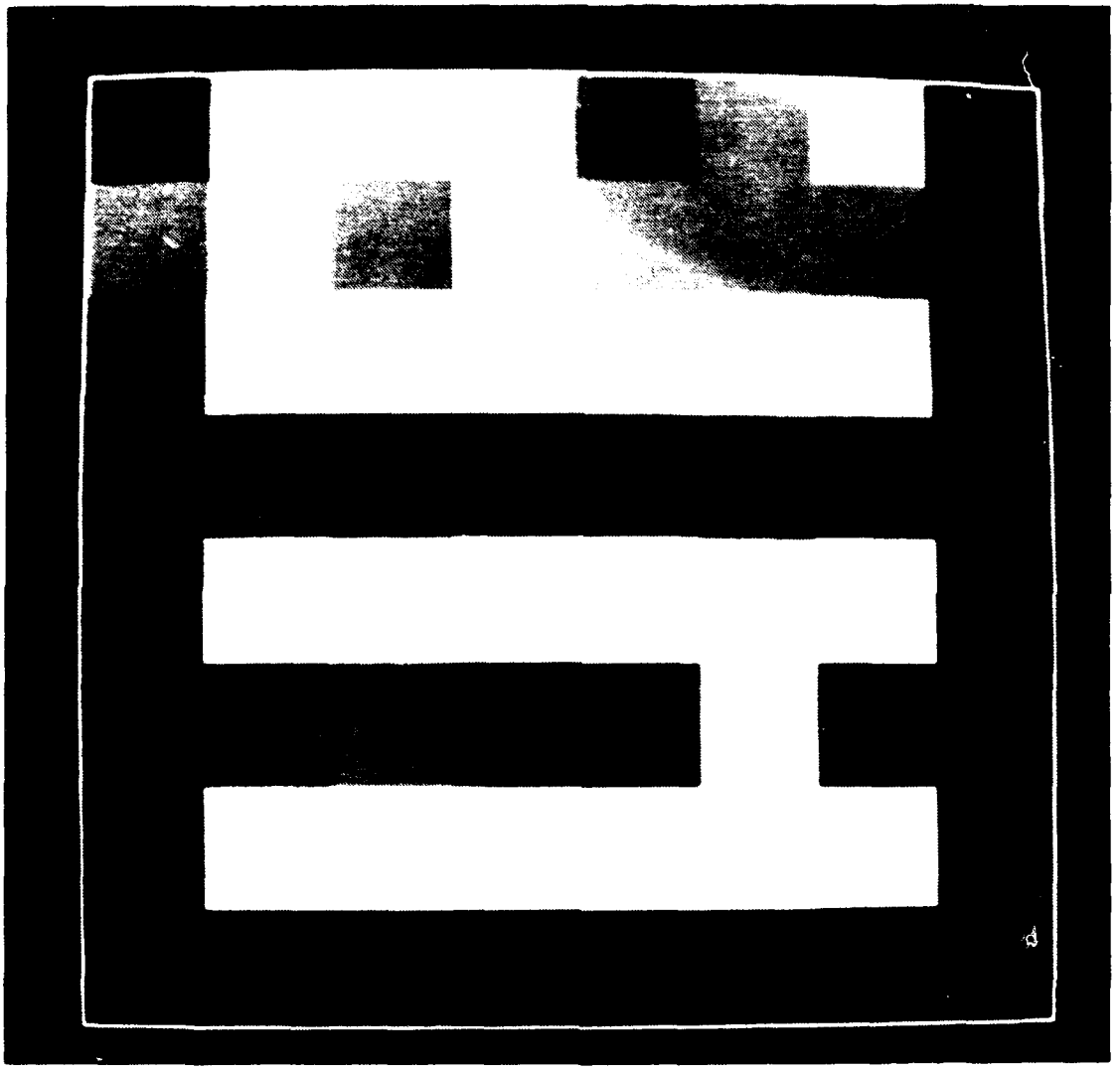

Figure VI-6 (d). Reproduced Image of Four-stripe Object Pattern Using Sixteen-level Gray Scale.

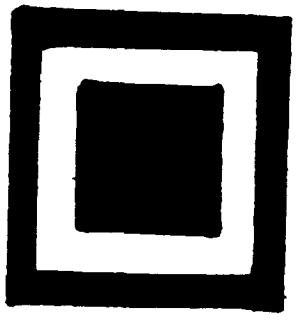

Figure VI-7. Black Square Object Pattern.

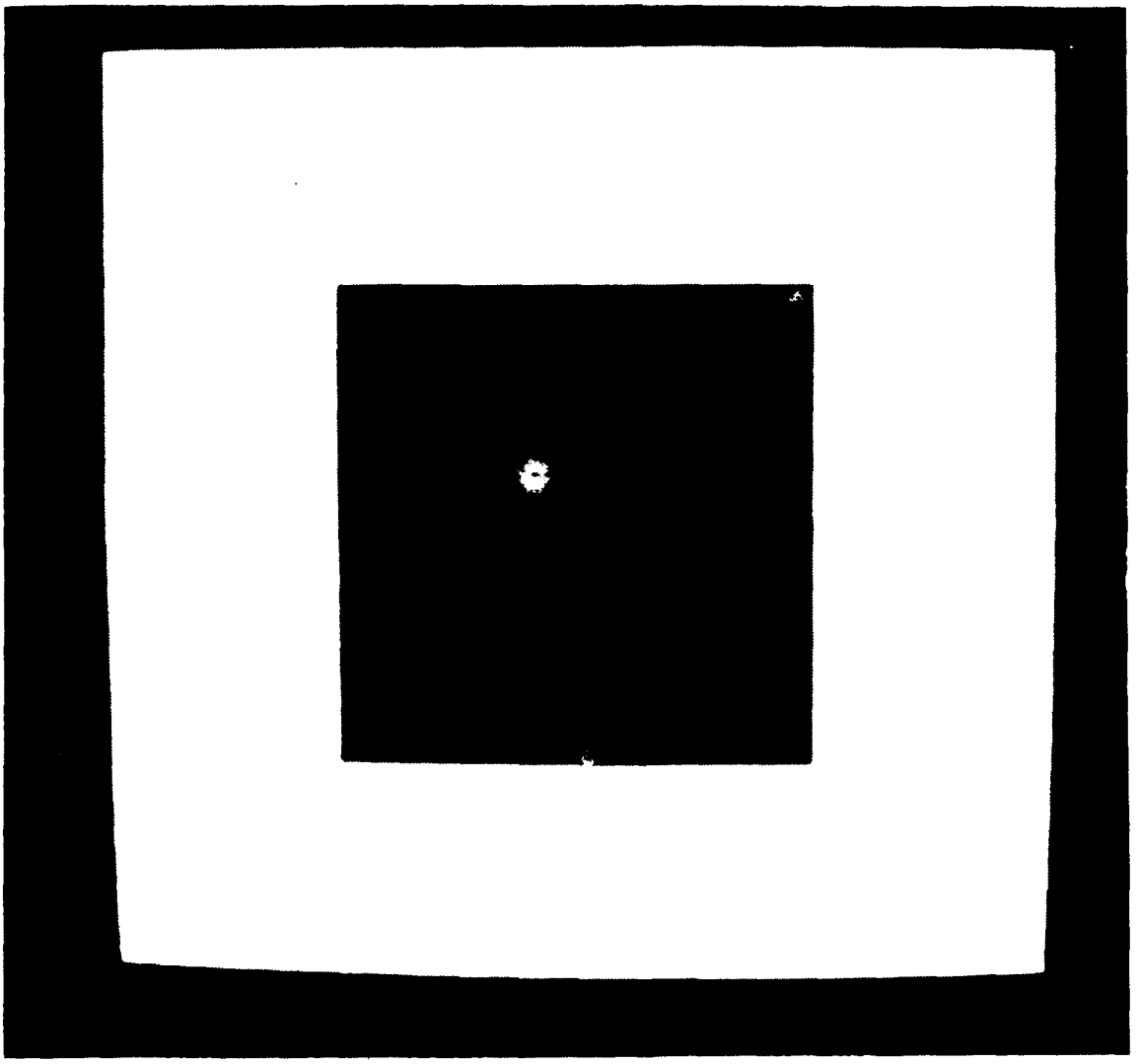

Figure VI-8 (a). Simulated Image of Black Square Object Pattern.

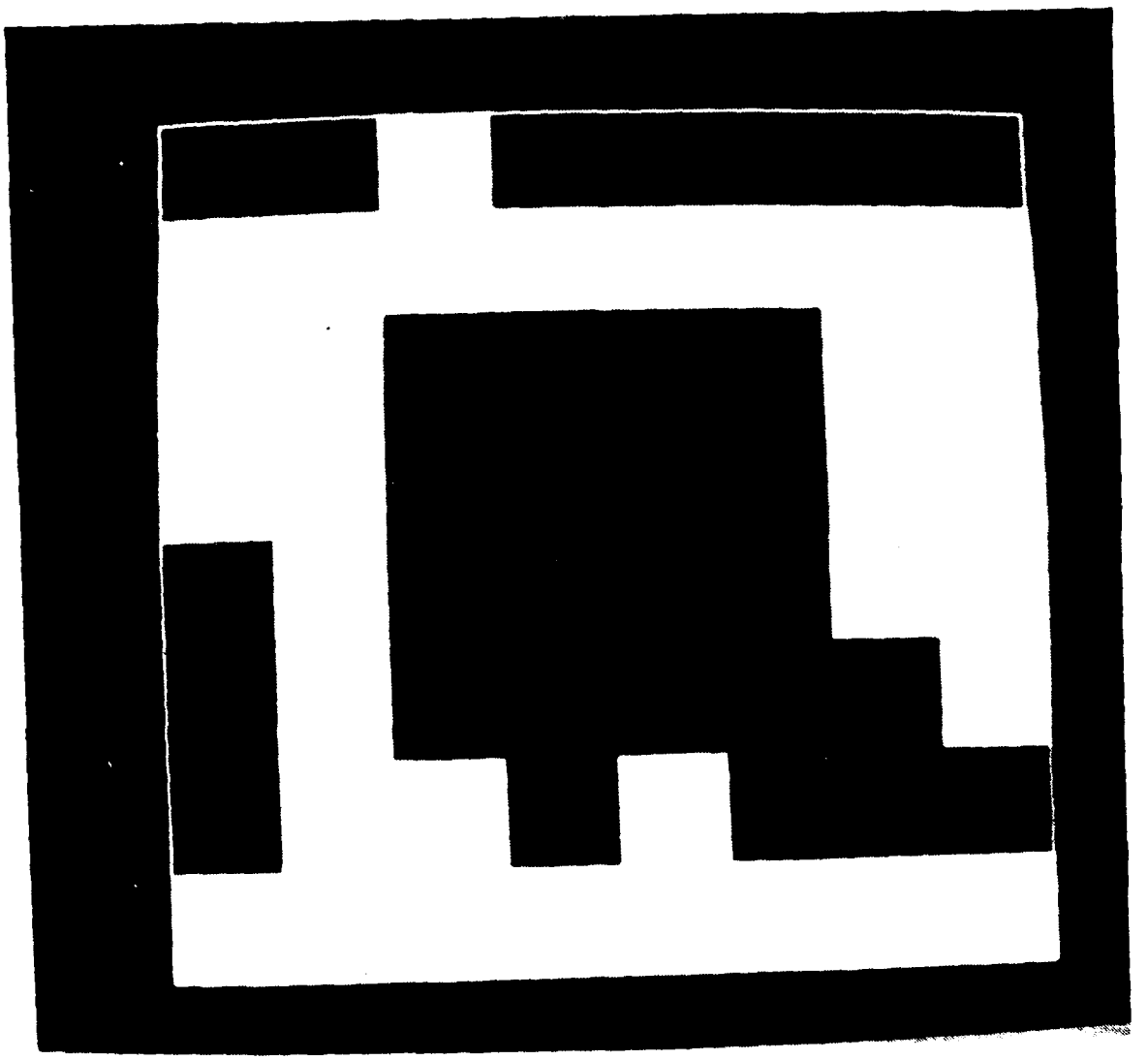

Figure VI-8 (b). Reproduced Image of Black Square Object Pattern Using Two-level Gray Scale.

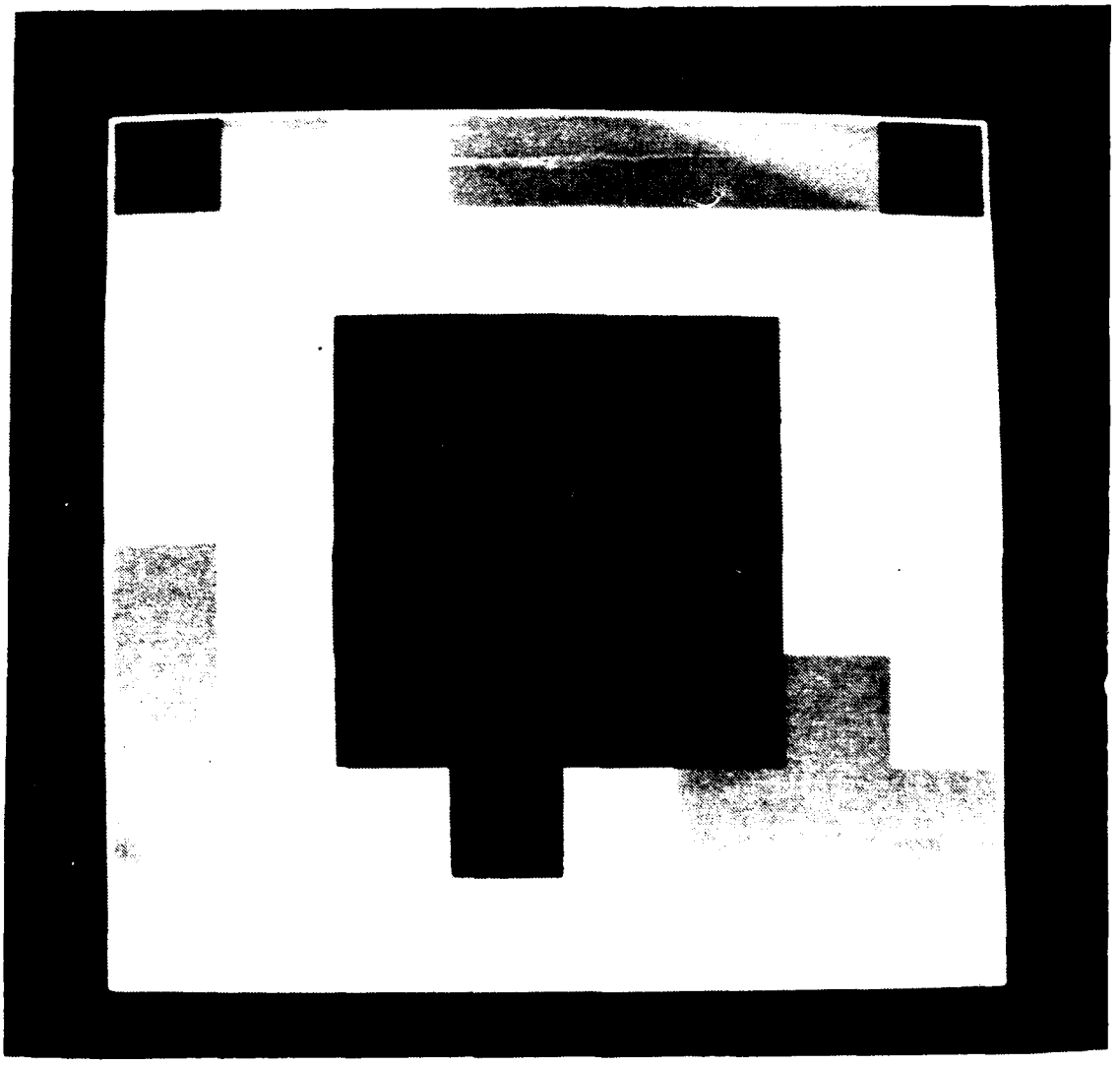

Figure VI-8 (c). Reproduced Image of Black Square Object Pattern Using Four-level Gray Scale.

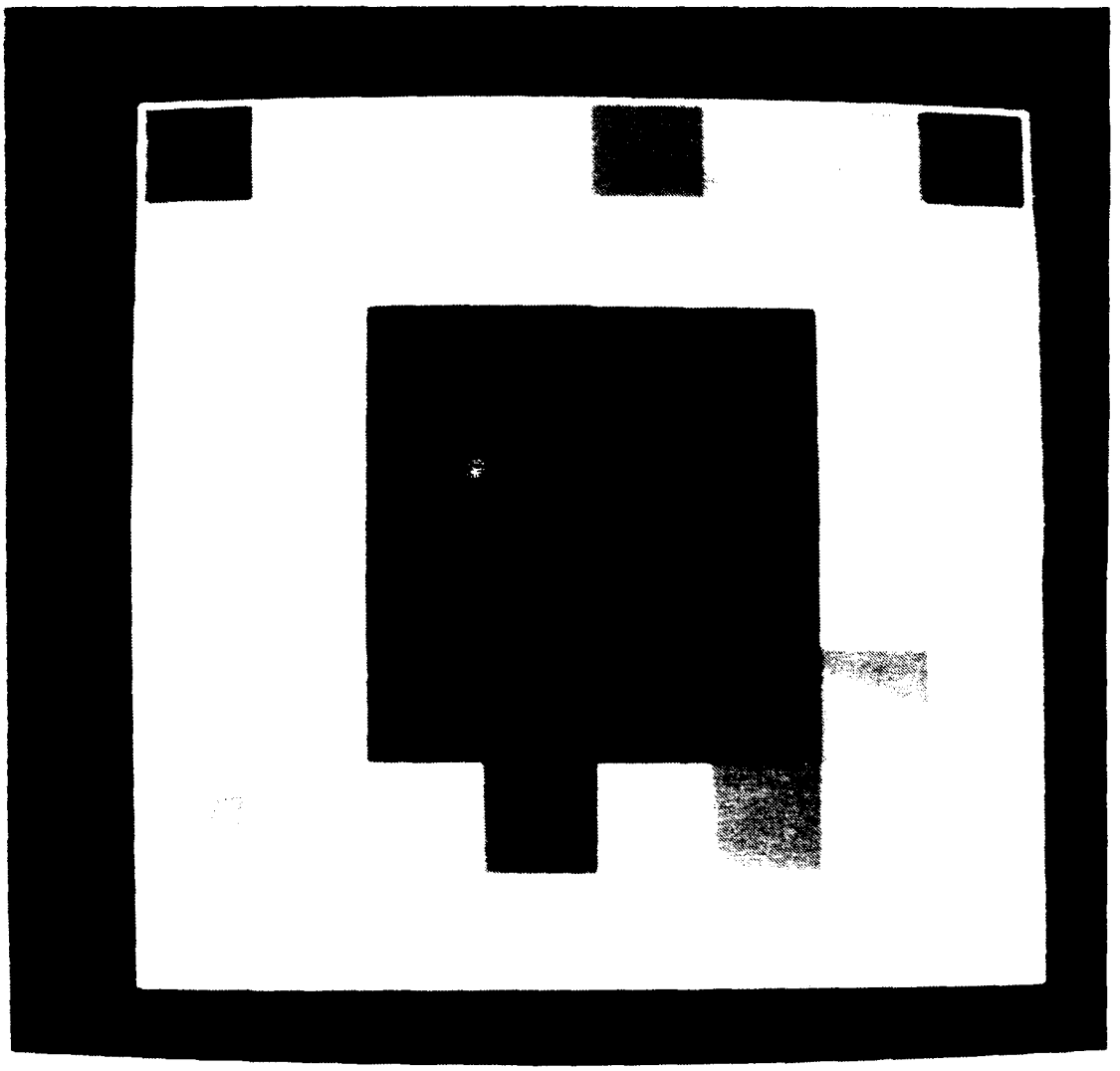

Figure VI-8 (d). Reproduced Image of Black Square Object Pattern Using Sixteen-level Gray Scale.

stalk that was two blocks wide and six blocks high. Because of its shape, the projected image was also easy to center. Like the previous target, this object was also drawn by hand then photo-copied and reduced onto transparency film. Figure VI-9 shows this object pattern. These last three patterns could have been generated on the plotter, but hand drawing avoided the extra time involved with the plotter.

b. Success Again

Our encoding/decoding process reproduces distinctly the image of this modified letter "T." Appendix E lists the measured data. Figures VI-10 (a)-(The image of this modified letter "T" was reproduced distinctly by our encoding/decoding process. Simulated and measured data are listed in Appendix E. The simulated and actual images reproduced on the screen are shown in Figure VI-10 (a)-(d).

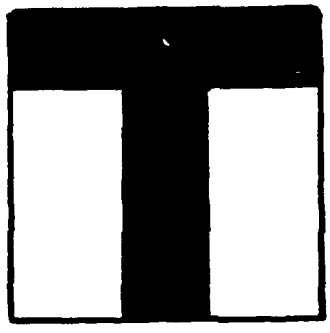

Figure VI-9. Modified "T" Object Pattern.

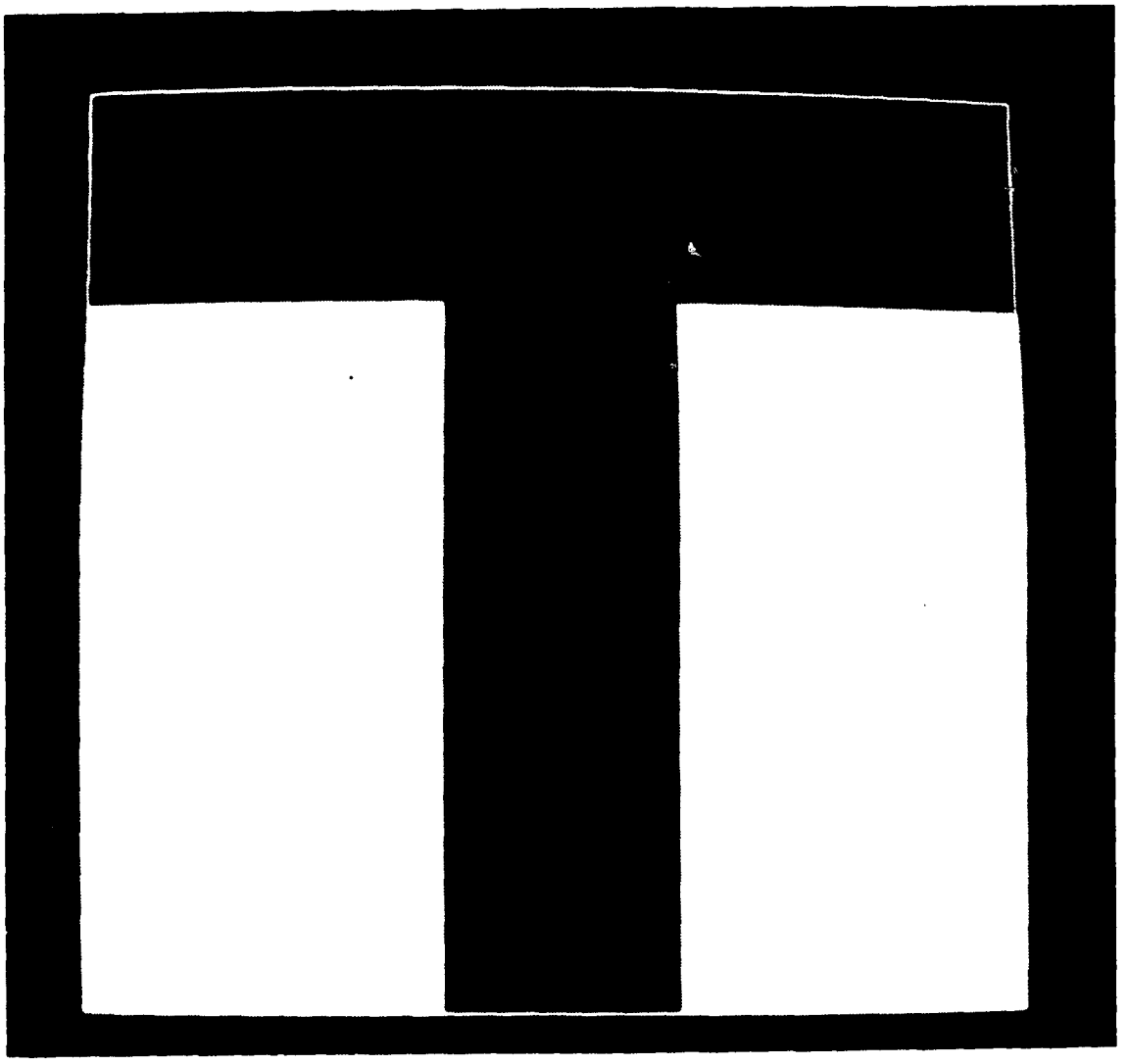

Figure VI-10 (a). Simulated Image of Modified "T" Object Pattern.

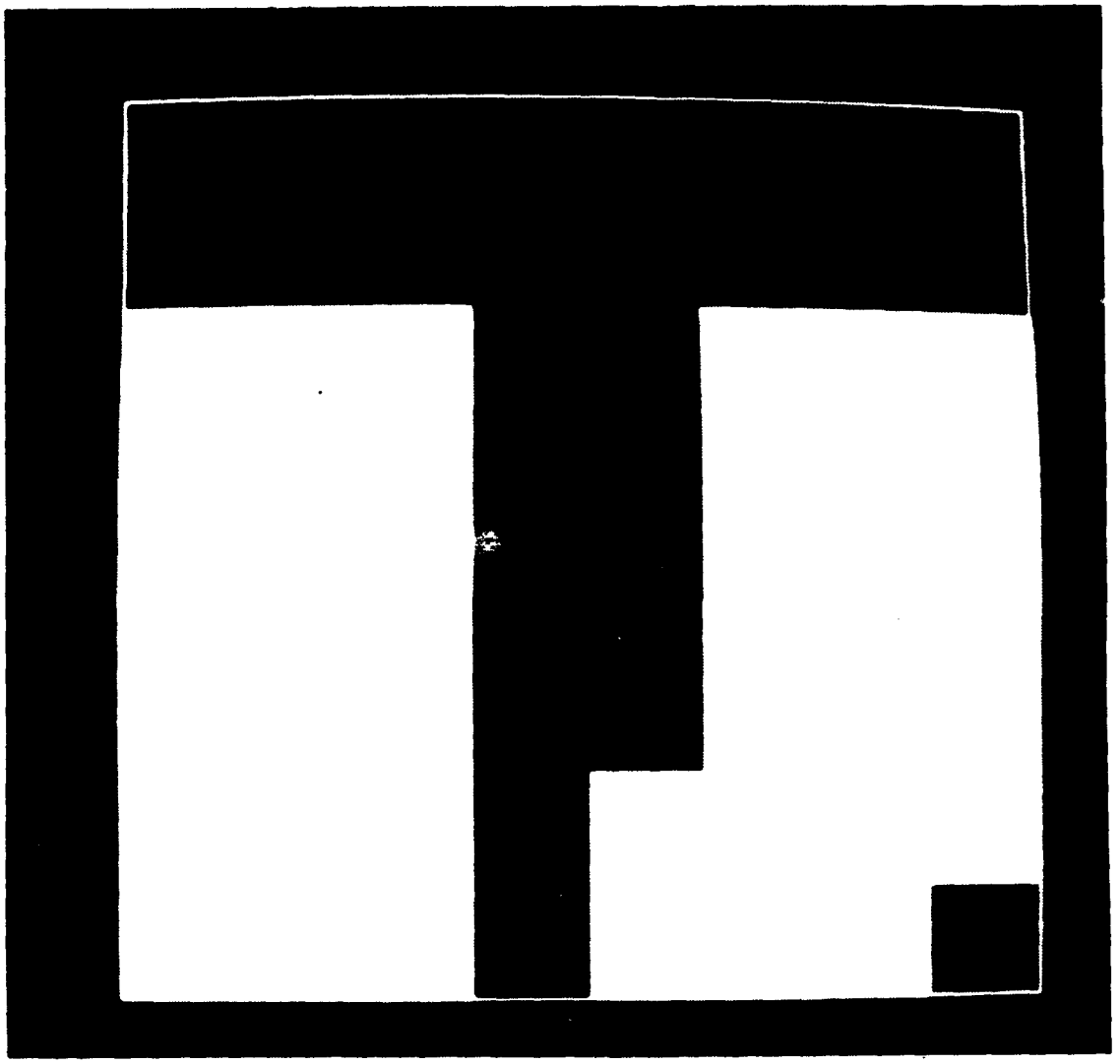

Figure VI-10 (b). Reproduced Image of Modified "T" Object Pattern Using Two-level Gray Scale.

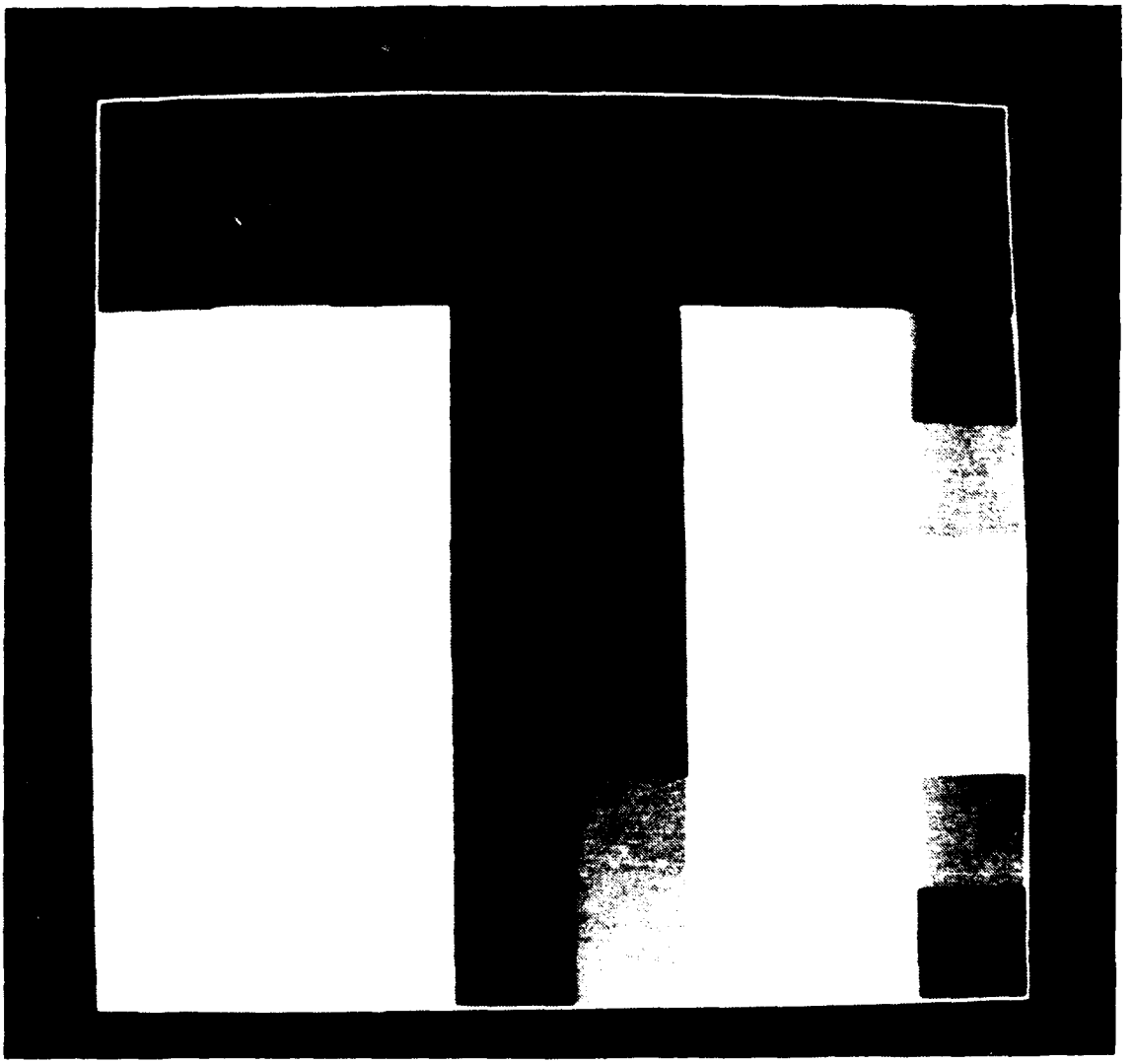

Figure VI-10 (c). Reproduced Image of Modified "T" Object Pattern Using Four-level Gray Sale.

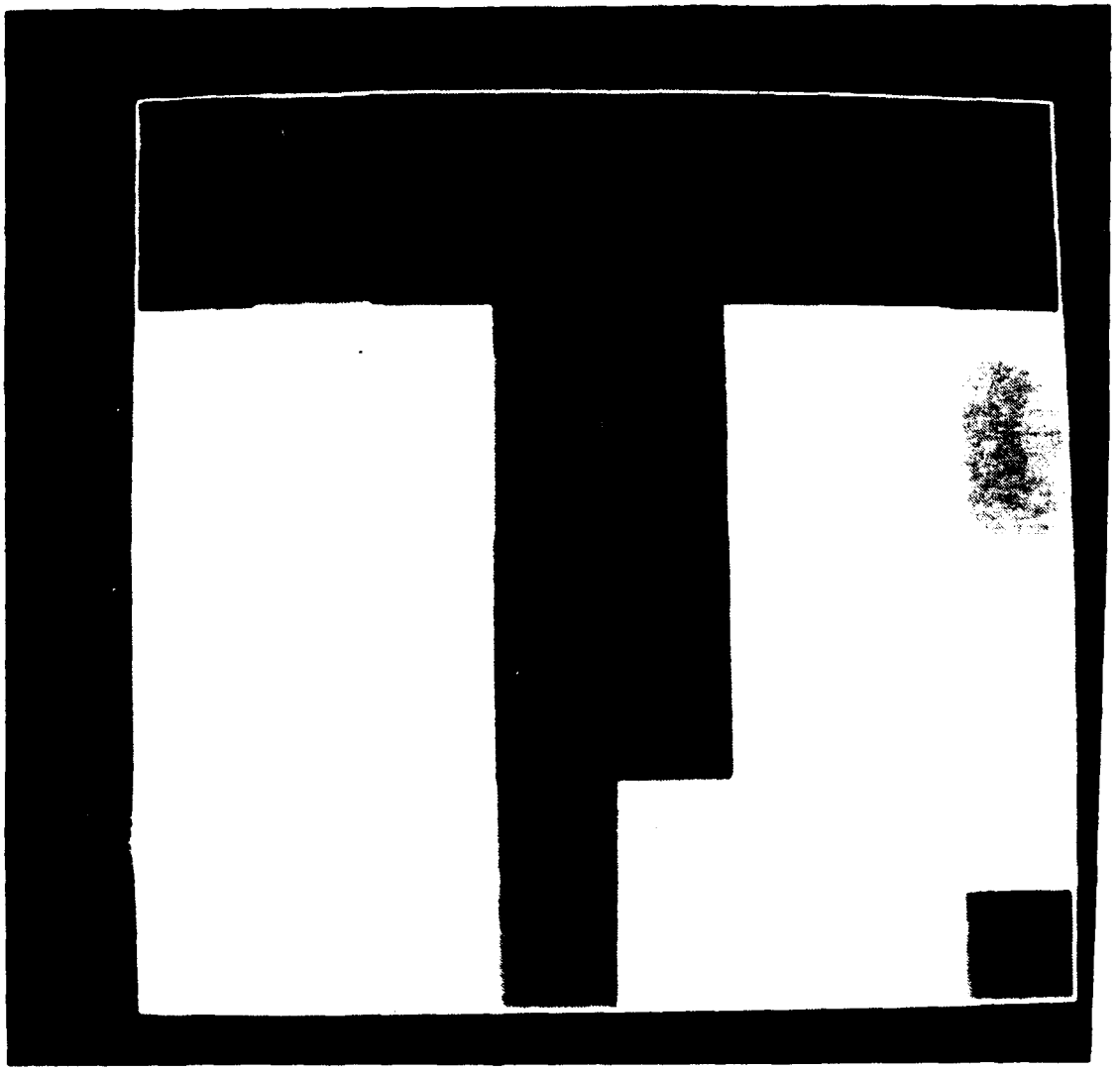

Figure VI-10 (d). Reproduced Image of Modified "T" Object Pattern Using Sixteen-level Gray Scale.

VII. CONCLUSIONS/RECOMMENDATIONS

A. CONCLUSIONS

As stated in the introduction, the primary goal of this thesis project was to develop and to implement a proof-of-concept validation of the proposed multiplexed encoding technique for images. The photographs in Chapter VI offer incontestable proof that this goal has been achieved. While the demonstration of the method's viability is far from perfect, it has shown that the technique's underlying concepts are sound.

Design of the masks using the plotter was a non-trivial task due to the finite pen thickness. Ideal masks would have no ink bleed-over and no border. Experiments with a laser-type printer might result in higher quality masks.

Proper alignment of the masks during the encoding process proved to be the most difficult portion of the project. The crude manual positioners and operator eye fatigue contributed to the difficulties and resulted in poor resolution. Resolution improved by using target objects whose symmetry and shape enabled them to be centered more easily on the masks. Automation of the mask positioning would further improve resolution.

B. RECOMMENDATIONS

Based on the successful proof of Davis' concept, it is recommended that research in this area be expanded to develop fully an infrared imaging system. Improved resolution will require a larger number of Walsh functions. The completed realization of the proposed technique will actually be able to generate the 2-D encoding masks by optical means, requiring far fewer actual masks than a simple extension of this thesis' approach would imply. For IR applications, there is a need to devise a method of putting transmitting/reflecting patterns on masks using materials which do not absorb the incident photon energy at infrared wavelengths. These masks must be precisely and quickly moved into position, requiring an automatic servocontrol system. A rugged, compact optical system and a method of automatically recording and storing the encoded data for each target object must also be designed. Computer software to transform the data into useful displays needs to be developed. It is anticipated that these challenging tasks will be undertaken as future student thesis topics at the Naval Postgraduate School under the direction of Professor Davis.

APPENDIX A

```
{*************************************************************}

{DOCUMENTATION}


{TITLE      : WALSHPRODUCTS
 AUTHOR     : R. H. MCKENZIE
 DATE       : 13 JULY 1990
 REVISED    : 29 JULY 1990
 SYSTEM     : IBM PS/2 MODEL 70 386
 COMPILER   : TURBO PASCAL 4.0
 UTILITY    :

 1. GENERATES WALSH FUNCTIONS UP TO A SPECIFIED ORDER AND
    OUTPUTS DATA TO TWO SEPARATE FILES.
 2. MULTIPLIES THE CONTENTS OF THE TWO FILES AND PRODUCES A
    TEXT FILE .THE CONTENTS OF WHICH ARE USED BY THE PROGRAM
    PRODPLOT TO PLOT THE MASK PATTERNS.}


{*************************************************************}

{DECLARATIONS}

Program WalProds;

const Order = 8;
      Plus = '+';
      Minus = '-';

type  Walsharray = array[1..Order, 1..Order] of char;
      Smallarray = array[1..Order] of char;

var   VDatafil : text;
      HDatafil : text;
      Prodfile : text;
      w : Walsharray;
      VSigns : String[8];
      HSigns : String[8];
      orderby2 : integer;
      row : integer;
      col : integer;
      prow: integer;
      pcol: integer;
```

```
    K,L,M,N: integer;
    sign: char;
    Prod: char;



{************************************************************}

{GENERATION}

begin {PROGRAM}
  {CREATE OUTPUT DATA FILES}
  assign (VDatafil,'VDATA.TXT');
  rewrite (VDatafil);
  assign(HDatafil,'HDATA.TXT');
  rewrite(HDatafil);

  {GENERATE WALSH FUNCTIONS UP TO ORDER 8 FROM RECURSIVE METHOD}

  orderby2 := order div 2;
  for col:= 1 to order do
  w[1,col] := plus;
  for row := 2 to order do
  begin
    pcol := 1;
    prow := (row-1) div 2 + 1;
    if w[prow,pcol] = plus then
      sign := plus
    else
      sign := minus;
    for col := orderby2 + 1 to order do
    begin
      if w[prow,pcol] = sign then
        w[row,col] := plus
      else
        w[row,col] := minus;
      pcol := pcol + 2;
    end;
    pcol := orderby2 + 1;
    if ODD(row) then
      sign := plus
    else
      sign := minus;
    for col := orderby2 downto 1 do
    begin
      if w[row,pcol] = sign then
        w[row,col] := plus
      else
        w[row,col] := minus;
```

```
      pcol := pcol + 1;
    end;

  end;

{*************************************************************}



  for row := 1 to order do  { OUTPUT TO DATA FILES }
  begin
    for col := 1 to order do
    begin
      write(VDatafil,w[row,col]);
      write(HDatafil,w[row,col]);
    end;
    writeln(VDatafil);
    writeln(HDatafil);
  end;


{*************************************************************}

{MULTIPLICATION}

  reset(VDatafil);
  reset(HDatafil);

  {CREATE OUTPUT DATA FILE FOR PRODUCTS}

  assign(Prodfile,'PDATA.TXT');
  rewrite(Prodfile);

  {MULTIPLY EACH VALUE IN THE FIRST FILE BY EACH VALUE IN
   THE SECOND FILE}

  for K := 1 to order do
  begin
    reset(VDatafil);
    readln(HDatafil.HSigns);
    for L := 1 to order do
    begin
      readln(VDatafil.VSigns);
      for M := 1 to order do
      begin
        for N := 1 to order do
        begin
          if (Vsigns[M]= '+') and (HSigns[N]= '+') then
            Prod := '+'
          else if (VSigns[M]= '+') and (HSigns[N]= '-') then
```

```
            Prod := '-'
          else if (Vsigns[M]= '-') and (HSigns[N]= '-') then
            Prod := '+'
          else if (VSigns[M]= '-') and (HSigns[N]= '+') then
            Prod := '-';

          write(Prodfile.Prod);
        end;
      end;
      writeln(Prodfile);  {MOVE DOWN ONE LINE IN OUTPUT FILE}
    end;
  end;

  {CLOSE ALL DATA FILES CREATED}

  close(VDatafil);
  close(HDatafil);
  close(Prodfile);

{*****************************************************************}

{OUTPUT NOTE}

  writeln('*******************************************************');
  writeln('*  THE PRODUCT DATA IS STORED IN THE TEXT FILE:  *');
  writeln('*                  PDATA.TXT                    *');
  writeln('*******************************************************');

end. {PROGRAM}


{*****************************************************************}
```

APPENDIX B

```
{*****************************************************************}

{DOCUMENTATION}

{ TITLE       : PRODUCTPLOT
  AUTHOR      : R.H. MCKENZIE
  DATE        : 26 JULY 1990
  REVISED     : 03 AUG 1990
  SYSTEM      : IBM PS/2 MODEL 70 386
  COMPILER    : TURBO PASCAL 4.0
  UTILITY     : PLOTS WALSH FUNCTION PRODUCTS }

{*****************************************************************}

Program Prodplot;

var
  Datafile:text;
  Plotfile:text;
  K,L,M,N:integer;
  Signs:string[8];

begin  {PROGRAM}
  {OPEN DATA FILES
  assign(Plotfile,'COM1');
  rewrite(Plotfile);
  assign(Datafile,'PDATA.TXT');
  reset(Datafile);  {DATAFILE HOLDS A 64x64 ARRAY OF CHAR}
  writeln(Plotfile,'SP1;');  {SELECT PEN # 1}
  writeln(Plotfile,'PA250,250;');  {MOVES PEN TO START POSITION}    for K := 1 to 8 do  {ROWS OF WINDOWS}
  begin
    for L := 1 to 8 do  {COLUMNS OF WINDOWS}
    begin
      for M := 1 to 8 do  {ROWS OF BLOCKS}
      begin
        read(Datafile,signs);
        for N := 1 to 8 do  {COLUMNS OF BLOCKS}
        begin
          if signs[N] = '+' then
          begin  {FILL BLOCK}
            writeln(Plotfile,'PR2,2;');
            writeln(Plotfile,'PT.1;FT1;RR98,98;');
```

```
            writeln(Plotfile,'PT.1;FT1;RR98,98;');
            writeln(Plotfile,'PR-2,-2;');
          end;
          writeln(Plotfile,'PR100,0;');  {MOVE RIGHT}
        end;
        writeln(Plotfile,'PR-800,100;');  {MOVE LEFT & UP}          end;

      writeln(Plotfile,'PR-5,-805;');
      writeln(Plotfile,'ER810,810;');  {EDGES WINDOW}
      writeln(Plotfile,'ER810,810;');                    writeln(Plotfile,'PR5,955;');  {MOVE UP/NEXT ROW}
      readln(Datafile);
    end;
    writeln(Plotfile,'PR950,-7600;');  {MOVE RIGHT&DOWN/NEXT COL}    end;

  writeln(Plotfile,'SPO;');  {RETURNS PEN}
  writeln(Plotfile,'PG;');  {UNLOADS PLOTTER}

  {CLOSE ALL DATA FILES}
  close(Plotfile);
  close(Datafile);

end.  {PROGRAM}
```

APPENDIX C

```
{*****************************************************************}

{*DOCUMENTATION*}

{*TITLE      : IMAGE
 AUTHOR     : R. H. MCKENZIE
 DATE       : 14 SEPT 1990
 REVISED    : 01 OCT  1990
 SYSTEM     : IBM PS/2 MODEL 70 386
 COMPILER   : TURBO PASCAL 4.0
 UTILITY    :

1. READS LIGHT INTENSITY MEASUREMENT DATA FROM THE FILE

2. RECALLS 64 X 64 WALSH MATRIX USED TO GENERRATE WALSH MASKS.
   CONVERTS THIS MATRIX OF +/- SIGNS TO MATRIX OF +/-1.
3. PERFORMS MATRIX MULTIPLICATION AND OUTPUTS MATRIX OF
   IMAGERY DATA INTO FILE IMAGDATA.TXT }

{*****************************************************************}

{*DECLARATIONS*}

Program Image;

const order = 64;

type   smallarray = array[1..order] of integer;
       walsharray = arrray[1..order,1..order] of integer;
       signarray = array[1..order,1..order] of char;

var
       Limfile:text;
       Walfile:text;
       Imagfile:text;
       I,J,sum:integer;
       clrvalu:integer;
       Datavalu:smallarray;
       Seqvvalu:smallarray;
       Imagvalu:smallarray;
       w:singarray;
       wvalu:walsharray;
```

```
{*************************************************************}

{PROGRAM}

begin
        {OPEN DATAFILES}
        assign(limfile,'LIMDATA.TXT');
        reset(Limfile);
        for I :=1 to order do
        begin  {READ DATA INTO AN ARRAY}
                readln(Limfile,Datavalu[I]);
eend;

{*************************************************************}

{CONVERT MATRIX}

        assig(Walfile, 'PDATA.TXT');   {RECALL ARRAY OF +/- SIGNS }
        reset(Walfile);
        for I :=1 to order do  {CONVERT +/- SIGNS TO +1/-1}
        begin
                for J :=1 to order do
                begin
                        read(Walfile,w[I,J]);
                                if w[I,J] = '+' then
                                        wvalu[I,J] :=1;
                                if w[I,J] = '-' then
                                        wvalu[I,J] :=-1
                end
                readln(Walfile);
        end

{*************************************************************}

{MATRIX MULTIPLICATION]

        assign(Imagfile,'IMAGDATA.TXT');  {OPEN FILE FOR IMAGE DATA}
        rewrite(IMAGFILE);

        for I := 1 to order do    {PERFORM MATRIX MULTIPLICATION}
        begin
                sum := 0;
                for J := 1 to order do
                begin
                        sum  := sum + wvalu[J,I] * Datavalu[J];  {TRANSPOSE}
                end;
                Imagvalu[I] :=sum;
                writeln(Imagfile,Imagvalu[I]);
        end;

        {CLOSE ALL DATA FILE FILES}
```

```
        close(Imagfile);
        close(Walfile);
        close(Limfile);

{*************************************************************}

{OUTPUT NOTE}

        writeln('*************************************************');
        writeln('*  THE DECODED DATA IS STORED IN THE TEXT FILE:  *');
        writeln('*                 IMAGDATA.TXT                  *');
        writeln('*************************************************');

end.  {PROGRAM}

{*************************************************************}
```

APPENDIX D

```
/*****************************************************************/

/*DOCUMENTATION*/

/*TITLE$      : WALSQR
  AUTHOR      : D. S. DAVIS
  DATE        : 17 SEPT 1990
  REVISED     : 07 NOV  1990
  SYSTEM      : IBM PS/2 MODEL 70 386
  COMPILER    : MICROSOFT C 5.1
  UTILITY     : RECREATES IMAGE ON CRT USING 64 PIXELS AND A GRAY SCALE OF 2,4,8,16 LEVELS*/

/*****************************************************************/

/*PROGRAM*/

#include <stdio.h>
#include <conio.h>
#include <graph.h>
#include <math.h>
#include <process.h>

#define MAXBASIS 64

void iointerface (int *, int *, float *);
void squaredisplay (int, int, float *);

main (void)
  { int greyscale, basis;
    float picture[MAXBASIS];
    iointerface (& greyscale, & basis, picture);
    squaredisplay (greyscale, basis, picture);
    return; }

void iointerface (int * greyscale, int * basis, float * picture)   { int a;
    char filename[40];
    FILE * instream;
    system ("CLS");
    for (a = 1; a <= 79; a ++)
      putch ('*');
    printf ("\n\r");
    for (a = 1; a <= 15; a ++)
      putch (' ');
```

```
  printf ("Walsqr    Walsh-multiplexed Square Image Display\n\r");    for (a = 1; a <= 79; a ++)
    putch ('*');
  printf ("\n\n\n\r");
  printf ("Name of input data file ? ");
  scanf ("%s", filename);
  if ((instream = fopen (filename, "rt")) == NULL)
    { fprintf (stderr, "Can't open input data file!\n");
      exit (0); }
  printf ("\n\n\r");
  * greyscale = 0;
  while ((* greyscale != 2) && (* greyscale != 4) && (* greyscale != 8) &&    (* greyscale != 16))
    { printf ("Number of greyscale levels (2, 4, 8, 16) ?"); scanf ("%d", greyscale); }
  * basis = 0;
  while (fscanf (instream, "%d", & a) != EOF)
    { * picture = a;
      (* basis) ++;
      picture ++; }
  fclose (instream);
  return; }

void squaredisplay (int greyscale, int basis, float * picture)   { long int tints[16];
  int row, column, side, xstart, ystart, yul, ylr, xul, xlr, color;    float picturemin, picturemax, * sample;
  struct videoconfig vc;
  if (greyscale == 16)
    { tints[0] = 0x00000000;
      tints[1] = 0x00040404;
      tints[2] = 0x00080808;
      tints[3] = 0x000c0c0c;
      tints[4] = 0x00101010;
      tints[5] = 0x00141414;
      tints[6] = 0x00181818;
      tints[7] = 0x001c1c1c;
      tints[8] = 0x00202020;
      tints[9] = 0x00242424;
      tints[10] = 0x00282828;
      tints[11] = 0x002c2c2c;
      tints[12] = 0x00303030;
      tints[13] = 0x00343434;
      tints[14] = 0x00383838;
      tints[15] = 0x003c3c3c; }
   else if (greyscale == 8)
    { tints[0] = 0x00000000;
      tints[1] = 0x000c0c0c;
      tints[2] = 0x00141414;
      tints[3] = 0x001c1c1c;
      tints[4] = 0x00242424;
      tints[5] = 0x002c2c2c;
      tints[6] = 0x00343434;
      tints[7] = 0x003c3c3c;
      tints[8] = 0x00000000;
      tints[9] = 0x00000000;
```

```
        tints[10] = 0x00000000;
        tints[11] = 0x00000000;
        tints[12] = 0x00000000;
        tints[13] = 0x00000000;
        tints[14] = 0x00000000;
        tints[15] = 0x003c3c3c; }
    else if (greyscale == 4)
     { tints[0] = 0x00000000;
        tints[1] = 0x001c1c1c;
        tints[2] = 0x002c2c2c;
        tints[3] = 0x003c3c3c;
        tints[4] = 0x00000000;
        tints[5] = 0x00000000;
        tints[6] = 0x00000000;
        tints[7] = 0x00000000;
        tints[8] = 0x00000000;
        tints[9] = 0x00000000;
        tints[10] = 0x00000000;
        tints[11] = 0x00000000;
        tints[12] = 0x00000000;
        tints[13] = 0x00000000;
        tints[14] = 0x00000000;
        tints[15] = 0x003c3c3c; }
    else if (greyscale == 2)
     { tints[0] = 0x00000000;
        tints[1] = 0x003c3c3c;
        tints[2] = 0x00000000;
        tints[3] = 0x00000000;
        tints[4] = 0x00000000;
        tints[5] = 0x00000000;
        tints[6] = 0x00000000;
        tints[7] = 0x00000000;
        tints[8] = 0x00000000;
        tints[9] = 0x00000000;
        tints[10] = 0x00000000;
        tints[11] = 0x00000000;
        tints[12] = 0x00000000;
        tints[13] = 0x00000000;
        tints[14] = 0x00000000;
        tints[15] = 0x003c3c3c; }
    basis = floor (sqrt ((double) basis) + 0.5);
    picturemin = picturemax = 0.0;
    sample = picture;
    for (row = 0; row < basis; row ++)
     for (column = 0; column < basis; column ++)
        { if (* sample < picturemin)
            picturemin = * sample;
          else if (* sample > picturemax)
            picturemax = * sample;
          sample ++; }
    _setvideomode (_VRES16COLOR);
```

```
_remapallpalette (tints);
_getvideoconfig (& vc);
_clearscreen (_GCLEARSCREEN);
side = vc.numypixels / basis - 1;
xstart = (vc.numxpixels - (side * basis)) / 2;
ystart = (vc.numypixels - (side * basis)) / 2;
sample = picture;
yul = ystart;
ylr = yul + side;
for (row = 0; row < basis; row ++)
  { xul = xstart;
      xlr = xul + side;
      for (column = 0; column < basis; column ++)
        { color = floor ((greyscale - 1) * (* sample - picturemin) /     (picturemax - picturemin) + 0.5);
          _setcolor (color);
          _rectangle (_GFILLINTERIOR, xul, yul, xlr, ylr);
          ++ sample;
          xul = xlr;
          xlr += side; }
      yul = ylr;
      ylr += side; }
_setcolor (vc.numcolors - 1);
_rectangle (_GBORDER, xstart, ystart, xul, yul);
while (! kbhit ())
  ;
_clearscreen (_GCLEARSCREEN);
_setvideomode (_DEFAULTMODE);
return; }
```

APPENDIX E

LIGHT INTENSITY MEASUREMENTS USING WALSH MASKS
DATE: 17 OCT 1990 OBJECT: 4 STRIPES

MASK #1

	1	2	3	4	5	6	7	8
1	4.82	2.58	2.89	2.57	2.41	2.59	2.98	2.97
2	2.44	2.49	2.54	2.63	2.66	2.80	2.81	2.86
3	2.6[illegible]	2.52	2.60	2.64	2.61	2.60	2.71	2.67
4	[illegible]	2.50	2.52	2.53	2.45	2.46	2.59	2.60
5	2.23	2.53	2.50	2.46	2.42	2.34	2.46	2.60
6	2.52	2.50	2.44	2.37	2.38	2.32	2.40	2.53
7	2.62	2.65	2.54	2.59	2.61	2.58	2.61	2.76
8	3.89	2.61	2.81	2.58	2.57	2.66	2.93	2.91

MASK #2

	1	2	3	4	5	6	7	8
1	0.09	2.66	2.26	2.46	2.93	2.74	2.45	2.98
2	2.34	2.47	2.54	2.62	2.67	2.67	2.85	2.88
3	2.34	2.43	2.57	2.57	2.64	2.58	2.67	2.60
4	2.34	2.48	2.53	2.52	2.42	2.53	2.49	2.58
5	2.79	2.53	2.58	2.51	2.43	2.40	2.30	2.50
6	[illegible]	2.50	2.47	2.45	2.36	2.24	2.33	2.48
7	2.16	2.47	2.54	2.47	2.39	2.50	2.35	2.61
8	2.99	2.52	2.44	2.49	2.75	2.61	2.45	2.75

LIGHT INTENSITY MEASUREMENTS USING WALSH MARKS

DATE: 17 OCT 1990 OBJECT: 4 STRIPES

DIFFERENCE: [MASK #1] - [MASK #2]

	1	2	3	4	5	6	7	8
1	4.73	-0.08	0.63	0.11	-0.52	-0.15	0.53	-0.01
2	0.10	0.02	0.00	0.01	-0.01	0.13	-0.04	-0.02
3	0.29	0.09	0.08	0.07	-0.03	0.02	0.04	0.07
4	0.10	0.02	-0.01	0.01	0.03	-0.07	0.10	0.02
5	-0.56	0.00	-0.08	-0.05	-0.01	-0.06	0.16	0.10
6	0.10	0.00	-0.03	-0.08	0.02	0.08	0.07	0.05
7	0.46	0.18	0.00	0.12	0.22	0.08	0.26	0.15
8	0.90	0.09	0.37	0.09	-0.18	0.05	0.48	0.16

LIGHT INTENSITYY MEASUREMENTS USING WALSH MARKS
DATE: 22 OCT 90 OBJECT: SQUARE

MASK #1

	1	2	3	4	5	6	7	8
1	4.82	2.44	1.87	2.46	2.43	3.50	3.00	2.93
2	2.46	2.49	2.62	2.59	2.71	2.68	2.73	2.74
3	1.65	2.42	1.80	2.52	2.72	2.69	2.54	2.85
4	2.37	2.51	2.55	2.45	2.46	2.42	2.51	2.55
5	2.43	2.56	2.63	2.40	2.42	2.30	2.48	2.57
6	3.04	2.58	2.50	2.40	2.38	2.30	2.47	2.50
7	2.57	2.59	2.43	2.53	2.55	2.48	2.62	2.65
8	1.72	2.38	2.28	2.45	2.57	2.61	2.66	2.70

MASK #2

	1	2	3	4	5	6	7	8
1	0.14	2.44	3.13	2.32	3.00	2.76	2.65	2.88
2	2.33	2.50	2.48	2.56	2.66	2.37	2.75	2.72
3	3.25	2.41	3.36	2.51	2.54	2.70	2.79	2.78
4	2.58	2.51	2.44	2.51	2.54	2.55	2.52	2.59
5	2.53	2.49	2.35	2.46	2.43	2.37	2.39	2.46
6	2.01	2.44	2.50	2.39	2.39	2.34	2.32	2.46
7	2.43	2.48	2.59	2.43	2.52	2.50	2.48	2.54
8	2.93	2.54	2.52	2.48	2.60	2.62	2.75	2.62

LIGHT INTENSITY MEASUREMENTS USING WALSH MARKS
DATE: 22 OCT 1990 OBJECT: SQUARE

DIFFERENCE: [MASK #1] - [MASK #2]

	1	2	3	4	5	6	7	8
1	4.68	0.00	-1.26	0.14	-0.57	0.74	0.35	0.05
2	0.13	-0.01	0.14	0.03	0.05	0.31	-0.02	0.02
3	-1.60	0.01	-1.56	0.01	0.18	-0.01	-0.25	0.07
4	-0.21	0.00	0.11	-0.06	-0.08	-0.13	-0.01	-0.04
5	-0.10	0.07	0.28	-0.06	-0.01	-0.07	0.09	0.11
6	1.03	0.14	0.00	0.01	-0.01	-0.04	0.15	0.04
7	0.14	0.11	-0.16	0.10	0.03	-0.02	0.14	0.11
8	1.21	-0.16	-0.24	-0.03	-0.03	-0.01	-0.09	0.08

LIGHT INTENSITY MEASUREMENTS USING WALSH MARKS
DATE: 23 OCT 1990 OBJECT: MODIFIED 'T'

MASK #1

	1	2	3	4	5	6	7	8
1	5.03	2.58	2.10	3.74	2.06	2.77	2.40	2.78
2	3.52	2.62	2.54	2.69	2.61	2.87	2.79	2.88
3	3.49	2.60	2.43	2.56	2.41	2.66	2.54	2.83
4	1.88	2.57	2.81	2.52	2.81	2.46	2.73	2.64
5	2.48	2.54	2.62	2.52	2.53	2.31	2.48	2.55
6	2.49	2.57	2.58	2.53	2.45	2.34	2.53	2.60
7	2.68	2.66	2.65	2.62	2.61	2.62	2.75	2.80
8	2.54	2.60	2.66	2.64	2.70	2.67	2.84	2.86

MASK #2

	1	2	3	4	5	6	7	8
1	0.14	2.49	3.20	3.29	3.69	2.89	2.26	2.84
2	2.06	2.55	2.81	2.71	3.03	2.92	3.07	2.94
3	1.67	2.59	2.99	2.81	3.04	2.80	3.13	2.82
4	3.19	2.60	2.47	2.64	2.31	2.58	2.54	2.71
5	2.68	2.51	2.58	2.53	2.51	2.43	2.40	2.68
6	2.52	2.55	2.61	2.51	2.48	2.41	2.46	2.73
7	2.50	2.59	2.69	2.60	2.69	2.60	2.72	2.96
8	2.60	2.60	2.69	2.64	2.75	2.70	2.80	3.08

LIGHT INTENSITY MEASUREMENTS USING WALSH MASKS

DATE: 23 OCT 1990 OBJECT: MODIFIED 'T'

DIFFERENCE: [MASK #1] - [MASK #2]

	1	2	3	4	5	6	7	8
1	4.89	0.09	-1.10	0.45	-1.63	-0.12	0.14	-0.06
2	1.46	0.07	-0.27	-0.02	-0.42	-0.05	-0.28	-0.06
3	1.82	0.01	-0.56	-0.25	-0.63	-0.14	-0.59	0.01
4	1.31	-0.03	-0.34	-0.12	0.50	-0.12	0.19	-0.13
5	-0.20	0.03	0.04	-0.01	0.02	-0.12	0.08	-0.13
6	-0.03	0.02	-0.03	0.02	-0.03	-0.07	0.07	-0.13
7	0.18	0.07	-0.04	0.02	-0.08	0.02	0.03	-0.16
8	-0.06	0.00	-0.03	0.00	-0.05	-0.03	0.04	-0.2

LIST OF REFERENCES

1. NASA Space and Earth Sciences Advisory Council, SOFIA: Stratospheric Observatory For Infrared Astronomy, pp. 1-14, Ames Research Center, 24 May 1988.

2. Davis, D.S., "A New Technique for Efficient Multiplex Imaging and Imaging Spectroscopy," paper in preparation.

3. Sakai, H., "High Resolving Power Fourier Spectroscopy," Spectrometric Techniques, Volume 1, Vanasse, G.A.(ed.), pp. 1-70, Academic Press, 1979.

4. Connes, P. and Michel, G., "Astronomical Fourier Spectrometer," Applied Optics, v. 14, p. 206, 1975.

5. Gebbie, A.H., "Walsh Functions and the Experimental Spectroscopist," Proceedings of the Symposium on the Applications of Walsh Functions, Bass, C.A. (ed.), pp. 99-100, National Technical Information Service Document No. AD-707 431, 1970.

6. Decker, J.A., "Hadamard-Transform Spectroscopy," Spectrometric Techniques, Volume 1, Vanasse, G.A.(ed.), pp. 189-289, Academic Press, 1979.

7. Decker, J.A., "Experimental Hadamard-Transform Spectroscopy," Proceedings of the Symposium on the Applications of Walsh Functions, Bass, C.A. (ed.), pp. 101-105, National Technical Information Service Document No. AD-707 431, 1970.

8. Harmuth, H.F., "Sequency Theory: Foundations and Applications," Advances in Electronics and Electron Physics, Marton, L.(ed.) pp. 1- 65, Academic Press, 1977.

9. Walsh, J.L., "A Closed Set of Normal Orthogonal Functions," American Journal of Mathematics, v. 45, pp. 5-24, 1923.

10. Beauchamp, K.G., Applications of Walsh and Related Functions, Academic Press, 1984.

11. Proceedings of the Symposium on the Applications of Walsh Functions, Bass, C.A. (ed.), National Technical Information Service Document No. AD-707 431, 1970.

12. Proceedings of the Symposium on the Applications of Walsh Functions, Zeek, R.W. and Showalter, A.E. (eds.), National Technical Information Service Document No. AD-744 650, 1972.

13. Chandrasekhar, S., Radiative Transfer, Dover Publications, 1960.

14. Boyd, R.W., Radiometry and the Detection of Optical Radiation, John Wiley and Sons, 1983.

15. Hecht, E., Optics, 2d ed., pp. 128-125, Addison-Wesley, 1987.

16. Connes, J., "Computing Problems in Fourier Spectroscopy," Aspen Conference on Fourier Spectoscopy 1970, Vanasse, G.A., Stain, A.T., Baker, D.J. (eds.), Air Force Cambridge Research Laboratory, AFCRL-710019, Special Report No. 114, 1971.

17. Connes, P., "High Resolution and High Information Fourier Spectroscopy," Aspen Conference on Fourier Spectoscopy 1970, Vanasse, G.A., Stain, A.T., Baker, D.J. (eds.), Air Force Cambridge Research Laboratory, AFCRL-710019, Special Report No. 114, 1971.

18. Davis, D., Larson, H.P., Williams, M., Michel, G., and Connes, P., "Infrared Fourier Spectrometer for Airborne and Ground-based Astronomy," Applied Optics, v. 19, p. 4238, 1980.

19. Hewlett-Packard Corporation, HP 7550A Graphics Plotter Interfacing and Programming Manual, Part No. 07550-900001, July 1986.

20. Horowitz, P., and Hill, W., The Art of Electronics, 2d ed., pp. 184-185, Cambridge University Press, 1989.

21. Texas Instruments Inc., Linear Circuits Data Book, Volume 1, p. II-191, 1989.

INITIAL DISTRIBUTION LIST

1.	Defense Technical Information Center Cameron Station Alexandria, VA 22304-6145	2
2.	Library, Code 52 Naval Postgraduate School Monterey, CA 93943-5002	2
3.	Professor K.E. Woehler, Code PH/Wh Chairman, Department of Physics Naval Postgraduate School Monterey, CA 93943-5000	1
4.	Assoc. Professor D.S. Davis, Code PH/Dv Department of Physics Naval Postgraduate School Monterey, CA 93943-50002	3
5.	Assoc. Professor D.L. Walters, Code PH/We Department of Physics Naval Postgraduate School Monterey, CA 93943-5000	1
6.	Department of Physics Library Naval Postgraduate School Monterey, CA 93943-5000	2
7.	Commandant of the Marine Corps Code TE 06 Headquarters, U.S. Marine Corps Washington, D.C. 20380-0001	1
8.	Capt. R.H. McKenzie III, USMC Depot Maintenance Activity Marine Corps Logistics Base Barstow, CA 92311-5087	3